

**Analysis of the Auger Lineshape of
Palladium and Tin using
Auger Photoelectron Coincidence Spectroscopy**

by Christine Ann Creagh

**This thesis is presented as part of the requirement for the Doctor of
Philosophy in Physics at Murdoch University**

Date of submission: 20/6/2002

Declaration of Originality

I declare that this thesis does not incorporate without acknowledgment any material previously submitted for a degree in any university, and that to the best of my knowledge it does not contain any material previously published or written by another person except where due reference is made in the text.

Research data for this thesis has been published as the following journal articles. The Palladium data was also presented as a poster at the Eighth International Conference on Electronic Spectroscopy and Structure in Berkeley California, August 2000

Creagh C. A., S. M. Thurgate, et al. (2002). "Investigating the Structure of the Tin $M_{45}N_{45}N_{45}$ Auger Spectrum Using Auger Photoelectron Coincidence Spectroscopy." Journal of Electron Spectroscopy and Related Phenomena **ELSPEC 4311**.

Creagh C. A., and S. M. Thurgate (2001). "The Use of Auger Photoelectron Coincidence Spectroscopy to Deconvolute the $M_{45}N_{45}N_{45}$ AES of Palladium." Journal of Electron Spectroscopy and Related Phenomena **114 - 116: 69 - 74**.

Other publications relating to my work in APECS are

Creagh C. A., S. M. Thurgate, R. P. Craig and C. P. Lund (1999). "Auger Photoelectron Coincidence Spectroscopy of the $2p_{1/2}$ Line in Coincidence with the $L_3-M_{45}M_{45}$ Peak of Copper." Surface Science **432: 297 - 304**.

Thurgate S. M., C. P. Lund, C. A. Creagh and R. Craig (1998). "More Auger Photoelectron Coincidence Spectra from Copper." Journal of Electron Spectroscopy and Related Phenomena **93: 209-214**.

Acknowledgments

This work would not have been possible without the patience and confidence shown by my supervisor A/Prof. Stephen Thurgate. He was unswerving in his belief that I could do this even when I found my spirits flagging.

I would not have embarked upon my honours year without the encouragement and support of Dr Chris Lund. My thanks go to him for his faith in my ability.

Peter Wilkie, as well as fixing everything in sight, has given me many thought provoking hours of discussion on APECS equipment and life in general. Thank you for seeing the world from "outside the box".

It would have been impossible to achieve the results I have in this thesis using the Commodore 64 that ran the system for my honours project. My heart-felt thanks go to Kurt Friday who developed the acquisition and data processing software I have been using.

Richard Craig stepped into the role of Post Doc. in the APECS lab. for a sort time while working on his own PhD in the adjoining lab. I would like to thank him for commitment above and beyond the call of duty.

Dr. Zhong-Tao Jiang arrived at Murdoch towards the end of the experimental period of my PhD and was happy to take a roster for weekend data acquisition. He has since upgraded the system and is producing some exciting coincidence spectra. I would like to thank him for those weekends when I got to sleep in and his organisational abilities.

Grant van Riessen has been the confusion and delusion seeker. Thank you for helping me focus.

Without the scholarship provided by Murdoch University for three and one half years of study my PhD would have just been a dream. Thank you for making it a reality.

The Australian Research Council has funded the APECS project for 12 years rest assured your money is being well spent.

I would like to thank my family. They have taken good care of me through all my trials and tribulations. Ron gave me the freedom to follow a dream while Robyn and Helen made sure I did not lose sight of reality. I have grown as a person by being part of their lives. Many things would have been impossible without them.

A short note

I would like to thank you for taking the time to read this thesis. Apart from my family it has been the most important thing in my life for the past four years. It is with a certain amount of satisfaction that I present this thesis to you in its final form. This satisfaction comes from the knowledge that I have done my best, I have enjoyed the journey and I am pleased with the result.

There are two sides of this thesis. One side is the research content. The showcase for the late nights, early mornings and weekends not to mention ordinary working hours that have been dedicated to the pursuit of knowledge.

The other side of this thesis is science communication. I am the first PhD student in the APECS laboratory at Murdoch University. The best legacy I can leave future students is a document describing the theory behind APECS as we see it at the moment. My aim is to communicate this theory as painlessly as possible ie. minimal mathematics and many diagrams. References are placed at the end of each chapter so that each section can be taken as a whole. The referenced papers themselves will provide a starting point for students who wish to investigate the subject further.

TABLE OF CONTENTS

Part 1 Background Information

1. XPS and AES	
1.1. Introduction	1
1.2. The XPS Lineshape	3
1.3. The AES Lineshape	7
1.3.1. The basic 2-hole Auger process	8
1.3.2. Auger plasmon gain peaks	15
1.3.3. Auger plasmon loss peaks	16
1.3.4. Auger 3-hole processes	17
1.3.4.1. <i>Coster-Kronig process</i>	17
1.3.4.2. <i>Initial-state shake processes</i>	22
1.3.4.3. <i>Final-state shake processes</i>	24
1.3.5. Process notation	25
1.3.6. 4-hole and other cascade processes	26
1.3.7. Other Factors complicate the Auger spectrum	26
1.3.7.1. <i>Band to band transitions</i>	26
1.3.7.2. <i>Overlapping lines</i>	27
1.3.7.3. <i>Chemical and other environmental effects</i>	27
1.3.7.4. <i>Transitions between atoms</i>	29
2. Cini-Sawatzky Theory and the Auger Lineshape	35
3. Background Subtraction	
3.1. Introduction	50

3.2. Intrinsic Coster-Kronig & Shake-off Processes	50
3.3. Extrinsic Processes	52
3.3.1. Plasmon loss	52
3.3.2. Inelastic scattering	52
3.3.3. Elastic scattering	54
3.4. Background Subtraction Techniques	57

Part 2 The APECS Experiment

4. APECS	
4.1. Introduction	64
4.2. Equipment	65
4.2.1. X-ray Source	66
4.2.2. Sample	66
4.2.3. Lenses and Analysers	68
4.2.4. Hemispherical Analysers	72
4.2.5. Channel Plates	74
4.2.6. Pre-amplifiers	74
4.2.7. Noise Antenna	74
4.2.8. TAC Spectra	75
4.2.9. Resolution	77
4.2.10. Data Collection	79
4.3. Historical Perspective of APECS	82
4.4. The Advantages of APECS Spectra	85
4.4.1. Selection of specific decay processes	85
4.4.2. Reduction of non-related background	87
4.4.3. Reduction of low kinetic energy broadening of the Auger peak	87

4.4.4. Identification of shake processes	89
4.5. The Work of the Murdoch Group	92
4.6. Other APECS Research	101

Part 3 Palladium and Tin APECS Spectra

5. Experimental Results

5.1. Introduction	112
5.2. Sample Preparation and Cleaning	112
5.3. Palladium Experimental Results	115
5.3.1. Weightman's model of the M ₄₅ NN Auger peak	115
5.3.2. Creating the Model Curves	117
5.3.3. Results	120
5.3.3.1. <i>Background subtraction</i>	120
5.3.3.2. <i>M₄₅NN: 3d_{5/2}</i>	126
5.3.3.3. <i>M₄₅NN: 3d_{3/2}</i>	127
5.3.3.4. <i>M₄:M₅:^{CK}NNN Coster-Kronig process</i>	129
5.3.4. Total Model of the M ₄₅ N ₄₅ N ₄₅ Auger Spectrum	131
5.3.5. Discussion	132
5.3.6. Palladium in summary	134
5.4. Tin Experimental Results	
5.4.1. Introduction	134
5.4.2. Constructing a model of the Tin Auger spectra using APECS data	
5.4.2.1. <i>M₄₅N₄₅N₄₅: 3d_{3/2}</i>	136
5.4.2.2. <i>M₄₅N₄₅N₄₅: 3d_{5/2}</i>	139
5.4.2.3. <i>M₄₅N₄₅N₄₅: 3p_{3/2}</i>	140
5.4.3. Comparing the model and high resolution Auger spectra	142

5.4.4. Oxidation and coincidence data	146
5.4.5. Tin in summary	148
6. Conclusion	151

Appendix

- i Acronyms
- ii Auger Process Notation
- iii Electron Path Length Definitions
- iv The Use of APECS to Investigate Various Decay Processes
- v List of APECS Researchers
- vi Optimising the Magnetic Fields
- vii Cleaning and Experimental Settings

Diagram index

Table index

Part 1

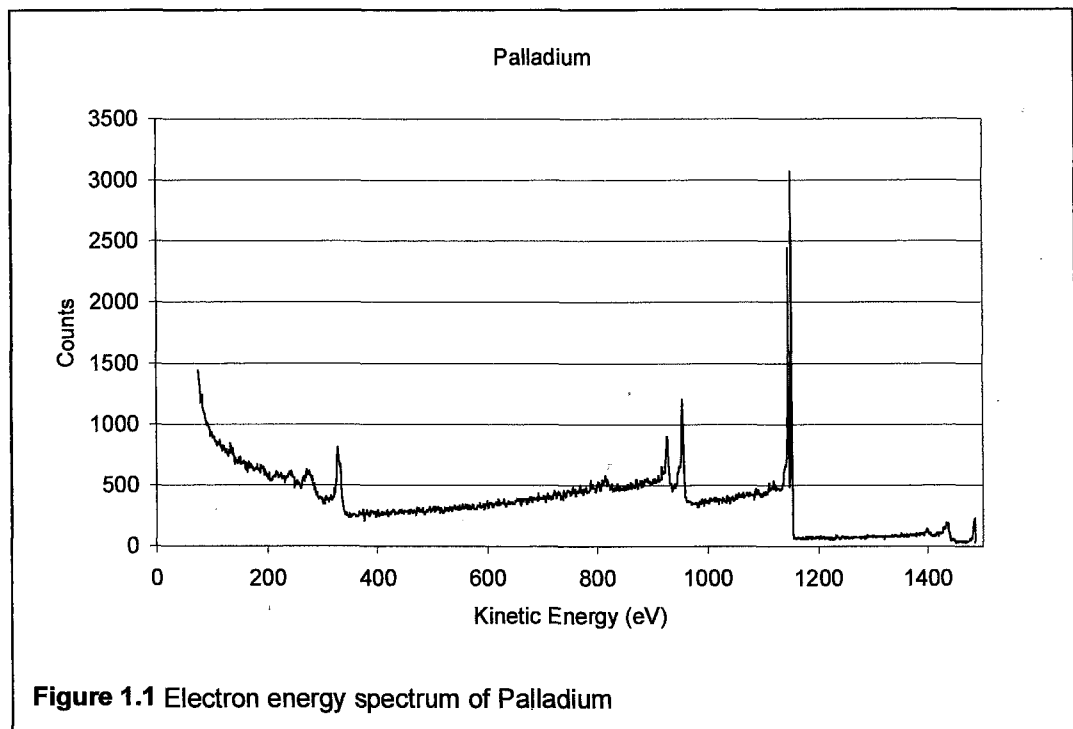
Background Information

Chapter 1.

XPS and AES

1.1. Introduction

When a metal surface is irradiated with low energy X-rays, UV rays or bombarded with electrons, electrons may be released. A plot of the number of electrons released against their energy gives the characteristic electron energy spectrum for that material (Figure 1.1).



The bulk of the intensity in the electron energy spectrum is background intensity, which has high intensity at low kinetic energies and low intensity at high kinetic energies. Superimposed on this background are photoelectron

lines, which together form the X-ray photoelectron spectrum and Auger peaks, creating the Auger electron spectrum.

X-ray photoelectron spectroscopy (XPS) is routinely used to investigate the chemical composition of materials. Its great strength is its ability to determine the chemical state of surface atoms. If the complex Auger spectrum were better understood Auger electron spectroscopy (AES) could also provide quantitative information about the chemical state of the material. A way to better understand the Auger lineshape is to use Auger photoelectron coincidence spectroscopy (APECS), which collects only those Auger electrons resulting from specific photoionisations. In this way intensity in the Auger peak from all other sources is removed. This makes it possible to independently examine the processes that produce intensity in the Auger peak. As the resolution of AES systems increases and AES is more widely used, the necessity to understand the Auger lineshape becomes important because the validity of the data rests on an understanding of the spectra.

To be able to understand APECS spectra it is necessary first to understand XPS and AES spectra and the relationship between the two, which is the topic of this chapter. For the purpose of this thesis photoelectron curves will be referred to as lines and Auger curves will be referred to as peaks to reduce the confusion when dealing with both in coincidence. The series of events taking place in an atom that result in the emission of one or more

electrons will be termed a process. A named process therefore identifies a particular series of electron transitions between the atomic energy levels as well as the electrons that are involved in the transitions.

1.2. The XPS Lineshape

This section will examine the origin and complexity of the photoelectron lines in the electron emission spectrum. A low energy X-ray photon transfers its energy to an inner shell electron of an atom and this electron escapes the atom with a fixed amount of kinetic energy (Figure 1.2). The use of monochromatic incident radiation eliminates complications in the XPS spectrum arising from satellites in the incident radiation. The photoelectron lines appear to be a series of narrow, high intensity lines whose energy position changes if the energy of the incident radiation changes.

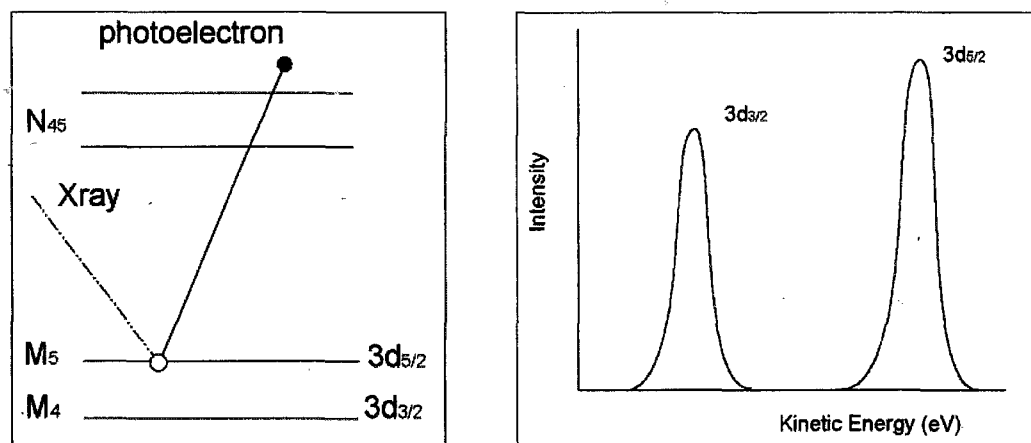


Figure 1.2 XPS process and spectrum

The energy separation between the XPS peaks of the photoelectron spectrum is the same as that of the energy levels.

A photoelectron line in the XPS spectrum is named using quantum number notation (Figure 1.3), which indicates the original energy level of the photoelectron.

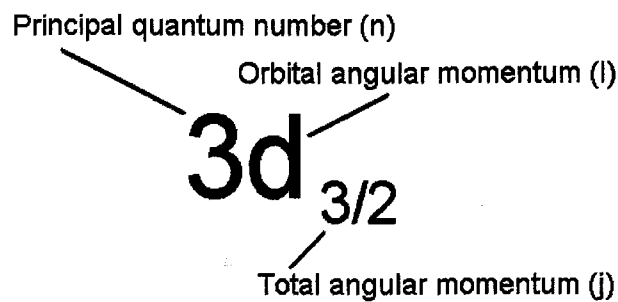


Figure 1.3 XPS notation – photoelectron lines are named using the quantum number notation representing the original energy level of the photoelectron.

Einstein determined that, in an isolated atom, the maximum kinetic energy of a photoelectron is equivalent to the energy of the incident photon, less the energy needed to remove the electron from its energy level in the atom (Equation 1.1).

Einstein's photoelectric equation

$$E_{\text{photon}} = E_{k_{p-e}} - E_{b_{\text{core-e}}} + \phi \quad (\text{Equation 1.1})$$

Where

E_{photon} is the energy of the incident photon

$E_{k_{p-e}}$ is the kinetic energy of the photoelectron

$E_{b_{\text{core-e}}}$ is the binding energy of the photoelectron - binding energies are negative values. The closer to the core the more negative the value is.

ϕ is the work function of the spectrometer – the energy required to remove the electron from the metal to empty space

If the photoelectron has high kinetic energy then any changes that take place in the atom and surrounding atoms due to the removal of the photoelectron

will have negligible effect on the energy of the photoelectron (sudden approximation theory). For atoms in a solid energy is also needed to remove the electron from the material (work function). The work function may be different for different materials in the same environment.

An XPS spectrum of isolated atoms, such as those in a gas, consists of several tall thin Gaussian curves at characteristic electron energies. The width of a curve is related to the lifetime of the excited state (see section on the Coster-Kronig process). The detection system (see chapter on APECS) has a finite energy resolution which also adds to the width of the curve.

Atoms in solids have inner energy levels, which may have multiplet splitting. Where there is multiplet splitting the lineshape of the photoelectron line is composed of the sum of several curves each representing the individual multiplet energy level. In a solid the atom is not isolated and the discrete outer valence level may broaden into a band. Photoelectrons arising from this valence band may therefore take on a range of energies reflecting the density of states (DOS) of the band.

Inelastic collisions between the photoelectron and other atoms in the solid as the electron escapes from the material will reduced the energy of the photoelectron and create a low kinetic energy tail to the main peak. Electrons with energy that places them in the most intense part of a photoelectron line

have not lost energy between leaving the atom and escaping from the material. This is more likely to happen if the atom the electron escapes from is close to the surface. The average depth for electrons to escape without losing energy is proportional to the inelastic mean free path (IMFP), which is related to the kinetic energy of the photoelectron. Specific IMFP values have been tabulated by Tanuma, Powell and Penn [1-7]. On average the distance that an electron can travel without collisions in a solid is of the order of $5 \times 10^{-10} \text{m}$ to $20 \times 10^{-10} \text{m}$ [8]. XPS is therefore sensitive to surface changes, which show up as changes in the intensity and position of the lines in the XPS spectrum.

Other processes may modify the lineshape of the photoelectron line such as plasmon loss, shake-up and shake-off. Photoelectrons can cause excitation of the electron gas (plasmons) as they leave the metal reducing the kinetic energy of the photoelectron by a characteristic amount. Plasmons may be seen in the XPS spectrum as a low intensity, lower kinetic energy satellites to the main line, removed by a characteristic amount of energy. During core level photoionisation an additional electron from the valence band may be excited to a higher energy level (shake-up) or even to the continuum (shake-off). In both situations the kinetic energy of the photoelectron is reduced producing low kinetic energy satellite peak(s) to the main peak.

The simplest electron energy spectra of solids come from clean pure elemental materials. Complications arise where there is more than one element in the sample and the photoelectron lines of the individual elements overlap other features in the emission spectrum. If the overlap is between photoelectron lines and Auger peaks then changing the energy of the initiating photons will shift the photoelectron lines away from the Auger peaks. If there are other structures overlapping the photoelectron lines surface analysis may still be performed by looking at the Auger peaks of the individual elements.

1.3. The AES Lineshape

The advantage of AES over XPS is that the kinetic energy of the Auger electron does not depend on the way the initial photoionisation was made. It is therefore possible to use non-monochromatic sources such as electrons, ultra-violet light or X-rays. Auger peaks are not as well defined as photoelectron lines, broader, of lower intensity, and do not change their energy when the energy of the incident radiation is changed because their energy is related to the electronic structure of the atoms. Auger electron peaks are named using atomic shell notation and indicate the sequence in which electron vacancies occur in the orbitals. A comparison of XPS and AES notation for several energy levels is given in Table 1.1 and an explanation of the naming of Auger peaks is given in Figure 1.4.

Table 1.1 Comparison of XPS and AES Notation

XPS	AES		XPS	AES		XPS	AES
1s	K		3s	M ₁		4s	N ₁
2s	L ₁		3p _{1/2}	M ₂		4p _{1/2}	N ₂
2p _{1/2}	L ₂		3p _{3/2}	M ₃		4p _{3/2}	N ₃
2p _{3/2}	L ₃		3d _{3/2}	M ₄		4d _{3/2}	N ₄
			3d _{5/2}	M ₅		4d _{5/2}	N ₅

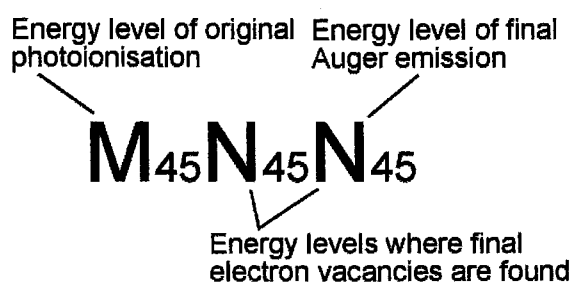


Figure 1.4 AES notation – Auger electron peaks are named using atomic shell notation. In this situation the initial photoionisation takes place in the 4d_{3/2} or 4d_{5/2} energy level (M₄₅). The subsequent decay process leaves two holes in the valence band.

1.3.1. The basic 2-hole Auger process

A simple two-step explanation of the Auger process begins with the initially photoionised atom with a missing electron or a ‘hole’ in one of its core energy levels. An electron from an outer energy level may fill this core hole and the process releases an amount of energy equivalent to the difference in binding energy between the two levels. The energy can either be emitted as a photon (fluorescence) or transferred to an electron in an outer orbital enabling it to escape from the atom (Figure 1.5). This secondary electron is the Auger

electron and the basic Auger process is sometimes called a 2-hole Auger process because of the 2 additional holes remaining in the valence band.

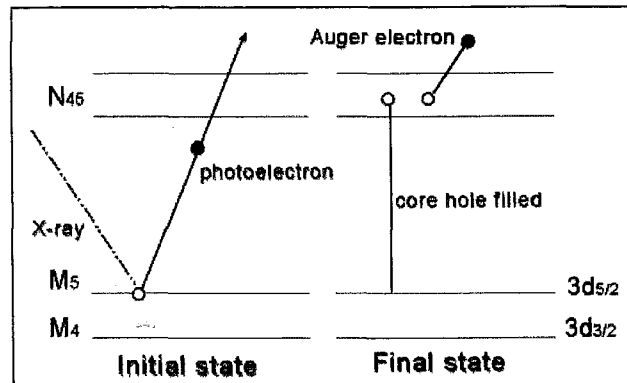


Figure 1.5 $M_5-N_{45}N_{45}$ basic 2-hole Auger process. Initial photoionisation of a core level is followed by an outer electron filling the core hole. The amount of energy released is transferred to another outer electron - the 'Auger' electron that escapes with a characteristic energy.

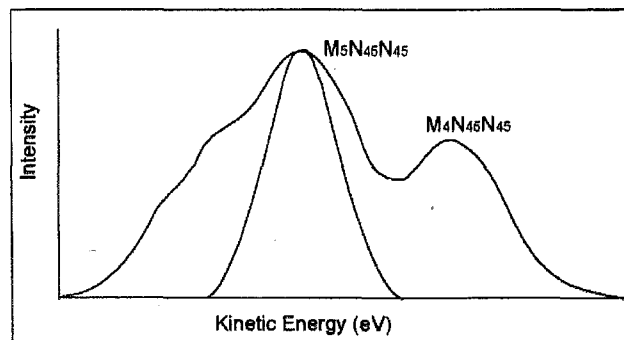


Figure 1.6 Auger curve from a 4d metal, which appears to be mainly, formed from the sum of two basic 2-hole Auger processes $M_5-N_{45}N_{45}$ (shown as the Gaussian curve under the full curve) and $M_4-N_{45}N_{45}$. This diagram makes many assumptions – there is no interaction between the holes made in the valence band and there is no multiplet splitting of the energy levels.

In an isolated atom where all electron energy levels are sharply defined and many-bodied effects are ignored, the basic Auger process between a core and valence level produces a symmetric distribution of electron energies about a single peak position (symmetrical curve Figure 1.6). This simplistic

explanation ignores the effect of Coulomb interaction between holes in the valence band, which will be dealt with in the chapter on Cini-Sawatzky theory.

The competition between fluorescence and Auger electron release changes with atomic number and is also dependent on the energy level of the initial photoionisation. Figure 1.7 plots the fluorescence yield as determined by McGuire and Fink against atomic number ([9-11] as cited in [12]). If the assumption is made that the atom relaxes after core-hole ionisation by either emitting a photon or an Auger electron then the Auger electron yield is the complement of the fluorescence yield. For Palladium and Tin ($Z = 46, 50$) with an initial ionisation in the M shell the probability of Auger decay is 100%.

Figure 1.7 has been removed for copyright purposes

The initial state of the Auger process is the final state of the photoelectron process. At this point the atom can be in a number of states depending on which energy level the photoelectron was ejected from. The final Auger process between these energy levels and an idealised discrete valence level of the isolated atom would produce a set of peaks with the same energy separation as the core energy levels e.g. $M_4N_{45}N_{45}$ and $M_5N_{45}N_{45}$ have the same energy separation as the $3d_{3/2}$ and $3d_{5/2}$ energy levels.

Each Auger transition could have several final states determined by quantum number selection rules [13]. The energy of the Auger electrons produced from the same initial state but ending with the atom in different final states would not differ greatly. The peaks in the Auger spectrum resulting from each of these transitions would overlap and sum to form the final Auger peak for that initial state. This would be described as an atomic-like spectrum with multiplet splitting.

Once an atom becomes part of a solid the surrounding atoms may influence its outer energy levels. In metallic bonding the influence of the surrounding atoms creates a continuum of energy levels in the valence level now called a band. An Auger electron released from this valence band could take on a range of energies determined by the width of the band (Figure 1.8), the initial occupancy of the band and the Coulomb force between the holes in the

band. This is discussed in greater depth in the chapter on the Cini-Sawatzky theory.

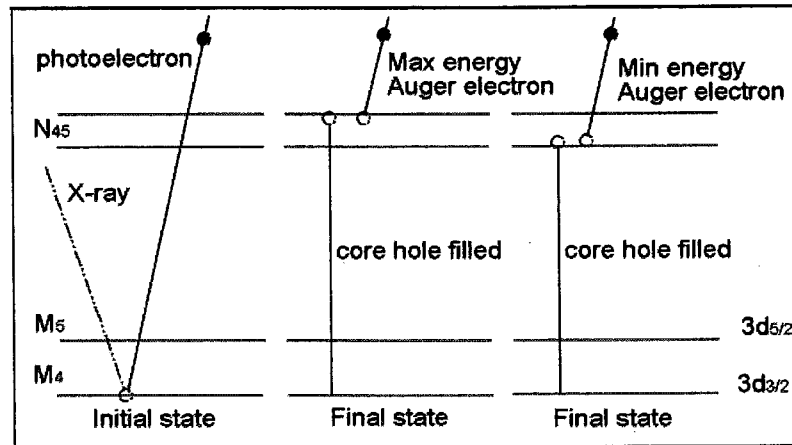


Figure 1.8 Basic Auger process involving the valence band and demonstrating the situations that produce maximum and minimum Auger electron energies.

The binding energy of the electrons in the ion after the initial photoionisation may not be the same as those of the neutral atom because the imbalance of charge within the atom may pull the outer electrons closer to the nucleus. This results in higher binding energies for the remaining electrons and the effect is called atomic relaxation. The nearest neighbours of the atom in a solid may also feel the effects of this changing potential producing extra-atomic relaxation [13]. Equation 1.2 gives the energy relationship between these processes.

The rate with which the atom and surrounding atoms relax can have an effect on the final kinetic energy of the Auger electron. The Auger electron will receive the most energy if the atom and surrounding atoms do not relax after

photoionisation and before the Auger electron is emitted. It will receive the least energy if relaxation has occurred fully.

$$\Delta E_{\text{atom}} + \Delta E_{\text{surround atoms}} + (E_{\text{b valence-e}} - E_{\text{b core-e}}) = E_{\text{K A-e}} - E_{\text{b valence-em}} \quad \text{(Equation 1.2)}$$

Where

ΔE_{atom}	is the change in energy of the atom due to relaxation
$\Delta E_{\text{surround atoms}}$	is the change in energy of the surrounding atoms due to relaxation
$E_{\text{b valence-e}} - E_{\text{b core-e}}$	is the difference in binding energy between valence and core level
$E_{\text{K A-e}}$	is the kinetic energy of the Auger electron
$E_{\text{b valence-e}}$	is the binding energy of a valence electron

Simple Auger processes involving core electrons occur within 10^{-15} s [8]. The energy released as the atom relaxes can be given to the surrounding atoms, atomic lattice, electron sea (in which case the energy is lost to the atom and its electrons), outer electrons within the same atom (see section on shake-up/off processes) or the Auger electron. If the energy is given to the Auger electron then the situation is indistinguishable from the Auger electron being released from the unrelaxed atom.

If the release of the Auger electron is assumed to take place from a fully relaxed atom then there is no correlation between the energy of the photoelectron and the Auger electron and the Auger process can be considered a two-step process. This is not always the case. The energy of two or more electrons released may be linked if the processes happen fast enough (core hole lifetime is short compared to the electronic relaxation time) and the ejected electrons travel slowly enough (near threshold ionisation

energy) [8]. Equation 1.3 combines Equation 1.1 and 1.2 however this is still not the full picture as one other assumption has been made here i.e. the energy released during the relaxation of the atom is lost to the system. The case where this assumption does not hold is dealt with in a later section.

$$E_{\text{photon}} = E_{k_{p-e}} + E_{k_{A-e}} - \Delta E_{\text{atom}} - \Delta E_{\text{surround atoms}} - 2E_{b_{\text{valence-e}}} \quad \text{(Equation 1.3)}$$

Where

E_{photon}	is the energy of the incident photon
$E_{k_{p-e}}$	is the kinetic energy of the photoelectron
$E_{k_{A-e}}$	is the kinetic energy of the Auger electron
ΔE_{atom}	is the change in energy of the atom due to relaxation
$\Delta E_{\text{surround atoms}}$	is the change in energy of the surrounding atoms due to relaxation
$E_{b_{\text{valence-e}}}$	is the binding energy of a valence electron

Examining Equation 1.3 may lead one to believe that a slight difference in the energy of the photon could cause changes in the energy of the Auger electron. The energy of the Auger electron however depends on the energy of the system at or shortly after the initial ionisation as can be seen in Equation 1.2 and it will be unaffected by changes in the photon energy. The photoelectron energy will change to accommodate the photon energy changes as indicated by Equation 1.1.

Equation 1.3 is however a useful tool for understanding the Auger process. When using a monochromatic photon source, Equation 1.3 indicates that photoelectrons of lower than average kinetic energy would produce Auger electrons of higher than average kinetic energy as demonstrated by Jensen [14].

We have looked at the composition of the Auger peak associated with the basic Auger process and how that differs with the electronic structure of the atoms and even the nearest neighbour atoms. We have also seen conservation of energy operating on the atomic scale and how AES is extremely sensitive to the electronic environment of the surface of the material. In all cases the Auger peak may have changed shape a little and even moved a few eV but the intensity has remained together under one peak. The following sections will discuss the processes whereby intensity can be shifted to other areas of the electron energy spectrum.

1.3.2. Auger plasmon gain peaks

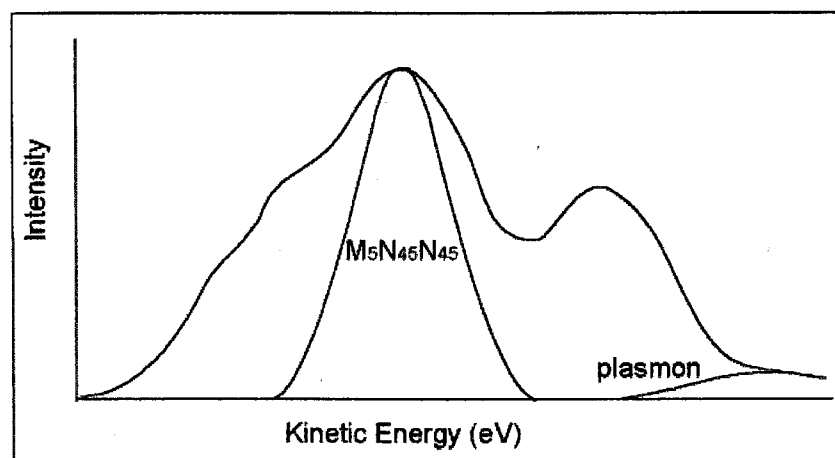


Figure 1.9 Auger plasmon gain satellite peak with primary peak.

Photoelectrons may lose energy as they leave the metal because they produce plasmons. The following Auger electron may then gain this energy from the electron gas as it leaves, effectively increasing its kinetic energy.

Plasmon gain peaks although unusual may be found on the high kinetic energy side of the Auger peak at characteristic distances from the peak (Figure 1.9). The corresponding XPS spectrum would show plasmon loss peaks [15].

1.3.3. Auger plasmon loss peaks

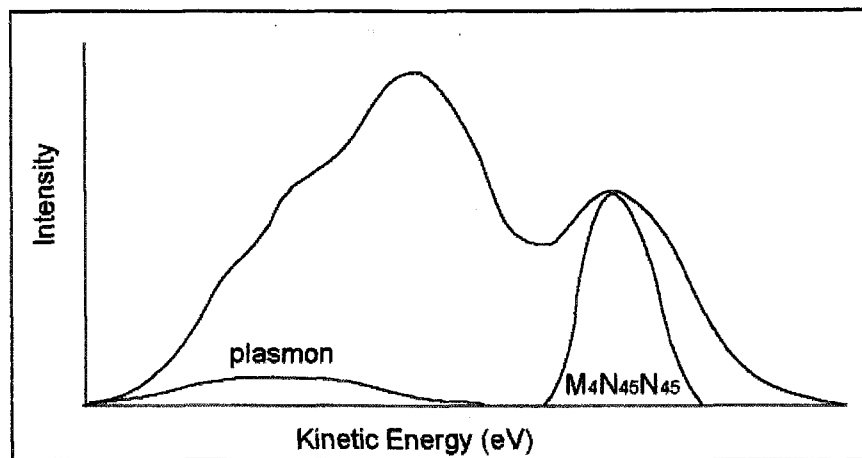


Figure 1.10 Auger plasmon loss satellite peak with main peak.

Equally spaced peaks, which decrease in intensity with distance from the main peak, may be found on the low kinetic energy side of an Auger peak Figure 1.10. The spacing of these peaks is characteristic of the metal being investigated and the energy loss from the Auger electrons is due to excitation of the electron gas (plasmon formation) by the Auger electron as it leaves the metal. For example the plasmon peak for Tin has a FWHM, which is twice that of the parent peak, its intensity is about 10% and it is shifted 14.6 eV to lower kinetic energies [16]. Plasmon formation can be in either the bulk or

surface of the metal and the spacing of the peaks is different for each case [17].

1.3.4. Auger 3-hole processes

1.3.4.1. Coster-Kronig process

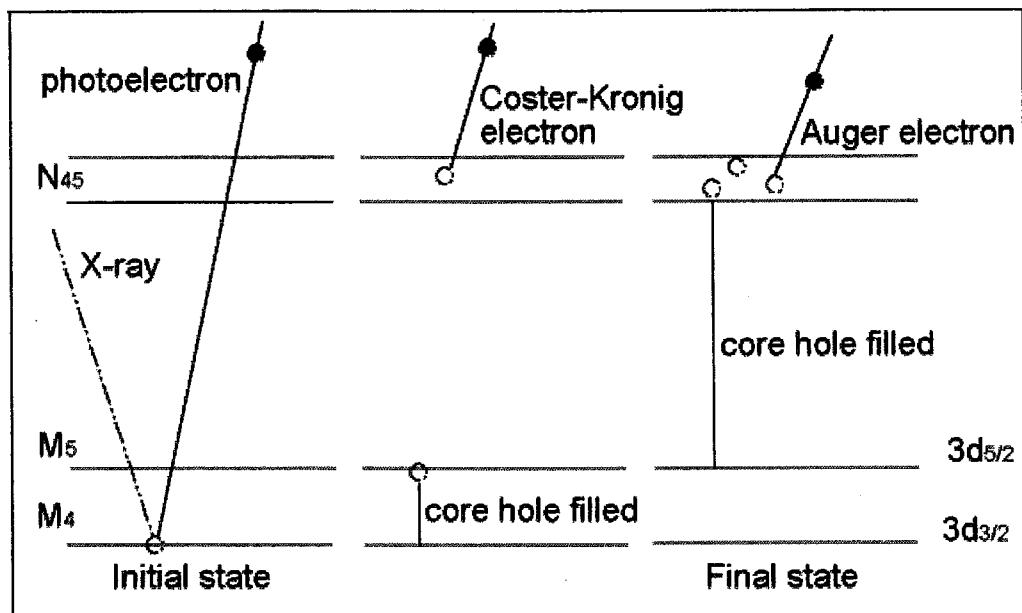


Figure 1.11 Coster-Kronig process. Photoionisation of inner core level. Core hole filled by an electron from a higher energy level with the same principle quantum number. The energy produced releases a Coster-Kronig electron from an outer orbital. Normal Auger process occurs in the presence of this spectator hole.

In the processes first described by D. Coster and R. de L. Kronig in 1935 [18] an initial photoionisation takes place in an inner core energy level and an electron from a higher energy level with the same principle quantum number drops down to fill the hole. This releases just enough energy to free a slow moving Coster-Kronig electron from an outer orbital, usually the valence band. The normal Auger process then occurs in the presence of this

spectator hole (Figure 1.11) and the Coster-Kronig electron adds intensity to the background at the low kinetic energy end of the electron emission spectrum. The spectator hole has little chance of moving out of the valence band into the conduction band before the Auger electron is emitted as the Coster-Kronig transition rate is usually large due to the overlap between the two inner orbitals [13].

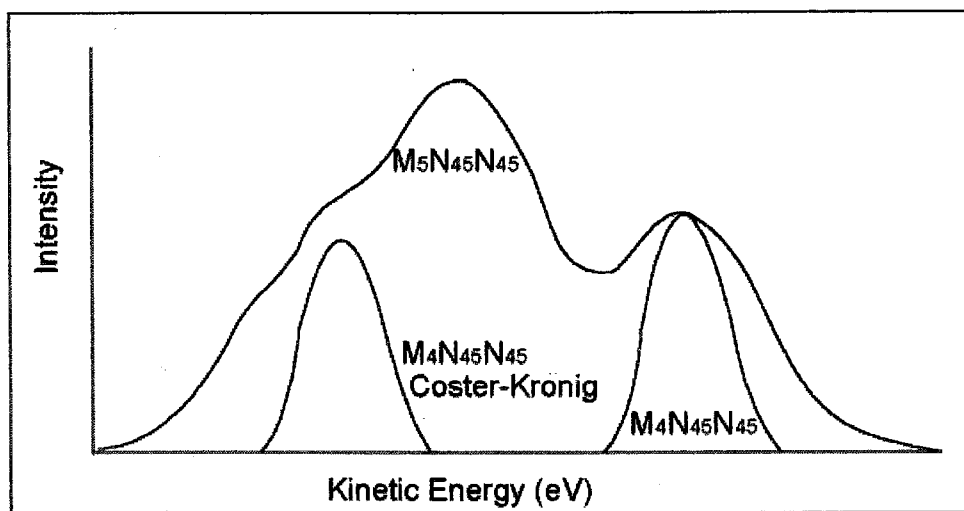


Figure 1.12 Auger spectrum showing the $M_4N_{45}N_{45}$ 2-hole Auger peak and its low kinetic energy Coster-Kronig satellite peak.

The effect of the Coster-Kronig process on the Auger spectrum can be dramatic. Intensity is moved from one Auger peak to another. If the $3d_{3/2}$ and the $3d_{5/2}$ are the two core energy levels involved in the Coster-Kronig transition then the initial ionisation takes place in the $3d_{3/2}$ energy level but the final Auger process occurs between the valence band and the $3d_{5/2}$ energy level. This places intensity in a low kinetic energy shoulder of the $M_5N_{45}N_{45}$ Auger peak (Figure 1.12). The simple 2-hole Auger process would

have placed intensity in the $M_4N_{45}N_{45}$ Auger peak. Intensity has effectively been shifted from the $M_4N_{45}N_{45}$ peak to a satellite peak in the same energy range as the $M_5N_{45}N_{45}$ peak.

There are several possible reasons why the Coster-Kronig satellite peak is on the low kinetic energy shoulder of the $M_5N_{45}N_{45}$ Auger peak instead of directly under the main intensity of the peak.

- The spectator hole changes the intra-atomic relaxation energy i.e. the positive potential of the atom is increased and more energy is needed to overcome this potential as the Auger electron escapes.
- The spectator hole changes the intra-atomic relaxation energy and an energy level is pulled below the valence band. If the Auger electron originates from this energy level then the peak will be atomic-like and on the low side of the $M_5N_{45}N_{45}$ peak because the energy difference between the core and valence levels in the final Auger process is reduced [19].
- The spectator hole in the valence band increases the effective hole-hole interaction energy (see Cini-Sawatzky chapter), which results in the peak moving to lower kinetic energies and becoming more atomic-like [20].
- The spectator hole changes the inter-atomic relaxation energy reducing the energy available to the atom and its electrons.

In using Auger spectra for any quantitative work it is therefore necessary to determine the area under the whole of the $M_{45}N_{45}N_{45}$ (or $L_{23}M_{45}M_{45}$) Auger peak, in order to account for any intensity that has been shifted from one part of the curve to another by the Coster-Kronig process. Information about the probability of the decay channels taken when the core hole is filled can be determined from the ratio of the 3-hole Coster-Kronig peak height, to the 2-hole Auger peak height, in the coincidence data from the same photoionisation. In Palladium this ratio was 1.45:1.00 and in Tin it was 0.30:1.00 indicating the Coster-Kronig process plays a larger part in the creation of the Auger lineshape in Palladium than it does in Tin.

The Coster-Kronig process can only happen if the difference in the binding energy of the core levels involved is greater than the binding energy of the valence electron. So the probability of the Coster-Kronig process varies across the periodic table as the energy levels of the atoms vary. If the whole Coster-Kronig and Auger process is limited to energy levels within the same principle quantum number then this is called a super Coster-Kronig process [9].

An indication of a possible Coster-Kronig process can be given by a difference in the FWHM of photoelectron lines from the same principal quantum number. Broadening of one indicates that the hole in the core level has extra decay paths or in other words a shorter core hole lifetime. If the X-

ray fluorescence for this line has a lower intensity than expected from its electron occupancy then a radiation-less decay process is indicated ie. the Coster-Kronig proceeded Auger process [9].

The relationship between the FWHM of a XPS line, the total transition rate (θ) and the core hole lifetime (τ) is given by McGuire [9] in Equation 1.4

$$\tau = 1 / \theta \quad \text{(Equation 1.4)}$$

$$\text{FWHM} = (h/2\pi) / \tau$$

$$\text{FWHM} = (h/2\pi) (\theta)$$

Where

- τ is the core hole lifetime
 - θ is the total transition rate
 - h is Planck's constant
-

The total transition rate depends on the sum of the Auger, Coster-Kronig and radiative transition rates. Eugene J. McGuire has calculated the Auger, Coster-Kronig and total transition rates for initial L and M shell initiated processes in elements with atomic numbers 18 to 90 [21-23].

Kochur et. al. have done some interesting work calculating the ion yield produced by the cascade decay of initial core holes using the construction of de-excitation trees [24, 25]. They include every possible pathway of decay in their calculations to produce branching ratios for each process. From these ratios the total Coster-Kronig, Auger and radiative yield can be determined

for initial holes in each energy level. So far they have studied Xenon, Neon, Argon, Krypton and Europium.

AES cannot differentiate between a basic 2-hole Auger process and a 3-hole Coster-Kronig process that places intensity in the same region of the Auger spectrum even though the two processes originated in different energy levels. As will be shown in a later section APECS can separate these overlapping peaks.

1.3.4.2. *Initial-state shake process*

The speed with which an atom relaxes compared to the lifetime of the initial core hole can influence the shape of both the XPS and AES spectrum. If the core-hole lifetime is long and the photoelectron is slow then the sudden approximation theory is not valid [13]. The emission of the photoelectron and relaxation of the energy levels may occur at the same time causing excitation of an outer electron to energy levels above the Fermi level as in the initial-state shake-up process (Figure 1.13). The electron may even escape to the continuum as in the initial-state shake-off process (Figure 1.14). The energy sharing by shake-up electrons may rob the photoelectron of discrete amounts of energy related to the discrete energy level transitions the shake-up electron is permitted to make. In the shake-off process the photoelectron could have its kinetic energy reduced by a variable amount dependant on the kinetic energy of the shake-off electron.

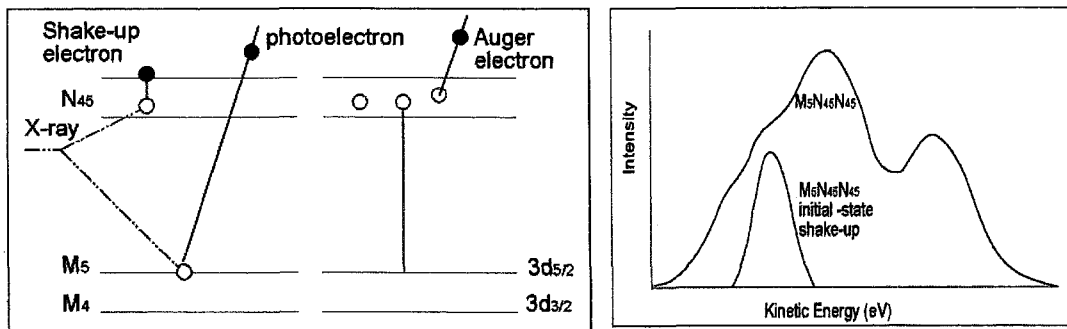


Figure 1.13 Initial-state shake-up process and resulting position of the satellite peak in the Auger spectrum. The shake-up electron is excited to higher levels within the valence band by the incident X-ray. This robs the photoelectron of discrete amounts of energy. The spectator hole in the valence band at the time of the Auger electron's release shifts the Auger peak to a lower kinetic energy.

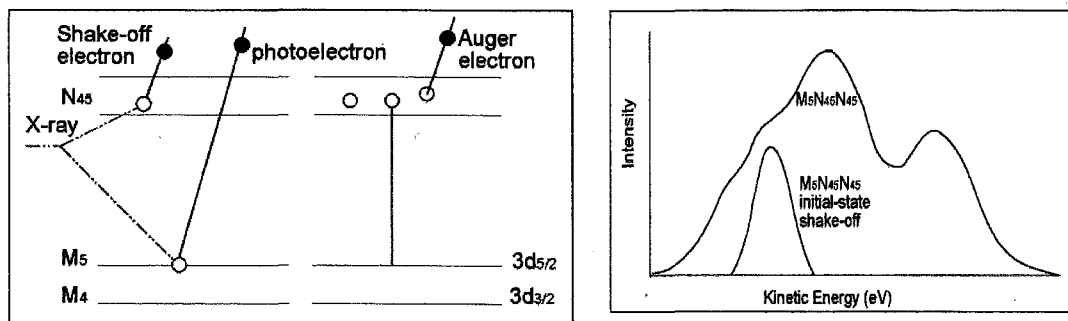


Figure 1.14 Initial-state shake-off process and resulting intensity of the initial-state shake-off satellite peak in the Auger spectrum. The end result is the same for the Auger spectrum but the photoelectron energy is reduced by a variable amount instead of discrete amounts.

The effect on the Auger spectrum will depend on how long the hole left by the shake electron persists in the outer energy level before it is filled by an electron from the conduction band (another way of looking at it is that the hole migrates to the conduction band). If this spectator hole is still present as the Auger electron leaves then intensity will be placed on the low kinetic

energy shoulder of the Auger peak. For valence electrons in isolated atoms shake-up and shake-off processes have approximately equal probability [26].

1.3.4.3. Final-state shake processes

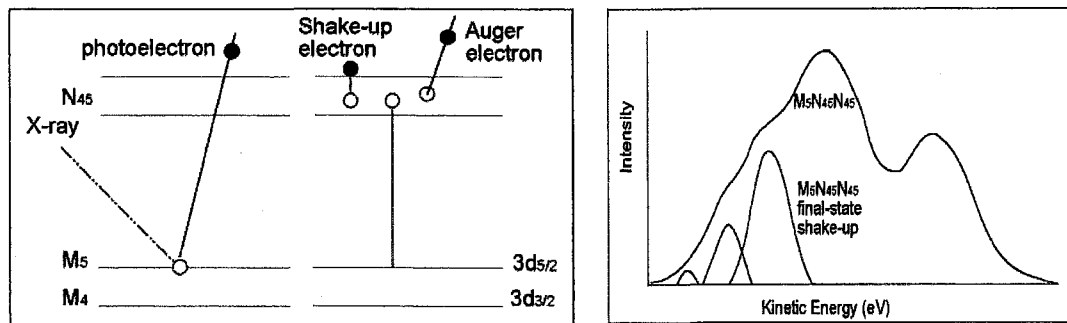


Figure 1.15 Final-state shake-up process and position of final-state shake-up satellite peaks in the Auger spectrum. The energy shift of the peaks is determined by the energy level to which the shake electron is raised.

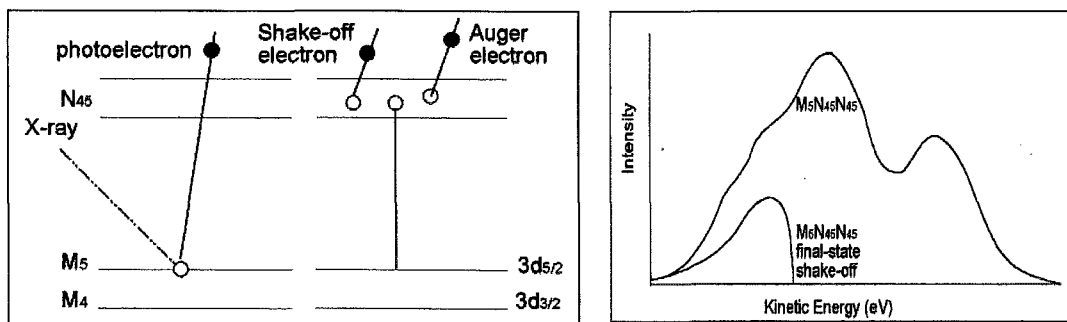


Figure 1.16 Final-state shake-off process and position of the final-state shake-off satellite peak. The maximum energy is the maximum energy of the Auger electron less the binding energy of the shake-off electron. There is only one peak, which gradually decreases in intensity with energy because the shake-off electron may remove a variable amount of energy from the Auger electron.

Similar shake processes due to incomplete relaxation of the atom can happen as energy is transferred to the Auger electron. A final-state shake-up electron will rob the Auger electron of discrete amounts of energy producing

discrete energy peaks on the low kinetic energy side of the main Auger peak (Figure 1.15) and a final-state shake-off electron will rob the Auger electron of a variable amount of energy (Figure 1.16). As these events take place in the final stage of the Auger process the photoelectron peak should not be affected.

1.3.5. Process notation

Several attempts have been made to create notation for the processes discussed so far in this section and it is worth noting a few here (Table 1.2). A more comprehensive table is given in Appendix ii. For reasons of clarity the simplified descriptive notation (N) will be used in place of N_{45} for the remainder of this thesis but other energy levels will retain their subscripts to avoid confusion. The full process notation will be used when specific processes are referred to.

Table 1.2 Notation for Possible Decay Processes

Process	Process notation	Descriptive notation	
Basic Auger	$M_4 - N_{45}N_{45}$	$M_4N_{45}N_{45}$	M_4NN
Coster-Kronig	$M_4-M_5N_{45} - N_{45}N_{45}(N_{45})$	$M_4-M_5N_{45}N_{45}(N_{45})$	$M_4:M_5^{CK}NNN$
Initial-state shake	$M_4N_{45} - N_{45}N_{45}(N_{45})$	$M_4N_{45}N_{45}(N_{45})$	$M_4^{is}NNN$
Final-state shake	$M_4 - N_{45}N_{45}N_{45}$	$M_4N_{45}N_{45}(N_{45})$	$M_4^{fs}NNN$
The bracketed holes in the process notation indicate the spectator holes created before the final Auger electron release. The bracketed holes in the descriptive notation indicate the spectrum is shifted to the 3-hole position of the respective Auger peak.			

1.3.6.4-hole and other cascade processes

It is possible that there are combinations of the above processes that result in four or even five additional holes in the valence band. It is not possible with the Murdoch APECS experiment at this stage to distinguish between them so individual description will be left to others. Cascade processes start with the ionisation of a core level very close to the nucleus which is then filled by an electron from a core level slightly further out, which in turn are filled by others yet further out. Each energy transition is accompanied by the release of either a photon or an electron. Photons are more likely from the inner energy level transitions and electrons from the outer energy level transitions [26]. A final Auger decay places intensity in the Auger spectrum related to the last transition and the history of the holes from previous transitions is lost.

1.3.7. Other Factors that Complicate the Auger Spectrum

1.3.7.1. *Band-to-band transitions*

If the kinetic energy of an emitted photoelectron or Auger electron from atom 'A' is large enough it could collide with another atom 'B' causing ionisation within that atom. The energy of the released photoelectron would be the energy of the initiating photoelectron or Auger electron from atom 'A' less the binding energy of the electron released from atom 'B' less the kinetic energy that the electron from atom 'A' retains after the collision. The two electrons would become part of the background intensity but any subsequent Auger

transition in atom 'B' would place intensity in the Auger peak of atom 'B'. This indirect intensity in the Auger peak of atom 'B' cannot be separated from intensity arising from internal processes within atom 'B' using AES. The indirect intensity can be removed using APECS because the final Auger electron is not linked to a photoelectron of proscribed energy from the same atom.

1.3.7.2. Overlapping lines

One of the reasons for studying Auger spectra was because sometimes XPS spectra have overlapping lines from different elements. The same situation occurs in the Auger spectrum and it is impossible to tell what percentage of the intensity of the Auger peak is due to which material. APECS is able to deal with this situation by selecting only the intensity in the Auger peak related to the specific element under investigation.

1.3.7.3. Chemical and other environmental effects

Changes to the surface potential of a metal either intentional by alloying or unintentional by oxidation; adsorption of carbon or other contaminants; electronic charge build up on the surface or changes in the topology, may all cause changes in the energy levels of the atom and hence the Auger and photoelectron spectra. These changes are seen as shifts in the photoelectron line and Auger peak position and changes in shape of the Auger peak.

The amount the atom relaxes after ionisation may also be determined by the chemical environment and even how the surrounding atoms react to the ionisation of the atom may change. While the energy shift in the XPS line and AES peaks are related to the movement of the energy levels of the atom the respective shifts are not the same. A shift of a core level and valence band towards the nucleus would result in the XPS line shifting to lower kinetic energy by the same amount as the core level. The Auger peak however would shift to lower kinetic energies by twice the change in the difference between the valence level and the core level.

The chemical environment may change the energy levels to such an extent that the probability of shake-up/off processes and even Coster-Kronig processes is changed. They may be allowable (turned on) when normally they are not (turned off) and vice versa [27]. If this happens in the photoelectron line or Auger peak being investigated, a change will be observed in the lineshape of that peak. If it happens in peaks other than the one under investigation then changes may be seen in the background intensity due to the shake-off and Coster-Kronig electrons produced. Chemical changes may also cause energy levels to pull free of the valence band changing the Auger spectrum from band-like to atomic-like (see Chapter on Cini-Sawatzky Theory).

Other ways chemical changes may affect the environment are by changing the work function of the material, changing the surface density of the atoms or changing the depth of the atoms under investigation. These changes will affect the background and intensity of both the XPS and AES spectrum (see the Chapter on Background Subtraction).

1.3.7.4. *Transitions between atoms*

It is possible for two atoms to participate in the photoelectron to Auger electron decay process. Electrons from the outer orbitals of one atom have been known to fill the core holes of another atom if the bonds between the two atoms are strong enough [28]. Transitions between atoms have also been noted between second layer and surface layer Ta atoms by Bartinski et al. [29]. Figure 1.17 presents some of the possible transitions they proposed. In the first case the core hole left by the photoelectron is filled by a valence electron from the same atom but the energy released allows an outer electron from a surface atom to escape. The second case involves "hole-hopping". An electron from a core energy level of a surface atom fills the initial core hole. The surface atom then undergoes Auger decay. Hole-hopping is also evident in the final situation. An electron from the same atom fills the initial core hole and the energy released excites a core electron in a surface atom to a shake-up position. This is the equivalent of the hole hopping from one valence band to another. This surface atom then undergoes Auger decay.

If the donating atom is different to the accepting atom the energy released by the transition may / may not result in the release of an Auger electron. Any Auger electron released under these conditions would not be part of the characteristic energy spectrum of either of the participating atoms. It would contribute to background intensity unless this type of transition was significant, in which case a new Auger peak would be formed [29].

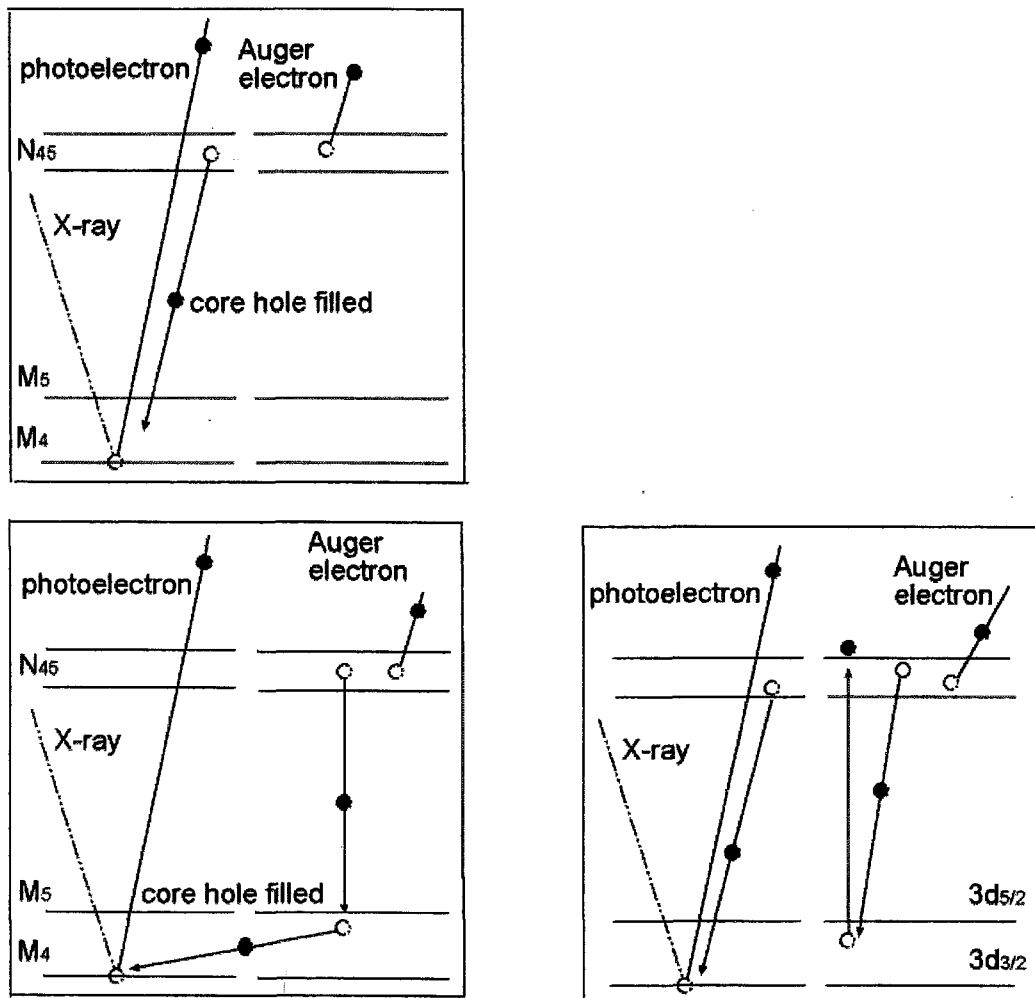


Figure 1.17 Hypothetical electronic transition between atoms

While the Auger peak can give a qualitative representation of the elements on the surface of a metal it is difficult to get a precise quantitative value for elemental concentrations. This is due to the number of processes, all originating with the same photoionisation, which place intensity in different parts of the Auger peak. Selecting corresponding parts of the Auger peak on different materials cannot guarantee the same Auger process is being selected for each material. If the area under the peak is used for analysis then it is not possible to know if intensity has been moved from the primary peak by any of the processes listed above. Until we know such things as "multiply the area under the M_{4NN} peak by δ to allow for the energy lost due to Coster-Kronig processes" then it will be difficult to use AES for quantitative analysis.

-
1. Tanuma, S., C.J. Powell, and D.R. Penn, *Calculations of Electron Inelastic Mean Free Paths (IMFPS) VI. Analysis of the Gries Inelastic Scattering Model and Predictive IMFP Equation*. Surface and Interface Analysis, 1997. **25**(1): p. 25 - 35.
 2. Tanuma, S., C.J. Powell, and D.R. Penn, *Calculations of Electron Inelastic Mean Free Paths for 31 Materials*. Surface and Interface Analysis, 1988. **11**: p. 577 - 589.
 3. Tanuma, S., C.J. Powell, and D.R. Penn, *Calculations of Electron Inelastic Mean Free Paths II. Data for 27 Elements Over the 50-2000 eV Range*. Surface and Interface Analysis, 1991. **17**: p. 911 - 926.
 4. Tanuma, S., C.J. Powell, and D.R. Penn, *Electron mean-Free-Path Calculations Using a Model Dielectric Function*. Surface and Interface Analysis, 1991. **17**(13): p. 927 - 939.
 5. Tanuma, S., C.J. Powell, and D.R. Penn, *Calculations of Electron Inelastic Mean Free Paths (IMFPS). IV. Evaluation of Calculated*

- IMFPs and of the Predictive IMFP Formula TPP-2 for Electron Energies Between 50 and 2000eV. Surface and Interface Analysis, 1993. 20(1): p. 77 - 89.*
6. Tanuma, S., C.J. Powell, and D.R. Penn, *Calculations of Electron Inelastic Mean Free paths V. Data for 14 Organic Compounds over the 50 - 2000eV Range. Surface and Interface Analysis, 1993. 21: p. 165 - 176.*
 7. Tanuma, S., C.J. Powell, and D.R. Penn, *Calculations of Electron Inelastic Mean Free Paths. V. Data for 14 Organic Compounds Over the 50 - 2000eV Range. Surface and Interface Analysis, 1994. 21(3): p. 165 - 176.*
 8. Haak, H.W., *Auger Photoelectron Coincidence Spectroscopy - A Study of Correlation Effects in Solids. 1983, University of Groningen: Groningen.*
 9. McGuire, E.J., *Atomic M-shell Coster-Kronig, Auger, and Radiative Rates, and Fluorescence Yields for Ca-Th. Physical Review A, 1972. 5(3): p. 1043 - 1047.*
 10. McGuire, E.J., *Atomic L-Shell Coster-Kronig, Auger, and Radiative Rates and Fluorescence Yields for Sodium-Thorium. Physical Review A, 1971. 3: p. 587 - 594.*
 11. Fink, R. W., R. C. Jopson, H. Mark and C. D. Swift, *Review of Modern Physics, 1966. 38(3): p. 513 - 540.*
 12. Tracy, J.C., *Auger Electron Spectroscopy for Surface Analysis, in Electron Emission Spectroscopy, L.F. W. Dekeyser, G. Vanderkelen, J. Vennik, Editor. 1972, D. Reidel Publishing Co.: Dordrecht, Boston. p. 313 - 315.*
 13. Weightman, P., *X-ray Excited Auger and Photoelectron Spectroscopy, in Report on Progress in Physics. 1982, The Institute of Physics. p. 753 - 814.*
 14. Jensen, E., et al., *Auger Photoelectron Coincidence Spectroscopy Using Synchrotron Radiation. Review of Scientific Instrumentation, 1992. 63(5): p. 3013 - 3026.*
 15. Fuggle, J.C., et al., *Plasmon Gains as a Monitor of Incomplete Relaxation, Interference Effects, and the Transition from Sudden to*

Adiabatic Limits in Electron Spectroscopies. Physical Review Letters, 1980. **44**(16): p. 1090 - 1093.

16. Parry-Jones, A.C., P. Weightman, and P.T. Andrews, *The $M_{4,5}N_{4,5}N_{4,5}$ Auger Spectra of Ag, Cd, In and Sn*. Journal of Physics C: Solid State Physics, 1979. **12**: p. 1587 - 1600.
17. Lund, C.P. and S.M. Thurgate, *Auger Photoelectron Coincidence Studies of the Intrinsic and Extrinsic Processes in the Ga $L_{23}M_{45}M_{45}$ Auger Line of GaAs*. Physical Review B, 1994. **50**: p. 17166 - 17171.
18. Coster, D. and R.D.L. Kronig, *A New Type of Auger Effect and its Influence on the X-ray Spectrum*. Physica, 1935. **2**: p. 13 - 24.
19. Thurgate, S.M., *Auger Spectroscopy and Surface Analysis*. Australian Journal of Physics, 1997. **50**: p. 745 - 757.
20. Thurgate, S.M., *Auger Photoelectron Coincidence Experiments from Solids*. Journal of Electron Spectroscopy and Related Phenomena, 1996. **81**: p. 1 - 31.
21. McGuire, E.J., *Atomic L-Shell Coster-Kronig, Auger, and Radiative Rates and Fluorescence Yields for Sodium-Thorium*. Physical Review A, 1971. **3**(2): p. 587 - 594.
22. McGuire, E.J., *L-Shell Auger and Coster-Kronig Electron Spectra*. Physical Review A, 1971. **3**(6): p. 1801 - 1810.
23. McGuire, E.J., *M-Shell Auger and Coster-Kronig Electron Spectra*. Physical Review A, 1972. **5**(3): p. 1052 - 1059.
24. Kochur, A.G., et al., *Direct Hartree-Fock Calculation of Multiple Xe^{i+} Ion Production Through Inner Shell Vacancy De-excitations*. Journal of Physics B: Atomic, Molecular and Optical Physics, 1994. **27**: p. 1709 - 1721.
25. Kochur, A.G. and V.L. Sukhorukov, *Low-Energy Auger Spectra of Xenon Emitted by Vacancy Cascades Following Inner-Shell Ionisations*. Journal of Physics B: Atomic, Molecular and Optical Physics, 1996. **29**: p. 3587 - 3598.
26. Carlson, T.A., *The Nature of Secondary Electrons Created as the Result of Electron Shake-off and Vacancy Cascades*. Radiation Research, 1975. **64**: p. 53 - 69.

27. Antonides, E. and G.A. Sawatzky., *The $L_2L_3M_{45}$ Coster-Kronig Process in Zn and ZnO in the Solid State*. Journal of Physics C: Solid State Physics, 1976. 9: p. L547 - L552.
28. Fuggle, J.C., *High Resolution Auger Spectroscopy of Solids and Surfaces*, in *Electron Spectroscopy: Theory, Techniques and Applications*, A.D.B. C. R. Brundle, Editor. 1981, Academic Press: London, New York, Toronto, Sydney, San Francisco. p. 102 - 105.
29. Bartinski, R.A., et al., *Surface Electronic Structure and Off-Site Auger transitions on TaC(111) Observed with Auger-Photoelectron Coincidence Spectroscopy*. Physical Review Letters, 1992. 68(14): p. 2247 - 2250.

Chapter 2

Cini-Sawatzky Theory and the Auger Lineshape

Figure 2.1 has been removed for copyright purposes

Figure 2.1 Generic figure showing the density of electron states near the Fermi energy. Assuming every transition between valence band and core hole is allowed and an electron may fill the core hole from any of the positions a-i. Also assume the transition probabilities are the same for each transition then the relative distribution of the transitions is determined by the DOS. The Auger electron can leave the valence band from any position r-z. If all transition probabilities are the same then the DOS determines the relative distribution of the Auger electrons. So for each possible transition that fills the core hole (set probability) there are a full range of Auger emissions with their own probabilities. The convolution of the valence band with itself therefore presents a first approximation to the shape of the Auger peak.

The shape of the Auger spectrum for atoms in a solid has been under theoretical consideration since 1953, when Lander [1] postulated that the shape and intensity of the spectrum would be determined by the self-convolution of the one-electron density of states (DOS) of the valence band (see Figure 2.1). This would produce an Auger spectrum for each

Auger process that was twice as wide as the valence band (Figure 2.2), rounded, fairly featureless and now described as band-like.

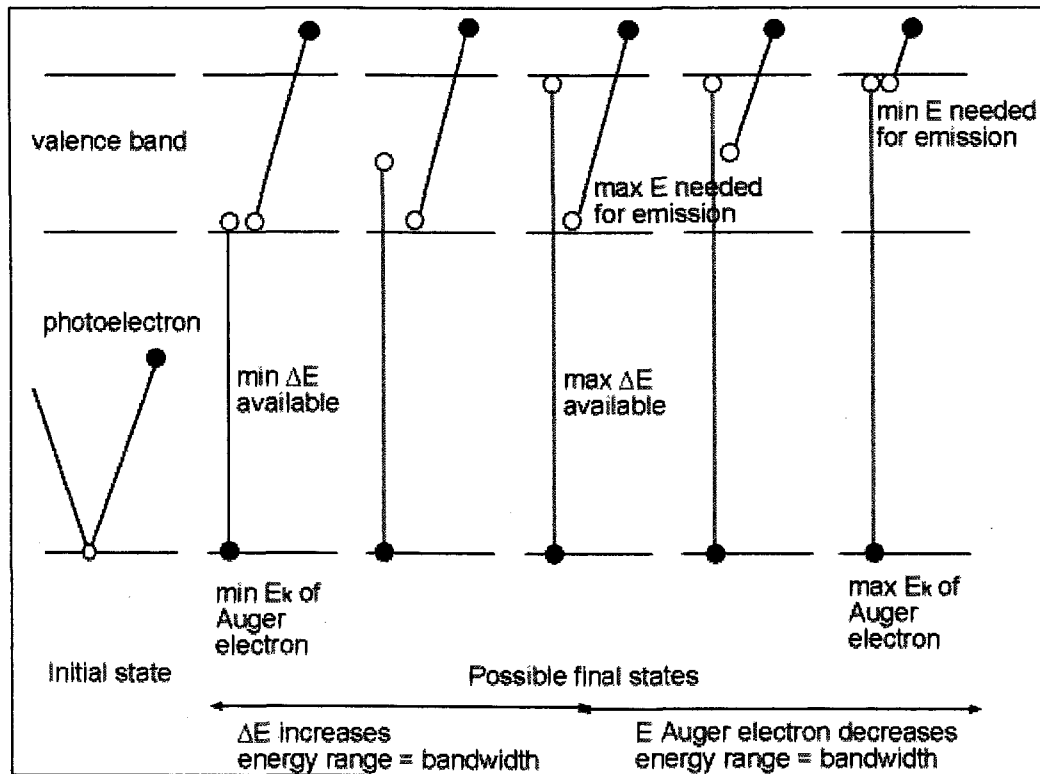


Figure 2.2 Kinetic energy range of the Auger electron in a core-valence-valence process. ΔE is the difference in binding energy between the energy levels, E is the binding energy of the Auger electron and E_k is the kinetic energy of the Auger electron.

The probability of the emission of an Auger electron with any given energy is determined by the DOS within the valence band. The DOS also determines the probability of an electron from the valence band filling the core hole. The actual DOS to be used comes into question here. Is it the DOS of: -

- an independent atom in the ground state
- an independent atom with a core hole
- an ion in a regular lattice with nearly free (whole range of energies to choose from) electron states in the conduction band

- a fully relaxed (internally within the atomic energy levels and externally between nearest neighbours) atom with a core hole
- a fully relaxed atom with a valence band hole
- a combination of the above

Mahan [2] proposed that for calculating the one-electron DOS the potential of a fully relaxed atom with a core hole should be used. Gunnarsson and Schonhammer [3] proposed that it would be more realistic if calculations of the DOS could take into account the

- response time of the screening of the core hole as the atom relaxes (inter-atomic relaxation)
- effect the core hole has on the surrounding atoms (intra-atomic relaxation)
- dynamic changes these effects would have on the Auger spectrum for differing core hole lifetimes.

This would be the ideal situation but applying these proposals to the experimental data in this work is a significant project in itself.

In the final step of the Auger process two holes are created in the valence band. If the valence bandwidth (W) is large and the holes delocalise the Auger peak is band-like and resembles the self-convolution of the DOS as proposed by Lander [1]. If however the holes remain close to the atom, then the valence band occupancy is changed as it would be in an isolated atom and the resulting Auger spectrum becomes atomic-like (Figure 2.3).

Sometimes metals, which should produce a band-like Auger spectrum, may have atomic-like qualities because the relaxation of the atom after photoionisation pulls outer energy levels below the valence band. If the final Auger decay is between this lowered energy level and the core energy level then the Auger peak will be sharp and atomic-like instead of broad and band-like.

Figures 2.3 a, b, and c have been removed for copyright purposes

Sawatzky [4] noted that the atomic-like spectra are found mainly in metals where the Auger process involves narrow d-bands. Where broad s-p bands are involved the Auger spectra appeared to be broad and band-like. The Auger process in both Palladium and Tin involve narrow d bands.

The bandwidth is not the only factor affecting the lineshape of the Auger spectrum. Cini [5] proposed that the DOS would be changed dynamically by the repulsive Coulomb interaction between the two holes formed in the valence band in the final stage of the Auger process. So the degree of change depends not only on the valence bandwidth but also on the

Coulomb interaction between the two holes (hole-hole interaction) (U). A large hole-hole interaction energy will produce a more atomic-like spectrum than a small hole-hole interaction energy for the same valence bandwidth. For narrow bands and significant hole-hole interaction energy the Auger spectrum becomes atomic-like possibly with multiplet structure [6].

A description of the effect differing values of U/W have on the Auger spectra was given by Sawatzky [4]. Auger peaks range from the completely band-like for $U/W \sim 0$ to almost atomic-like for $U/W \gg 2$. Between these two extremes Auger spectra composed of the sum of two curves can be found.

Of the two curves comprising the Auger lineshape for a single decay process one is narrow and atomic-like, the other broad based and band-like. The centroid of the atomic-like curve and the band-like are separated by approximately U [7] with the atomic-like curve being on the low kinetic energy side of the band-like curve and the width of the band-like curve being $2W$ (Figure 2.4). After the atomic-like curve has moved out of range of the band-like one ($U > W$) the intensity in the atomic-like curve will be around 90% of the total intensity [7]. So if atomic-like peaks are seen in the Auger spectrum of solids then Coulomb interaction between the two holes in the valence band (correlation effects) are important.

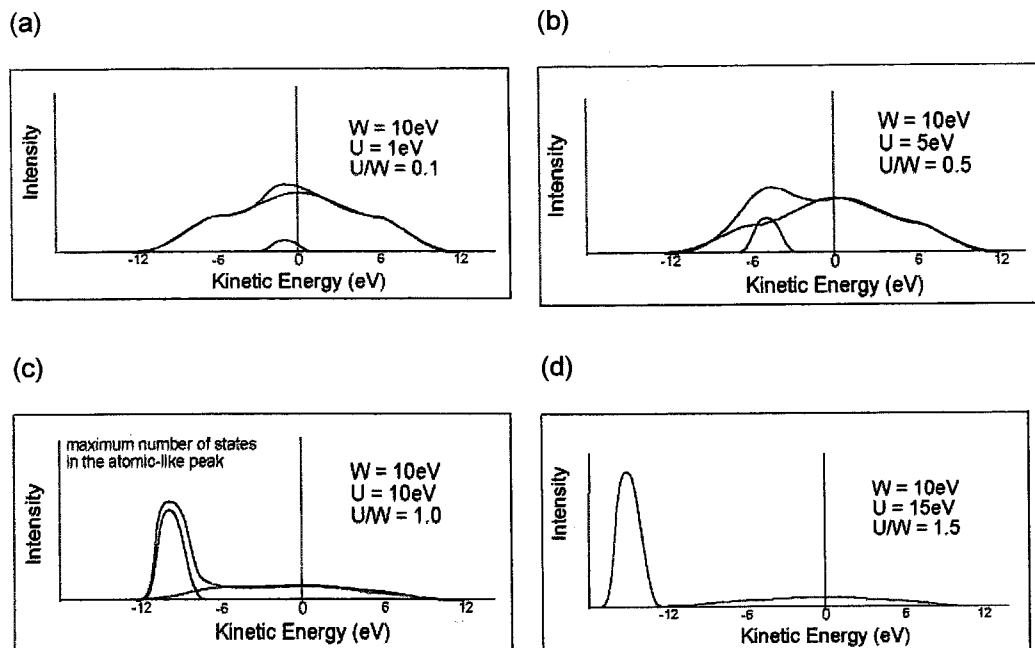


Figure 2.4 Hypothetical sketches of the band-like and atomic-like sections of the Auger spectrum. In (a) the valence band (W) is wide relative to the hole-hole interaction energy (U). Most of the intensity is in the broad low-intensity band-like peak with a small amount of intensity in the narrow atomic-like peak. The atomic-like peak is shifted to a lower kinetic energy from the centroid of the band-like peak by an amount approximately equal to U . The Auger peak is the sum of these band-like and atomic-like peaks. In (b, c and d) the ratio of U/W increases, as does the intensity in the atomic-like peak and the separation between the two peaks. In this way the Auger peak changes from band-like to atomic-like across the periodic table as the values of U and W change.

For this model to work the assumption that there is no interaction between the emitted Auger electron and the remaining ionised atom or the photoelectron was made. Instances where the sudden approximation is not valid will be discussed shortly. It has also been assumed by Cini and Sawatzky that the bands are tightly bound to the atom as a condition in the use of their particular mathematical model.

A mathematical relationship developed by Cini [8] described the effect of the hole-hole interaction energy on the shape of the Auger spectrum. It

assumed that the core energy levels and valence band of the atoms were full before the initial photoionisation and that there was no interaction between the atom and its neighbours.

$$d\sigma/d\varepsilon_k = \frac{D(\omega)}{[1-(U/W)F(\omega)]^2 + [\pi(U/W)D(\omega)]^2} \quad \text{(Equation 2.1)}$$

Where

$d\sigma/d\varepsilon_k$ is the transformed DOS at energy ω

$D(\omega)$ is the initial DOS at energy ω

U is the hole-hole interaction energy

W is the bandwidth

$$F(\omega) = P \int_{-\infty}^{+\infty} \frac{D(\omega')}{(\omega - \omega')} d\omega'$$

ω' is another energy in the initial DOS

Sawatzky and Lenselink [7] restated Cini's formula in the format given here (Equation 2.1) for an atom embedded in a cubic lattice. The atom has a tight binding s-band and initially had filled non-degenerative energy levels (no multiplet splitting). The photoelectron and Auger electron do not have any effect on the atom once they have been removed. This formula provides a numerical way of convoluting the one electron DOS and calculating the effect of the hole-hole interaction energy on the final Auger spectrum using a simple computer program. This is the mathematical model used in this thesis to probe the band structure of Palladium and Tin (Figure 2.5).

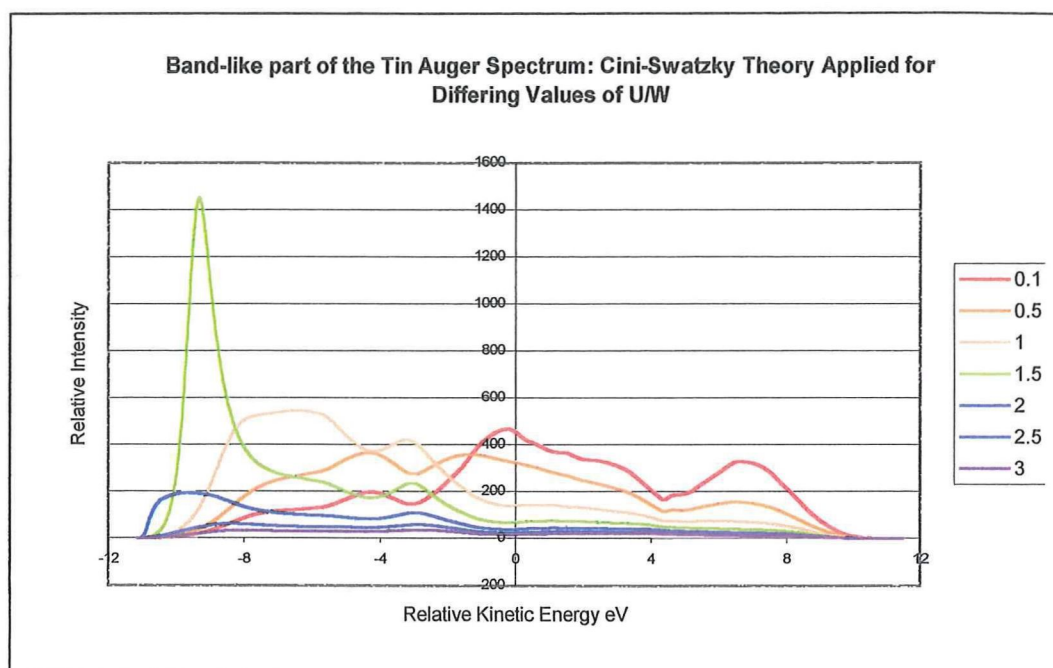


Figure 2.5 Band-like part of the Tin Auger spectrum produced using the Cini-Sawatzky theory. The kinetic energy scale is relative to the centroid of the band-like spectrum. The legend gives values of U/W . For U/W less than or equal to 1.5 the area under the curves is the same. For $U/W = 1.5$ the lineshape has formed an atomic-like spike about U below the centroid of the band-like curve. For $U/W > 1.5$ the atomic-like curve has separated from the band-like curve (so it is not shown on the diagram) and contains 90% or more of the total intensity of the atomic-like and band-like curves for that value of U/W .

In atoms that have multiplet splitting, a narrow valence band structure and to be completely accurate, filled energy levels, the Auger spectra consists of a set of atomic-like and related band-like curves. Each atomic-like/band-like pair of curves in the set will have their individual value of U [9]. Each value of U gives the distance between the centroid of the atomic-like and band-like parts. The energy spacing between the band-like curves reflects the splitting of the energy level within the atom. If U is the same for each multiplet situation then the spacing of the atomic-like curves will be the same as the band-like ones. For the purpose of investigating the structure

of the Tin Auger spectrum in this thesis it was assumed that U was constant. Sawatzky and Lensink [7] cautioned that when working with degenerative bands and ones that cannot be described with the tight binding approximation, effects resulting from differing probabilities and energy shifts for each possible decay pathway can have a strong influence on the Auger spectrum. This should be dealt with before effects due to hole-hole interaction are considered. Sawatzky [10] also cautioned against using the theory associated with Equation 2.1 for partially filled bands.

In 1979 Liebsch [11] was studying the valence band photoelectron spectrum of Nickel, which is partially filled and found features that could not be predicted by the one-electron DOS model alone. The one-electron DOS model predicts that photoelectron spectroscopy of the valence band would produce a peak whose shape is a direct reflection of the DOS of the band. The Nickel spectrum however was narrower than expected and there were atomic-like features as well as the anticipated band-like features. Liebsch explained the unexpected atomic-like features by considering the electrostatic interactions between the initial electrons (or holes) in the 3d band at the moment the photoelectron was produced. Nickel has 2 holes in the 3d band of the neutral atom (electronic configuration $\{\text{Ar}\}3d^84s^2$). The electron-electron, hole-hole and electron-hole interactions within the valence band determine the relative distribution of the hole created during photoionisation. So in Nickel with its partially filled band there are more possible states before photoionisation for the atom than one that has full energy levels and there will be more possible

states after photoionisation for the same reason. Each of the combinations of initial and final state has its own photoelectron spectrum and the weighted sum of these gives the resultant spectrum. Some initial and final states are more likely due to Coulomb interaction (correlations) between the electrons (or holes) in the band. It is these more likely states (resonances) that produce the atomic-like peak in the photoemission spectrum removing intensity from the band-like part of the spectrum. This phenomenon does not occur in Copper because it has a full 3d band (electronic configuration $\{\text{Ar}\}3d^{10}4s^1$) [11]. The comparison between the Nickel and Copper spectrum indicated how the assumption about completely filled bands in the initial state limited the model. From further studies of Nickel Liebsch [12] discovered that energy calculations involving the d-band were improved by considering both hole-hole interactions and electron-hole interactions.

The factor now to be considered is the effect of original holes in the valence band (partially filled band) on the Coulomb interaction energy of the two extra holes produced by the Auger process. By not considering this possibility previous discussions have assumed that before the initial photoionisation of the atom all the energy levels and valence band were full and the conduction band was empty.

Tin has the electronic configuration $\{\text{Kr}\}4d^{10}5s^25p^2$, which means there are 4 holes in the sp-band in the initial ground state but the d-band is full. So the effect of the holes does not have to be taken into consideration as

previously stated. Auger processes involving the d-band are more likely to show atomic-like peaks if the holes created in the d-band remain in that band and the bandwidth is narrow. The bandwidth of Tin is around 2eV, $U/W > 2$ for all components of the $4d^2$ states [13] and Tin does exhibit atomic-like structures in the Auger spectrum. In Palladium however there are 2 holes in the d-band (electronic configuration $\{Kr\}4d^85s^2$) of the ground state of a neutral atom. Even though there are electrons in the s-band the Auger processes involve the d-band and so the effect of initial holes in this area should be taken into consideration.

An interesting graphical demonstration was given by Treglia et. al. [14] which showed that as soon as there were any holes in the valence band the core-valence-valence (CVV) Auger spectra broadened. They found that both the full and unfilled part of the band are important in creating the final shape of the Auger spectra and that the relative emptiness of the band determines the amount of broadening. Other authors [15] [16] have gradually pushed the boundaries of our understanding using complex mathematical models to describe the effects of partially filled valence bands on the Auger spectrum.

Since 1979 Cini [17] has been attempting to formulate the mathematical models needed to describe the distortion of the Auger spectrum due to hole-hole interaction in partially filled valence bands. The calculations involve the total bandwidth not just the occupied part of the band and are complicated by the fact that all possible final states of the atom have to be

taken into consideration. A few predictions have arisen from this work. Firstly the atomic-like part of the Auger spectrum has a width that is related to the energy difference between the top of the valence band and the Fermi level. Secondly the atomic-like peaks may broaden because there are possible decay processes that result in electron-hole pairs (shake-up processes). The models so far have indicated that the CVV spectra are very sensitive to the comparative width of the unoccupied portion of the valence band (hole density). As the unoccupied section increases in size compared to the occupied section the atomic-like part of the Auger spectrum moves to higher kinetic energies, broadens and loses intensity. A broad shake-up structure also forms on the low kinetic energy side of the Auger peak.

A study of Nickel alloys was undertaken by Bennett et. al. in 1983 [18] to investigate the effect of varying hole densities on the Auger spectrum. They found that even though the hole densities varied there was little change in the distance between the atomic-like peak and the band-like peak (this distance is approximately U) for all of the 27 Nickel alloys studied. They attribute this lack of change in U to screening of the d-band by s-p orbitals and minimal variation in the screening as the chemical environment changed. Palladium as previously mentioned also has two holes in the d-band involved in the production of the Auger electron, which are screened by electrons in the s band. In this thesis it was assumed therefore that these holes would have little effect on the value of U and that Equation 3.1 could be used as a first-step approximation in creating

the model Auger curves for Palladium. As this proved to be adequate no further complexity was considered.

By 1992 Cini et. al. [19] [20] [21] had developed the mathematical model to the stage where they could make predictions about the shape of the Auger spectrum for atoms that have small U and closed bands, and atoms with reasonable U and small hole densities. It is not possible yet to make calculations for large U in partially filled bands or for situations in which the Auger process is not a two-step process. Cini et. al. have also investigated band degeneracy and multiplet splitting. They have applied their theories to the $M_{45}NN$ Auger spectrum of Palladium and achieved good agreement with the line shape.

Cini [21] has proposed a final holistic one-step model that describes the Auger process from the initial photo-ionisation of the core energy level through all possible decay processes. This would take into consideration modifications of U/W to allow for partially filled bands and the possible polarisation and shake-up effects they may create in the Auger spectrum. A computer program based on this model would be a valuable tool in understanding the Auger lineshape and its development is eagerly awaited.

-
1. Lander, J.J., *Auger Peaks in the Energy Spectra of Secondary Electrons from Various Materials*. Physical Review, 1953. **91**(6): p. 1382 - 1387.
 2. Mahan, G.D., *Final-State Potential in X-ray Spectra*. Physical Review B, 1980. **21**(4): p. 1421 - 1431.

3. Gunnarsson, O. and K. Schonhammer, *Dynamical Theory of Auger Processes*. Physical Review B, 1980. **22**(8): p. 3710 - 3733.
4. Sawatzky, G.A., *Quasiatomic Auger Spectra in Narrow-Band Metals*. Physical Review Letters, 1977. **39**(8): p. 504 - 507.
5. Cini, M., *Density of States of Two Interacting Holes in a Solid*. Solid State Communications, 1976. **20**: p. 605 - 607.
6. Cini, M., *Comment on Quasiatomic Auger Spectra in Narrow-Band Metals*. Physical Review B, 1978. **17**(6): p. 2788 - 2789.
7. Sawatzky, G.A. and A. Lenzelink, *Auger Line Shape in Narrow-Band Metals*. Physical Review B, 1980. **21**(5): p. 1790 - 1796.
8. Cini, M., *Two Hole Resonances in the XVV Auger Spectra of Solids*. Solid State Communications, 1977. **24**: p. 681 - 684.
9. Sawatzky, G.A., *Auger Photoelectron Coincidence Spectroscopy, in Treatise on Materials Science and Technology*. 1988, Academic Press Inc. p. 167 - 243.
10. Sawatzky, G.A., *Experimental Probes of Electron Correlation Effects and the Influence on the Electronic Structure*, in *Auger Spectroscopy and Electronic Structure*, G.M. G. Cubiotti, K. Wandelt, Editor. 1989, Springer-Verlag: Berlin, Heidelberg, New York, London, Paris, Tokyo, Hong Kong. p. 2 - 28.
11. Liebsch, A., *Effects of Self-Energy Corrections on the Valence-Band Photoemission Spectra of Ni*. Physics Review Letters, 1979. **43**(19): p. 1431 - 1434.
12. Liebsch, A., *Ni d-Band Self-Energy Beyond the Low-Density Limit*. Physical Review B, 1981. **23**(10): p. 5203 - 5212.
13. Weightman, P., *X-ray Excited Auger and Photoelectron Spectroscopy*, in *Report on Progress in Physics*. 1982, The Institute of Physics. p. 753 - 814.
14. Treglia, G., et al., *Correlation Effects on Auger Spectra in Unfilled d Band Metals*. Journal of Physics C: Solid State Physics, 1981. **14**: p. 4347 - 4355.
15. Drchal, V. and J. Kudrnovsky, *The Auger Spectra of Metals: Effects of Electron Correlations in Partially Filled Bands*. Journal of Physics F, 1984. **14**: p. 2443 - 2453.
16. Cubiotti, G., *Comments on the relationship Between Auger Lineshapes and Local Electronic Structure*, in *Auger Spectroscopy and Electronic Structure*, G.M. G. Cubiotti, K. Wandelt, Editor.

- 1989, Springer-Verlag: Berlin, Heidelberg, New York, London, Paris, Tokyo, Hong Kong. p. 51 - 56.
17. Cini, M., *Theory of Auger XVV Spectra of Solids : Many Body Effects in Incompletely Filled Bands*. Surface Science, 1979. **87**: p. 483 - 500.
 18. Bennett, P.A., et al., *Electronic Structure of Ni and Pd Alloys. III. Correlation Effects in the Auger Spectra of Ni Alloys*. Physical Review B, 1983. **27**(4): p. 2194 - 2209.
 19. Cini, M. and C. Verdozzi, *Photoemission and Auger Spectra of Incompletely Filled Bands: Intermediate-Coupling Theory and Application to Palladium Metal*. Journal of Physics: Condensed Matter, 1989. **1**: p. 7457 - 7470.
 20. Cini, M. and C. Verdozzi, *Correlation Effects in Photoemission and Auger Spectra of Palladium*, in *Auger Spectroscopy and Electronic Structure*, G. Cubiotti, G. Mondio, and K. Wandelt, Editors. 1989, Springer-Verlag: Berlin, Heidelberg, New York, London, Paris, Tokyo, Hong Kong. p. 122 - 126.
 21. Cini, M., *Correlation Effects in Auger CVV Spectra from Partially Filled Bands*. Physica Scripta, 1992. **T41**: p. 59 - 66.

Chapter 3

Background Subtraction

3.1. Introduction

Figure 1.1 and 3.1 show the emission electron energy spectrum for Palladium and Tin produced by incident Mg K_{α} X-rays. So far in this thesis we have been concerned with the lines and peaks sitting on the “background” curve because they are characteristic of the material under investigation. In this chapter the background curve that gently slopes from high intensity at the low kinetic energy end of the spectrum to low intensity at the high-energy end of the spectrum will be investigated.

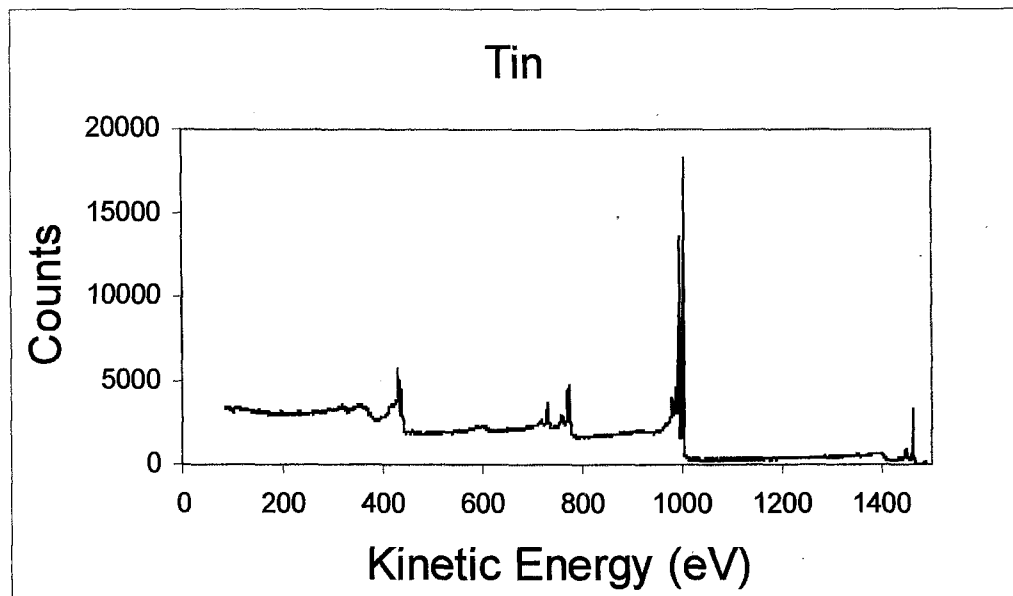


Figure 3.1 Tin emission-electron energy spectrum

3.2. Intrinsic Coster-Kronig and Shake-off Processes

In Chapter 1 the intensity on the low kinetic energy side of individual photoelectron lines and Auger peaks arising from intrinsic shake and

Coster-Kronig processes was discussed in detail so a description of these processes will not be given here. They do contribute to the asymmetry of the line or peak and can extend to 50eV below the main feature [1]. For the remainder of this chapter these energy-shifted electrons will be considered as part of the main photoelectron line or Auger peak.

For the purpose of this thesis, true primary electrons are those electrons contributing to the lineshape of the photoelectron lines or Auger peaks, which may be elastically scattered but have not lost any energy due to inelastic scattering. Those that would contribute to the lineshape but have suffered inelastic scattering as they leave the material will be called "diffuse primary electrons". Electrons, which arise from processes other than the initial photoionisation or final Auger emission, will be called "secondary electrons". Diffuse primary electrons associated with a photoelectron line can be distinguished from secondary electrons because the intensity from the diffuse primaries will retain their relationship with the photoelectron line even when the energy of the ionising radiation is changed [2].

Coster-Kronig and shake-off electrons are emitted at the same time as the final Auger electron and their energy is typically between 0-10 eV. They form part of the background intensity in the electron emission spectrum. The Coster-Kronig processes and shake processes depend on the energy levels of the electrons within the atom, how these energy levels are affected by being in an elemental or compound solid, the work function of

the material and the characteristics of the ionising radiation [3-6]. With higher energy ionising radiation deeper core levels can be reached, more shake and Coster-Kronig processes can be initiated providing more low kinetic energy electrons. These low kinetic energy electrons are therefore a potential source of information. Unfortunately it is not possible at this point in time to separate these electrons from "secondary electrons" found in this energy range.

3.3. Extrinsic Processes

3.3.1. Plasmon loss

Plasmon loss is an extrinsic process, which has definite energy associations with a characteristic line or peak, so the electrons affected by this process would be classified as diffuse primaries. The electron loses energy as it leaves the metal by causing a collective oscillation of the electron gas [7] in [2]. These oscillations can be excited in the bulk or the surface of the sample and the relative intensity of the two types varies with the sample thickness for the same initiating electron energy [8] in [2]. So there may be several low intensity broad peaks on the low kinetic energy side of the photoelectron line or Auger peak from plasmon formation.

3.3.2. Inelastic scattering

Inelastic scattering producing diffuse primary electrons is also associated with the characteristic lines and peaks of the electron energy spectrum. From studies of several materials and their oxides in 1953 Lander [9] came to the conclusion that the long tail on the low kinetic energy side of

Auger peaks was due to inelastic collisions of the Auger electrons as they made their way out of the material. This tail may extend over several hundred electron volts [10] having its maximum intensity nearest the photoelectron line or Auger peak with which it is associated and reducing intensity as the kinetic energy reduces. As photoelectron lines and Auger peaks are characteristic of the material and this intensity is related to them then this intensity is also characteristic of the material.

Inelastic scattering occurs when a photoelectron or an Auger electron excites or ionises another atom. The initiating electron loses energy and becomes part of the inelastic tail associated with the primary peak while the electrons produced from the second atom become part of the secondary electron background. These electrons may themselves ionise other atoms producing a cascade of low energy electrons.

The amount of energy lost by an Auger or photoelectron due to inelastic scattering is dependent on several properties of the material under investigation. One of these properties is the depth distribution of the emitting atoms [10]. In XPS and X-ray induced AES the depth the photons reach is much larger than the inelastic mean free path (IMFP) of the electrons. The depth distribution profile of the emitting atoms is therefore the same as the depth concentration profile of the atoms being investigated [10]. Tougaard et. al. [10] have indicated that the inelastic background will be different for different depth distribution profiles. These profiles may be homogeneous or that of an emitting layer hidden under a

surface layer with varying thicknesses of the submerged or surface layer. Even if the emitting layer is a surface layer of nano-meter thickness, the thickness of this layer plays a part in shaping the background [11].

3.3.3. Elastic scattering

A factor, which contributes to the number of times an electron is inelastically scattered, is the amount of elastic scattering the electron encounters. Inelastic scattering depends on the distance the electron travels in the solid. This distance in turn depends on the depth of the emitting atom and the amount of elastic scattering the electron encounters. Elastic electron scattering changes the direction of the electron even though it does not change the energy. So increased elastic scattering indirectly leads to greater inelastic scattering and energy loss for the emitted electron. Jablonski and Tougaard [12] determined a correction factor to account for elastic electron scattering in photoelectron intensity. The correction factor is strictly valid for close to normal electron emissions but only small deviations were observed for emission angles up to 30° .

There has been a great deal of investigation and discussion of the effects of elastic electron scattering on intensity and the terminology that should be used when discussing the path length of an electron in a solid. The one path length measurement that takes into account elastic electron scattering is the inelastic mean free path (IMFP). Penn [13] used experimental optical data to develop an algorithm for calculating IMFP's. This was applied by Tanuma et. al. [14-19] to do calculations for over 60

materials where emission electron energies were in the range 50 eV to 2000 eV. The resultant IMFP's were between 2 Å and 100 Å. The calculations were for bulk solids and therefore would need to be modified for surface studies in free-electron-like solids due to the excitation of surface plasmons [2, 20]. They used a modified form of the Bethe equation (named TPP-2M) as in Equation 3.1.

$$\lambda = E / \{ E_p^2 (\beta / \ln(\gamma E) - (C/E) + (D/E^2)) \} \quad \text{(Equation 3.1)}$$

Where

λ is the IMFP in Armstrong units

$E_p = 28.8(N_v \rho / M)^{1/2}$ is the free-electron plasmon energy in eV

N_v is the number of valence electrons per atom/molecule

Values characteristic of the material

$$\beta = -0.1 + 0.944 / (E_p^2 + E_g^2)^{1/2} + 0.069 \rho^{0.1}$$

$$\gamma = 0.191 \rho^{-0.50}$$

$$C = 1.97 - 0.91U$$

$$D = 53.4 - 20.8U$$

$$U = N_v \rho / M = E_p^2 / 829.4$$

E_g is the band gap energy in eV for non-conductors

From [2] [15] [19]

Clearly the IMFP is dependent on the electron energy and the atomic number of the material. It is not dependent on the experimental geometry of the system unlike other measures, which are sometimes used to indicate the surface sensitivity of XPS and AES. These other measures are

EAL effective attenuation length

MED mean escape depth

It was indicated (somewhat incorrectly) in early overlayer thickness experiments that the intensity of XPS and AES signals diminished exponentially with depth. The exponential parameter was called the EAL and is equivalent to the IMFP if there is no elastic electron scattering. Elastic electron scattering changes the emission depth distribution function (EDDF), which causes the EAL to be ~30% less than the IMFP [2] [21]. In other words the signal intensity does not vary exponentially with depth when the effects of elastic electron scatter are considered [22].

The MED [23] [24] is the average depth normal to the surface from which the detected signal electrons originated. It depends on the material, the electron energy and the geometry of the experiment. If there is no elastic electron scattering then the MED is given by Equation 3.2.

$$\text{MED} = \text{IMFP} \cos \alpha \quad \text{(Equation 3.2)}$$

Where

α is the electron emission angle with respect to the surface normal

In AES the MED is reduced by ~35% when elastic electron scattering is considered and the calculated XPS intensity can change by $\pm 30\%$ [23].

Elastic electron scattering is therefore responsible for the difference between the IMFP, the EAL and the MED and the variation of the EDDF from exponential decrease with depth. Further information on these terms can be found in Appendix iii.

3.4. Background Subtraction Techniques

The historical way of considering the background was to assume it contained no useful information and remove it from the spectrum. A horizontal, linear amount was removed bringing the high kinetic energy end of the spectrum to zero. Then a wedge shape amount running from zero at the high kinetic energy end, to the lowest intensity at the low kinetic energy end was also removed. Application of this technique however removed a great deal of intensity from shake processes and plasmon peaks as well as the intensity from inelastically scattered primary electrons.

Shirley [25], whilst studying gold-valence-band photoemission spectra, observed that the background contribution from inelastic scattering returned to a constant but higher intensity level at kinetic energies lower than the valence bands compared to the intensity above the valence bands. The difference in the background level was assumed to be entirely due to inelastic scattering of the electrons from the band spectra. To correct for this background a quantity was subtracted from the intensity at each energy point proportional to the area under the valence band peak at higher kinetic energies. This was the first acknowledgment that the background was related to the intensity of the peaks. This type of background removal is more realistic than the straight-line method but may remove intensity due to shake processes as well as that from inelastic scattering.

In the above techniques it is the responsibility of the person performing the lineshape analysis to decide how far the peak extends on the low kinetic energy side. As previously stated if too much intensity is removed, information about shake processes are also removed. Shake processes can change with the composition of the material so it is impossible for the analyst to standardise the background removal procedure. If it were possible to remove the intensity in the background due only to inelastic scattering and leave the background from intrinsic processes, more could be learned about the intensity in the spectrum due to shake processes. This is what Tougaard [10] has been able to do.

Tougaard's method [1] of background subtraction is superior to the Shirley and straight-line methods in both consistency and validity because the Tougaard method relies on a detailed description of the physical processes involved in creating the background. With the Shirley and straight-line methods, both the maximum and minimum energy for the line or curve have to be specified and by changing the minimum energy (low kinetic energy / high background intensity end of the feature) the area under the peak changes. With the Tougaard method this does not happen. Tougaard et. al. [1] [26] have made exhaustive comparisons of the three types of background subtraction and I have summarised these results in Table 3.1.

Table 3.1 Comparison of Three Types of Background Subtraction Techniques

	Straight Line	Shirley	Tougaard
Need to specify maximum energy	Yes	Yes	Yes
Peak area sensitive to position of maximum energy	Yes	No	No
Need to specify minimum energy	Yes	Yes	No
Peak area sensitive to position of minimum energy	Yes	Yes	No – minimum energy specified by background subtraction technique
Compensates for the method used to remove intensity from processes occurring at higher kinetic energies in the spectrum i.e. horizontal line or a line that decreases in intensity with a decrease in kinetic energy	Yes	No – the variations can be as high as 38%	Yes – difference in total intensity under the peaks is less than 2.5% between the two methods
Use in a restricted energy range produces variations in peak areas with variations in minimum energy	Most variation	Moderate variation	Least variation but energy range > 65eV to use available software
Does the x-ray source Mg K α or Al K α make a difference to the validity of the results of the peak intensity ratios?	Yes	Yes	No
RMS difference between experiment and theory for intensity ratio of two peaks from the same pure elemental solid	35%	35%	11%
Sensitivity to noise (RMS deviation from theory)	Sensitive (31%)	Sensitive (33%)	Least sensitive (14%)
Do changes in shake-up processes with chemical environment cause systematic errors?	Yes	Yes	Considerably less
Accuracy when applied to doublet peaks	Worse	Worse	No change

[1] [26]

When using Tougaard's method it is necessary to know the IMFP of the electron in the material and the inelastic electron scattering cross-section, which describes the inelastic scattering properties of the material.

Fortunately Tougaard [10] [27] found that for noble and transition metals the electron scattering cross-section was fairly constant and therefore for practical day-to-day work, removing inelastic background from spectra a 'Universal' cross-section was adequate. The Universal cross-section follows a scaling law. Starting on the high kinetic energy side of the peak the background is zero but gradually increases to a broad maximum 20 to 30eV below the peak and then trails off to zero much further from the peak. By using this Universal cross-section fine structure in the background is removed but this does not decrease the usefulness of the Universal cross-section. Electrons may undergo several inelastic collisions on the way out of the solid and this fine structure would be smeared leaving only the rough shape anyway [27]. The uncertainties in the Universal cross-section are no greater than uncertainties in other areas of peak shape analysis eg IMFP, influence of elastic electron scattering, role of surface roughness [28] and surface plasmons. For transition metals, their oxides and alloys the 2-parameter Universal cross-section [29] provides a reasonably accurate and robust description of the inelastic background.

-
1. Tougaard, S. and C. Jansson, *Comparison of Validity and Consistency of Methods for Quantitative XPS Peak Analysis*. Surface and Interface Analysis, 1993. **20**: p. 1013 - 1046.
 2. Powell, C.J., *Inelastic Interactions of Electrons with Surfaces - Application to Auger-Electron Spectroscopy and X-ray Photoelectron Spectroscopy (Review)*. Surface Science, 1994. **300**(1 - 3): p. 34 - 48.
 3. Weightman, P., *X-ray Excited Auger and Photoelectron Spectroscopy*, in *Report on Progress in Physics*. 1982, The Institute of Physics. p. 753 - 814.

4. Antonides, E. and G.A. Sawatzky., *The $L_2L_3M_{45}$ Coster-Kronig Process in Zn and ZnO in the Solid State*. Journal of Physics C: Solid State Physics, 1976. **9**: p. L547 - L552.
5. Thurgate, S.M. and C.P. Lund, *Comparison of the Auger Photoelectron Coincidence Spectroscopy (APECS) Spectra of Ag and InP with Cu and GaAs*. Surface and Interface Analysis, 1997. **25**: p. 10 - 16.
6. Thurgate, S.M. and C.P. Lund, *Auger-Photoelectron Coincidence Spectroscopy (APECS) A Tool for Understanding Auger Emission From Solids*. Journal of Electron Spectroscopy and Related Phenomena, 1995. **72**: p. 289 - 297.
7. Bohm, D. and D. Pines, Physical Review, 1952. **85**: p. 338.
8. Ritchie, R.H., Physical Review, 1957. **106**: p. 874.
9. Lander, J.J., *Auger Peaks in the Energy Spectra of Secondary Electrons from Various Materials*. Physical Review, 1953. **91**(6): p. 1382 - 1387.
10. Tougaard, S., *Quantitative Analysis of the Inelastic Background in Surface Electron Spectroscopy*. Surface and Interface Analysis, 1988. **11**: p. 453 - 472.
11. Tilinin, I.S., A. Jablonski, and S. Tougaard, *Path-Length Distribution of Photoelectrons Emitted from Homogeneous Noncrystalline Solids: Consequences for Inelastic-Background Analysis*. Physical Review B, 1995. **52**(8): p. 5935 - 5946.
12. Jablonski, A. and S. Tougaard, *Practical Correction Formula for Elastic Electron Scattering Effects in Attenuation of Auger Electrons and Photoelectrons*. Surface and Interface Analysis, 1998. **26**(1): p. 17 - 29.
13. Penn, D.R., *Electron mean-Free-Path Calculations Using a Model Dielectric Function*. Physical Review B: Condensed Matter, 1987. **35**(2): p. 482 - 486.
14. Tanuma, S., C.J. Powell, and D.R. Penn, *Calculations of Electron Inelastic Mean Free Paths for 31 Materials*. Surface and Interface Analysis, 1988. **11**: p. 577 - 589.
15. Tanuma, S., C.J. Powell, and D.R. Penn, *Calculations of Electron Inelastic Mean Free Paths II. Data for 27 Elements Over the 50-2000 eV Range*. Surface and Interface Analysis, 1991. **17**: p. 911 - 926.

16. Tanuma, S., C.J. Powell, and D.R. Penn, *Electron mean-Free-Path Calculations Using a Model Dielectric Function*. Surface and Interface Analysis, 1991. **17**(13): p. 927 - 939.
17. Tanuma, S., C.J. Powell, and D.R. Penn, *Calculations of Electron Inelastic Mean Free Paths (IMFPs). IV. Evaluation of Calculated IMFPs and of the Predictive IMFP Formula TPP-2 for Electron Energies Between 50 and 2000eV*. Surface and Interface Analysis, 1993. **20**(1): p. 77 - 89.
18. Tanuma, S., C.J. Powell, and D.R. Penn, *Calculations of Electron Inelastic Mean Free Paths. V. Data for 14 Organic Compounds Over the 50 - 2000eV Range*. Surface and Interface Analysis, 1994. **21**(3): p. 165 - 176.
19. Tanuma, S., C.J. Powell, and D.R. Penn, *Calculations of Electron Inelastic Mean Free paths V. Data for 14 Organic Compounds over the 50 - 2000eV Range*. Surface and Interface Analysis, 1993. **21**: p. 165 - 176.
20. Powell, C.J. and A. Jablonski, *Evaluation of Calculated and Measured Electron Inelastic Mean Free Paths Near Solid Surfaces [Review]*. Journal of Physical & Chemical Reference Data, 1999. **28**(1): p. 19 - 62.
21. Powell, C.J. and A. Jablonski, *Consistency of Calculated and Measured Electron Inelastic Mean Free Paths*. Journal of Vacuum Science and Technology A: Vacuum Surfaces and Films, 1999. **17**(4): p. 1122 - 1126.
22. Powell, C.J., et al., *Effects of Elastic and Inelastic Electron Scattering on Quantitative Surface Analyses by AES and XPS*. Journal of Electron Spectroscopy and Related Phenomena, 1994. **68**: p. 605 - 616.
23. Powell, C.J., et al., *Surface Sensitivity of Auger-Electron Spectroscopy and X-ray Photoelectron Spectroscopy*. Journal of Electron Spectroscopy and Related Phenomena, 1999. **99**: p. 1 - 15.
24. Jablonski, A. and C.J. Powell, *Evaluation of Correction Parameters for Elastic-Scattering Effects in X-Ray Photoelectron Spectroscopy and Auger Electron Spectroscopy*. Journal of Vacuum Science and Technology A: Vacuum Surfaces and Films, 1997. **15**(4): p. 2095 - 2106.
25. Shirley, D.A., *High-Resolution X-Ray Photoemission Spectrum of the Valence Bands of Gold*. Physical Review B, 1972. **5**(12): p. 4709 - 4714.

26. Jansson, C., et al., *Intercomparison of Algorithms for Background Correction in XPS*. *Surface and Interface Analysis*, 1995. **23**: p. 484 - 494.
27. Tougaard, S., *Low Energy Inelastic Electron Scattering Properties of Noble and Transition Metals*. *Solid State Communications*, 1987. **61(9)**: p. 547 - 549.
28. Tougaard, S., *Quantitative XPS: Non-destructive Analysis of Surface Nano-Structures*. *Applied Surface Science*, 1996. **100 / 101**: p. 1 - 10.
29. Tougaard, S., *Universality Classes of Inelastic Electron Scattering Cross-Sections*. *Surface and Interface Analysis*, 1997. **25(3)**: p. 137-154

Part 2

The APECS Experiment

Chapter 4.

APECS

4.1. Introduction

A way of understanding and reducing the complexity of the Auger spectrum is to do APECS experiments. The acronym APECS was first coined by Haak and Sawatzky around 1978 [1] and APECS notation retains the historic usage of quantum number identification for photoelectron lines and atomic shell notation for Auger peaks (Figure 4.1).

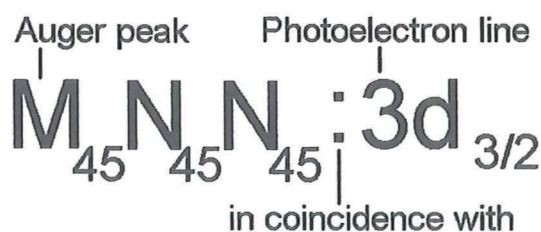


Figure 4.1 APECS notation. The symbols to the left of the colon represent the peak or line being scanned while the symbol to the right of the colon represents the particular part of the electron energy spectrum that determines the decay process being investigated.

Haak and Sawatzky devised the APECS experiment to detect both the photoelectron and the Auger electron from the same atom. By linking these two electrons only features arising from the selected photoionisation are recorded in the Auger spectrum. This allowed the Auger lineshape to be separated into its component peaks indicating the intensity arising from different decay paths.

This chapter looks at the equipment necessary to perform the APECS experiment, what information the APECS spectrum can give us that AES and XPS can not, the APECS results obtained by the Murdoch research group and will also touch on the work done by other APECS groups.

4.2. Equipment

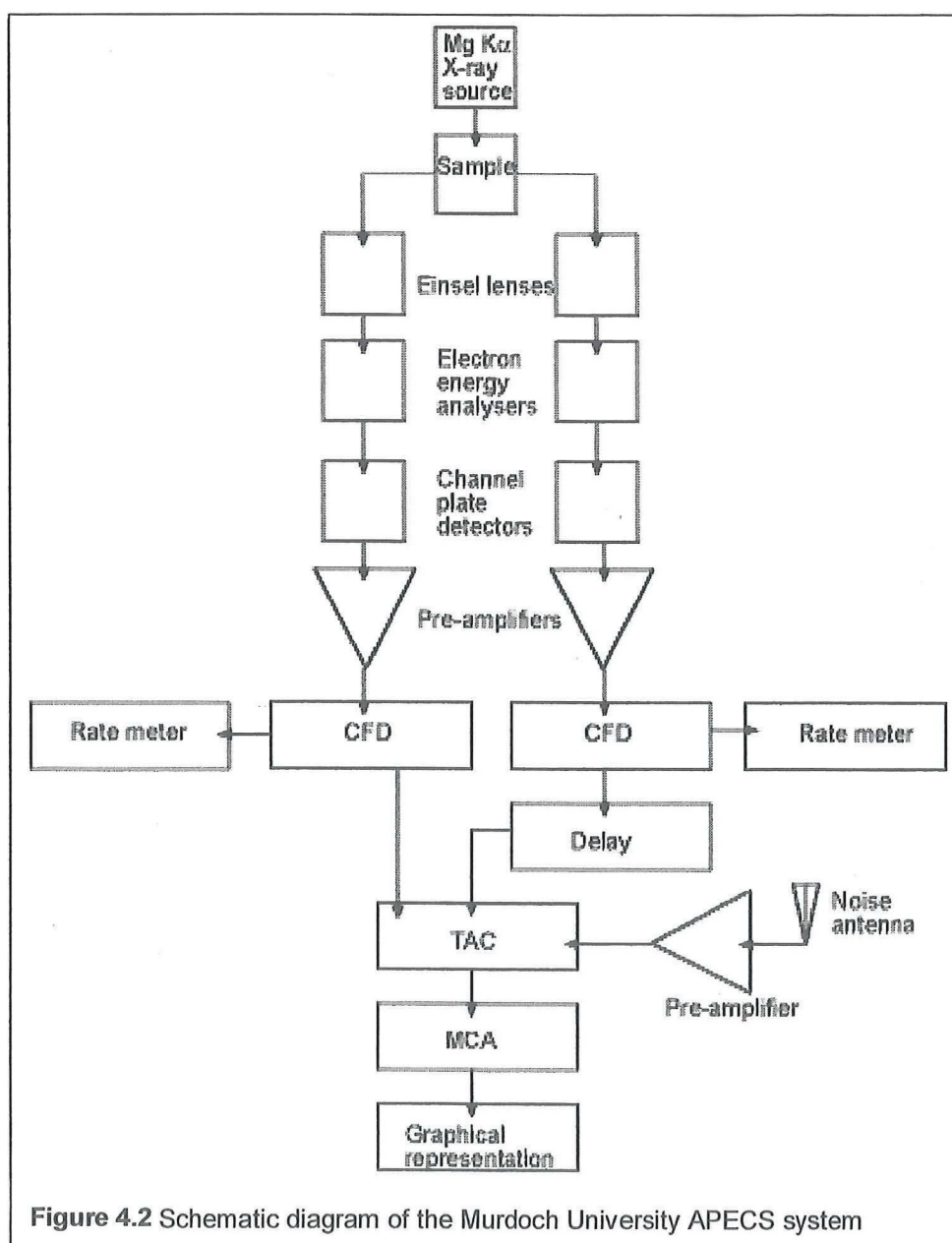


Figure 4.2 Schematic diagram of the Murdoch University APECS system

An ultra high vacuum (UHV) APECS system was built at Murdoch University to enable simultaneous studies of X-ray-initiated photoelectron and Auger-electron spectra. The details of the apparatus are described elsewhere [2, 3] and only those details will be touched on here that are necessary in understanding this experiment. Figure 4.2 provides an overview of the system.

4.2.1. X-ray Source

The X-ray source operating at 20 mA with 13 kV for Palladium and at 30 mA with 13.5 kV for Tin produced a constant flux of Magnesium $K\alpha$ non-monochromatic x-rays. In the X-ray spectrum of Magnesium there are three high intensity characteristic lines. These are the $K\alpha_1$ and $K\alpha_2$ lines, which overlap at a kinetic energy of 1253.6eV. The third line is the $K\alpha_3$ at 8.4eV higher kinetic energy and 8% of the height of the $K\alpha_{1,2}$ line [4]. These high intensity characteristic lines contribute to the lineshape of the resultant photoelectron spectrum. The $K\alpha_3$ line in particular produces a 'ghost' to the main spectrum that is 8% as intense and at 8.4eV higher kinetic energy.

4.2.2. Sample

Two 4d transition metals were examined using the APECS technique, 99.95% pure Palladium and 99.99% pure Tin both from Goodfellow Cambridge Ltd. The sample under investigation was cleaned daily within the

UHV chamber by Argon ion bombardment until the surface was free of contamination. This was confirmed using XPS. Palladium was also annealed but not the Tin sample because of its low melting point. The target area of the sample was 2mm x 2mm which was small compared to the area irradiated.

During each experiment the sample was positioned at an angle of 45° to both the x-ray flux and the Einsel lenses (Figure 4.3)

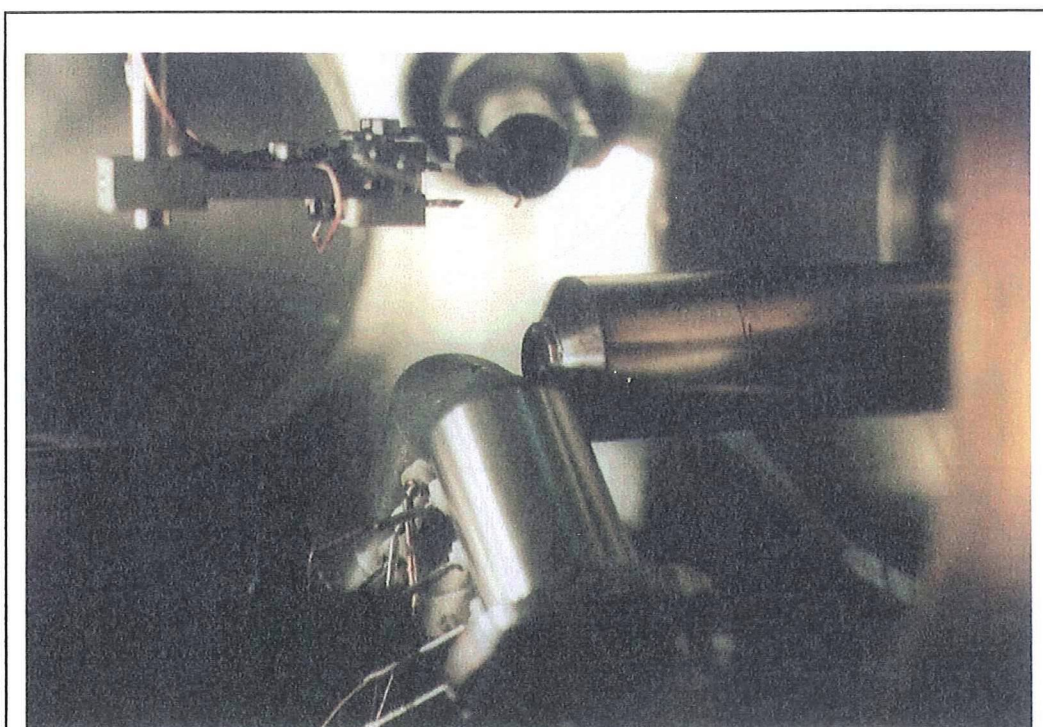
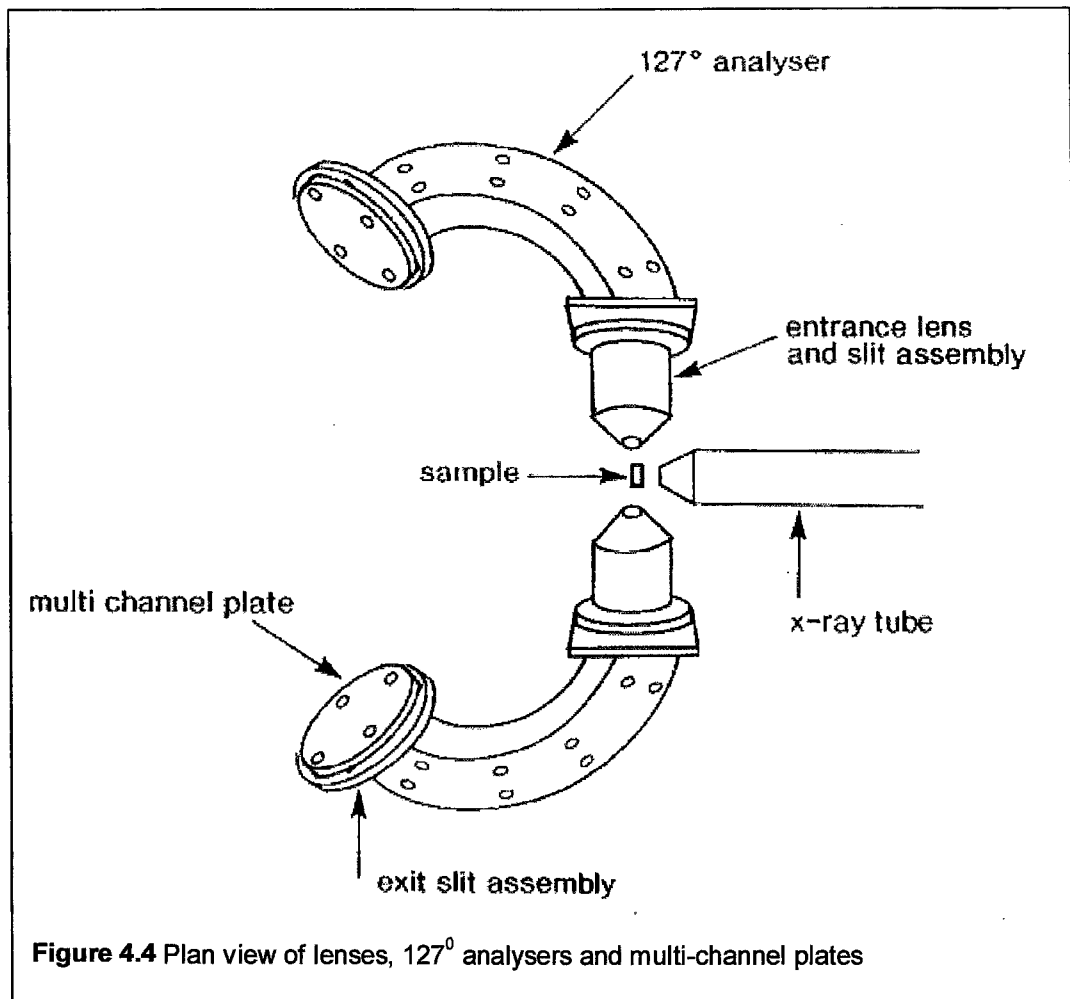


Figure 4.3 Position of x-ray source (right) and electron collection lenses (bottom). The sample holder (top left) has been raised so the sample can be cleaned by Argon ion bombardment. The sample normally sits at the focus of the of the lenses and X-ray source. A copper sample can be seen superimposed over the lower lip of the ion gun (top middle).

4.2.3. Lenses and Analysers



The Einsel lenses, positioned 90° to each other, collected the electrons released from the X-ray irradiated sample. Each lens was designed to have a magnification of 1 and was composed of five elements, which focused the electrons onto the entrance aperture of an electron energy analyser [3]. In the first series of experiments for this thesis two independent 127° cylindrical analysers (Figure 4.4, 4.5 and 4.6) were used to determine the energy of the

captured electrons. In the final section of the Tin experiment two high-resolution hemispherical analysers were employed.

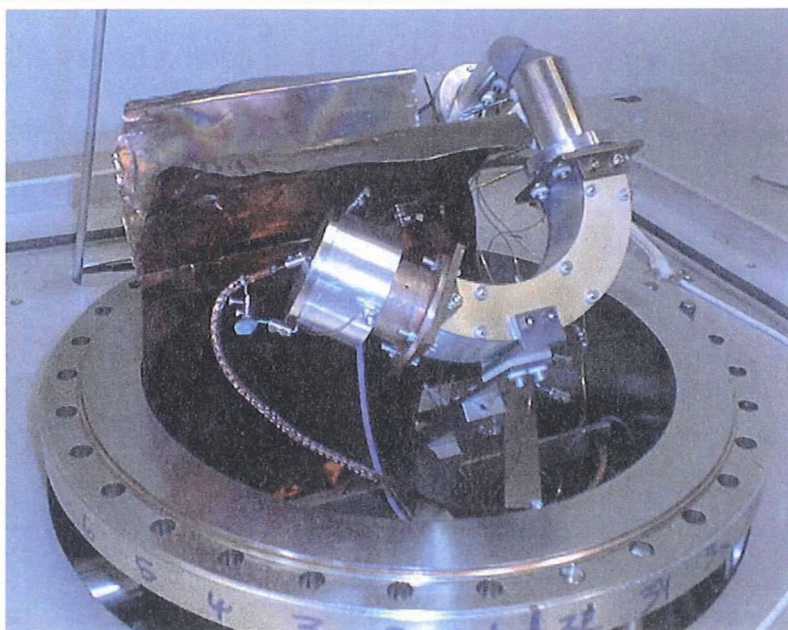


Figure 4.5 APECS lenses, 127° analyzers and channel plates.

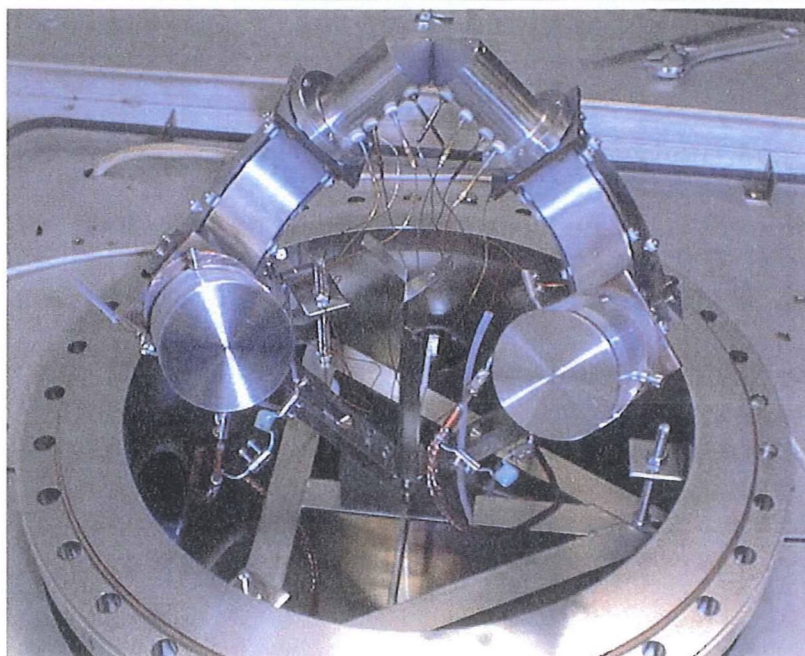
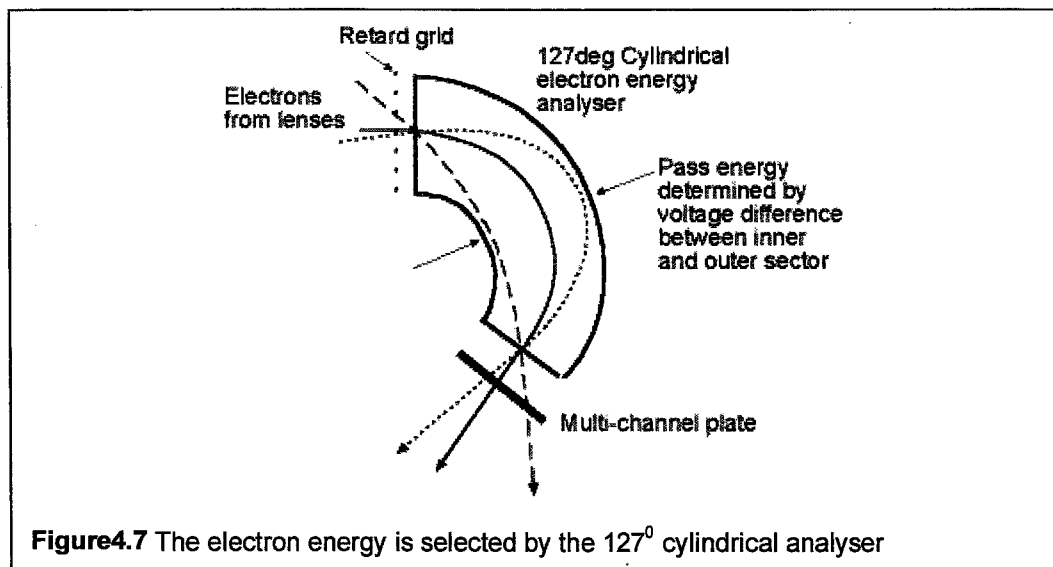


Figure 4.6 APCES lenses, 127° analyzers and channel plates.

The pass energy of both analysers was set at 150eV for the earlier experiments and 130eV (lower pass energy produces higher energy resolution) for the final experiment with the hemispherical analyser. By adjusting the retard potential of the grid at the entrance to each analyser it was possible to select the energy of the electrons under investigation (Figure 4.7).



One analyser was set to collect the initiating photoelectrons from the peak position of the photoelectron line under investigation. The retard potential of the other analyser was methodically incremented to allow the analyser to scan the energy range of the resultant Auger peak. The whole experiment was computer controlled and the analyser focus was maintained as the retard energy was ramped by electronically linking the focus values and the retard values [5].

Electrons arriving at both analysers within 10ns of each other were regarded as having a high probability of originating from the same atom. In this way it was possible to link parts of the Auger spectrum with their initiating photoelectrons. Several processes may place intensity in the same part of the Auger spectrum however using APECS it is possible to distinguish between each of these processes if the initiating photoelectrons have different energies.

The analysers were designed and built for B. D. Todd's Honours thesis in 1989 [6] and he has dedicated a significant section of his thesis to discussing their construction, energy resolution, timing resolution, slit design and how fringing fields were dealt with. A very brief summary of his analysis is given below.

The energy resolution of an electron energy analyser is $\Delta E/E_p$ where ΔE is the FWHM of the energy spread of a monochromatic electron beam passing through the analyser and E_p is the pass energy. For a spectrometer of fixed mean radius the FWHM decreases as the

- width of the entrance and exit apertures of the analysers decrease
- acceptance angle in the plane of deflection decreases
- acceptance angle perpendicular to the plane of deflection decreases

Minimising these parameters however decreases the count rate of the electrons successfully passing through the analysers. This is of major

concern in a coincidence experiment because of the intrinsically low count rate to begin with.

Another way of increasing the energy resolution of the analysers is to decrease the pass energy. This however would have the effect of increasing the time-of-flight spread of the electrons through the analysers, which in turn decreases the timing resolution. In designing the analysers for construction in the Murdoch University workshop, Todd had to balance each of these requirements and the physical limitations of the UHV system.

4.2.4. Hemispherical Analysers

For the final experiment of this thesis the apparatus was fitted with dual hemispherical electrostatic electron energy analysers (Figure 4.8 and 4.9). They were designed by Professor Steven Thurgate, built in the workshop at Murdoch University and optimised by Dr. Zhong-Tao Jiang. The new analysers had better collection efficiency producing an improved count rate. The energy resolution of the system is now good enough to allow the resolution of individual atom-like terms in the Cu $L_{23}VV$ Auger spectra [7].

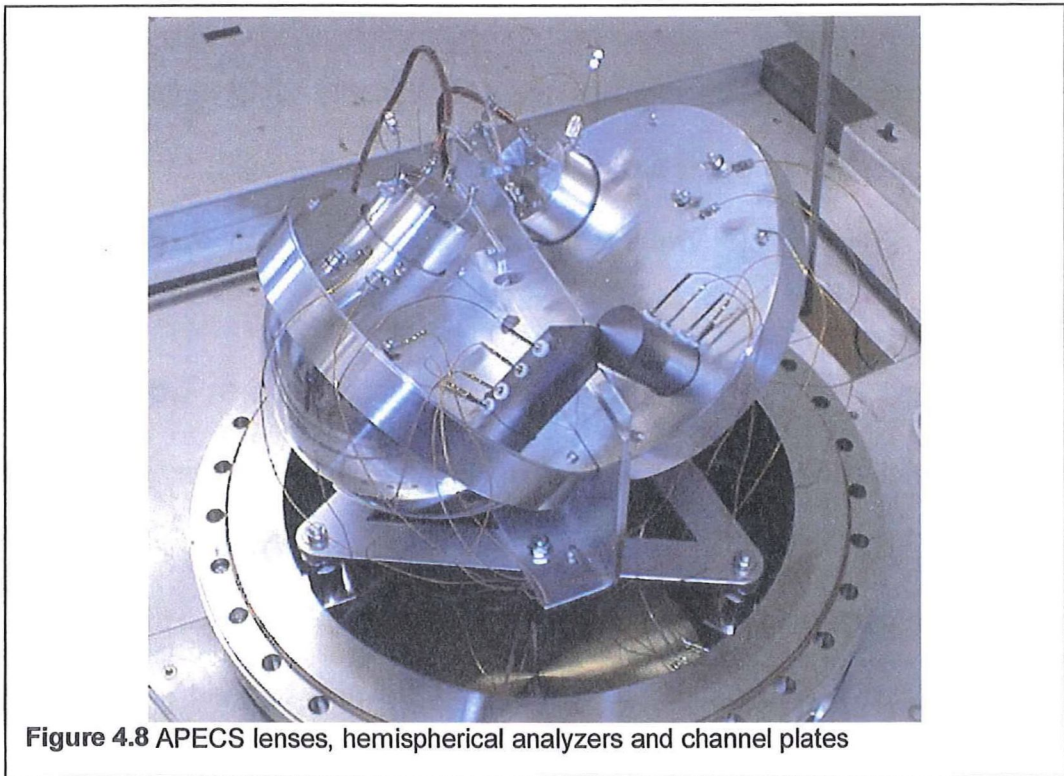


Figure 4.8 APECS lenses, hemispherical analyzers and channel plates

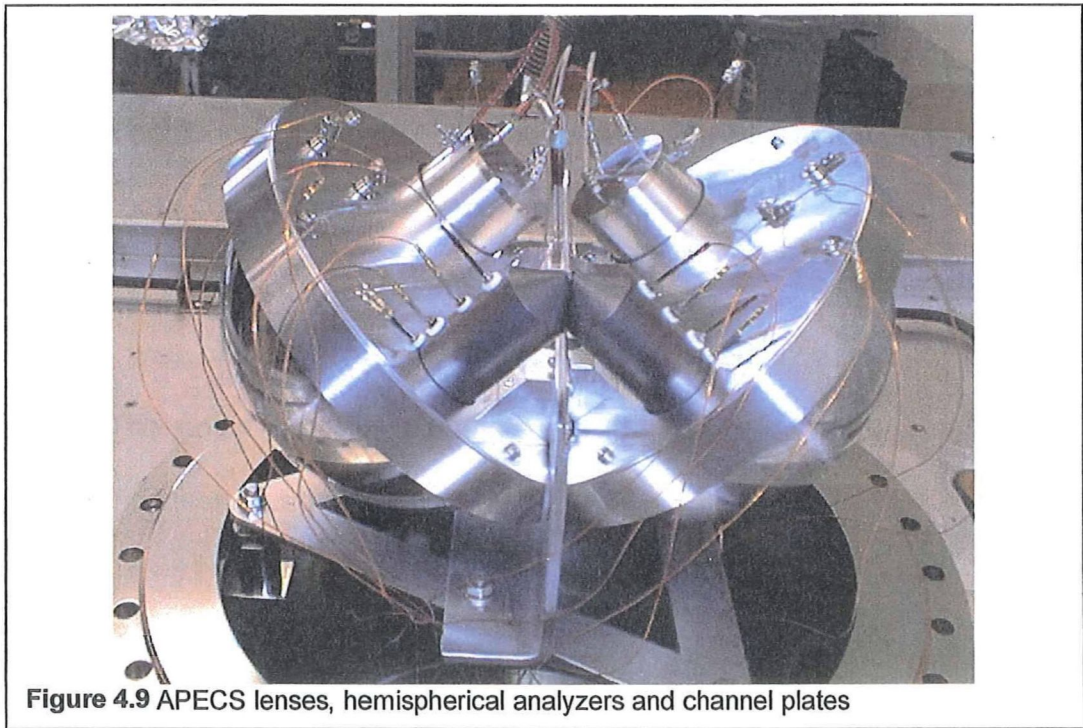


Figure 4.9 APECS lenses, hemispherical analyzers and channel plates

4.2.5. Channel Plates

A multi-channel plate electron detector was placed at the exit aperture of each analyser (Figure 5.4 and 5.5). The output pulse of each multi-channel plate had a rise time of 1.0ns and a height of 20mV [8].

4.2.6. Pre-amplifiers

The high timing resolution necessary for this experiment required excellent pre-amplifiers and these were found in kit form as VHF-UHF Masthead Amplifiers (uses the wideband amplifier IC MAR-6). Slight modification of the amplifier was needed to invert the output pulse so it could be detected by the electronics.

4.2.7. Noise Antenna

If the coincidence circuit detected noise from an external source it would occur in both channels at the same time and so would be included as a true coincidence count. To compensate for this a fast pre-amplifier with small antenna was placed near the electronics and used to detect such noise bursts. The noise circuit is connected to the anti-coincidence input of the TAC and cancels out the noise pulse [5].

4.2.8. TAC Spectra

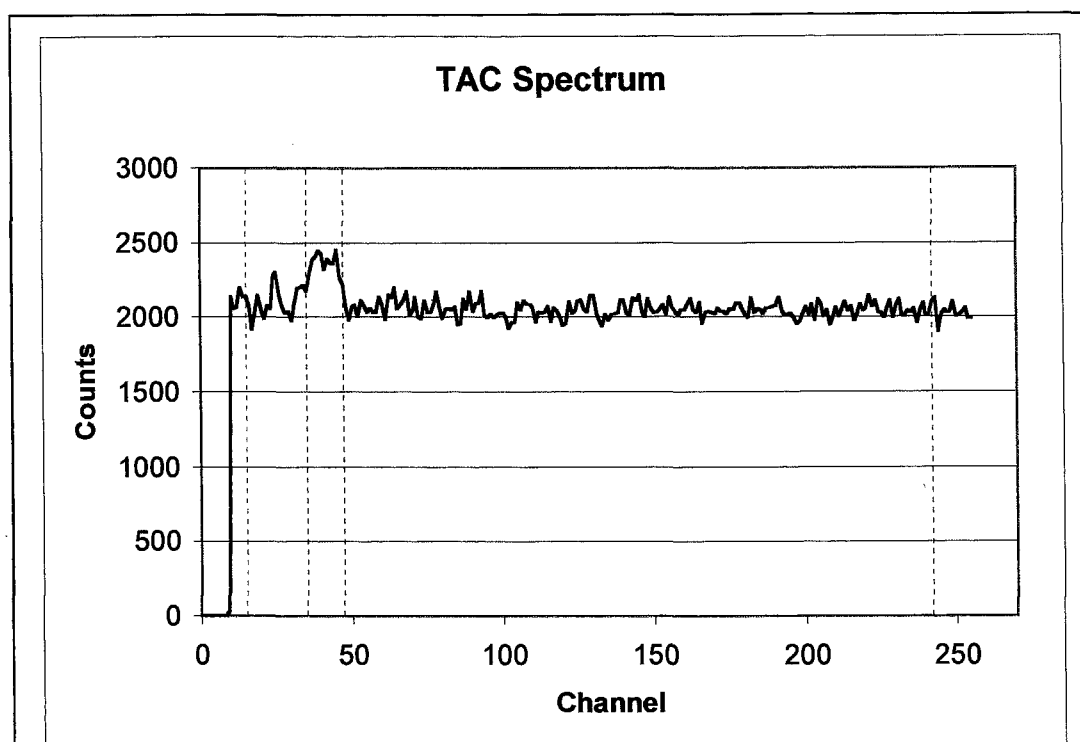


Figure 4.10 TAC spectrum. The x-axis is divided into 256 channels each representing $0.1 \times 10^{-6} / 256$ sec. Distance along the x-axis represents the delay between the start and the stop signal. The y-axis shows the number of start-stop events in each channel. The total number of events in all channels is the singles count for that particular combination of photoelectron and Auger electron energy. For the coincidence count only the events under the coincidence peak and above the background level are counted. The background level in the coincidence channels (35-47) is determined by fitting a cubic function to the other channels 15-34 and 48-242. The zero channel is 47.

The output pulse from each multi-channel plate detector was analysed by a constant fraction discriminator (CFD), which turned it into a square wave pulse of constant width. This pulse was then used as the start or stop signal for a time-to-amplitude converter (TAC), which changed the time difference between the pulses into a voltage. The output from the TAC was fed to a multi-channel analyser (MCA) producing a voltage distribution spectrum. The

x-axis of this TAC spectra was the voltage output of the TAC and hence the time difference between the arrival of the photoelectron and Auger electron at their respective multi-channel plate detectors. For most of the experiments the full-scale deflection of the x-axis was $0.1\mu\text{s}$ and this was divided into 256 increments or channels each of 0.39ns . The y-axis of the TAC spectra represents the number of start/stop events recorded at each time separation. Figure 4.1 contains a schematic of the coincidence circuitry. The pulse from one of the channel plate detectors was delayed for a small time before entering the TAC so that the channel that has electrons arriving with zero time difference does not occur in the first channel of the TAC spectrum. The coincident electrons therefore will peak to the left or right of the zero time channel in the TAC spectrum (Figure 4.10).

Which side of the zero channel the coincidence peak is on is determined by the energy of the two detected electrons. The delay is always placed in line with the pulse that is going to stop the TAC. If both the start and stop electrons from an event have the same energy i.e. the same speed, they arrive and pass through the analysers in the same amount of time. This will place intensity in the channel of the TAC spectrum determined by the introduced delay. If the starting electron is faster than the stopping electron the time between the two pulses will be longer and the coincidence peak will be to the right of the zero channel. If the starting electron is the slower of the

two then the delay will appear to be shortened and the coincidence peak will be to the left of the zero channel.

4.2.9. Resolution

There are two aspects to be considered when discussing the resolution of this system. One is the finite energy resolution of the analysers and the other is the timing resolution of the whole detection system, analysers and electronics.

Energy resolution is determined by the analyser's physical dimensions. Electrons within a small band of energies either side of the selected pass energy may make it through the analysers. The bandwidth of accepted electron energies depends on the path length of the electron within the analyser (determined by distance between the inner and outer sector and radius of curvature of the sectors), and the energy of the transient electrons. The greater the distance between the sectors the wider the energy band for any given pass energy.

The intense photoelectron lines used for chemical analysis are relatively symmetrical. Their width is a convolution of the linewidth of the incident X-rays, the instrument function and the natural linewidth of the state [4]. The wider the energy range of incident photons the wider the energy range of the electrons produced from photoionisation of the same energy level. This

however would not affect the energy distribution of the subsequently released Auger electron as long as the initial photoionisation took place in a discrete energy level.

The analysers also play a part in the timing resolution of the system due to the geometric spread of the paths through the analyser taken by electrons with the same energy [5]. The incident electron may not enter along the axis of the analyser but somewhere within the analyser acceptance angle and still be refocused on the exit aperture. The separation of the sectors within the analyser provides space for a small range of arcing paths through the analyser, all of which have different path lengths. It is possible to minimise this spread in path length by mapping out the position of same energy electrons at equal time intervals and by angling the channel plates to lie along one of these isochronal planes (Figure 4.7) as discussed by Volkel and Sander [9]. This set-up has been used for previous experiments at Murdoch but the channel plates were normal to the central flight path in the experiments for this thesis for mechanical reasons.

There is a time of flight spread through the analysers of 0.8 ns at a pass energy of 145 eV [8] and a time spread of about 0.5 ns is produced by the channel plates [5]. The width of the coincidence peak in the TAC spectrum however indicates a time spread of 4.7 ns (peak covers 12 channels and each channel is $0.1/256 \mu\text{s}$). This width includes the time spread through the

lenses, analysers, channel plates and the electronics. The time of flight spread through the electronics must therefore be 3.4 ns making this the main contributing factor to the width of the TAC coincidence peak. Changes to the time of flight through the analysers due to changes in the pass energy are therefore unimportant by comparison.

With the hemispherical analysers and a new MCA box the full-scale deflection of the TAC was 0.2 μ s for 256 channels instead of 0.1 μ s as with the old analysers. The coincidence peak on the TAC spectrum therefore covered half as many channels i.e. six instead of twelve.

The necessity for good timing resolution is discussed in the data collection section.

4.2.10. Data Collection

During the experiment the APECS spectrum was scanned several times in the twenty-four hour period between each cleaning of the sample. Each scan lasted approximately 90 minutes and consisted of a series of TAC spectra. One TAC spectra was collected for each photoelectron/Auger electron paired energy setting. In this way any effect due to the minimal build up of contamination on the surface was distributed uniformly across all the data.

The daily TAC spectra for each paired energy setting were then added

together and the coincidence and singles count for each paired setting was calculated. These values in turn produced the daily singles and coincidence spectra. Daily data was then added together to produce the final spectra which took a minimum of 4 weeks to collect with the system running 21.5 hours a day 7 days a week. This was a very slow process because of the low coincidence count rate.

The number of true coincidence counts is small, between 1 and 9 counts / hr depending upon the peaks under investigation, compared with the total number of Auger electrons detected (1.0×10^4 counts/sec) at the peak energy of the Auger spectrum. The total count rate is proportional to the x-ray beam flux. The accidental coincidence count rate increases as the square of the total count rate while the true coincidence count rate increases as the total count rate does. [10]. Thus the ratio of true coincidence counts to accidental coincidence counts is inversely proportional to the incident beam flux. A more mathematical discussion of the true to accidental coincidence count rate is given by Thurgate [5]. By reducing the incident beam flux the signal to noise ratio improves but it takes longer to get a reasonable amount of data.

In all cases the singles spectra and the coincidence spectra were generated from the same data set. A TAC spectrum was produced for each paired energy setting of the electron analysers with the number of events for each

start-stop time difference displayed on the y-axis. The coincidence counts therefore are the ones with zero time difference. In practice the coincidence peak spreads over ten of the 256 channels in the TAC spectrum. The delay introduced in either the start or stop signal moves the coincidence peak away from the zero channel by an amount determined by the length of the delay.

The total number of counts above background in these 10 channels gives the coincidence count. The total number of all counts in all the channels of the TAC spectrum gives the singles count for this Auger energy. Thus the value for the singles count and coincidence count are tied to the Auger energy settings being sampled and are measured at the same time. The background level in the TAC spectrum under the coincidence peak was determined by ignoring the coincidence peak and fitting a cubic least-squares fit to the remaining data.

Any difference in the final shape of coincidence and singles peaks over the scanned energy range is real and cannot be attributed to scaling factors or misalignment. It is expected that there will be differences between the singles and coincidence spectra because the singles spectrum contains intensity from all processes, no matter what their originating photoelectron energy. The coincidence spectrum however contains intensity from only those processes associated with photoelectrons of a specific energy.

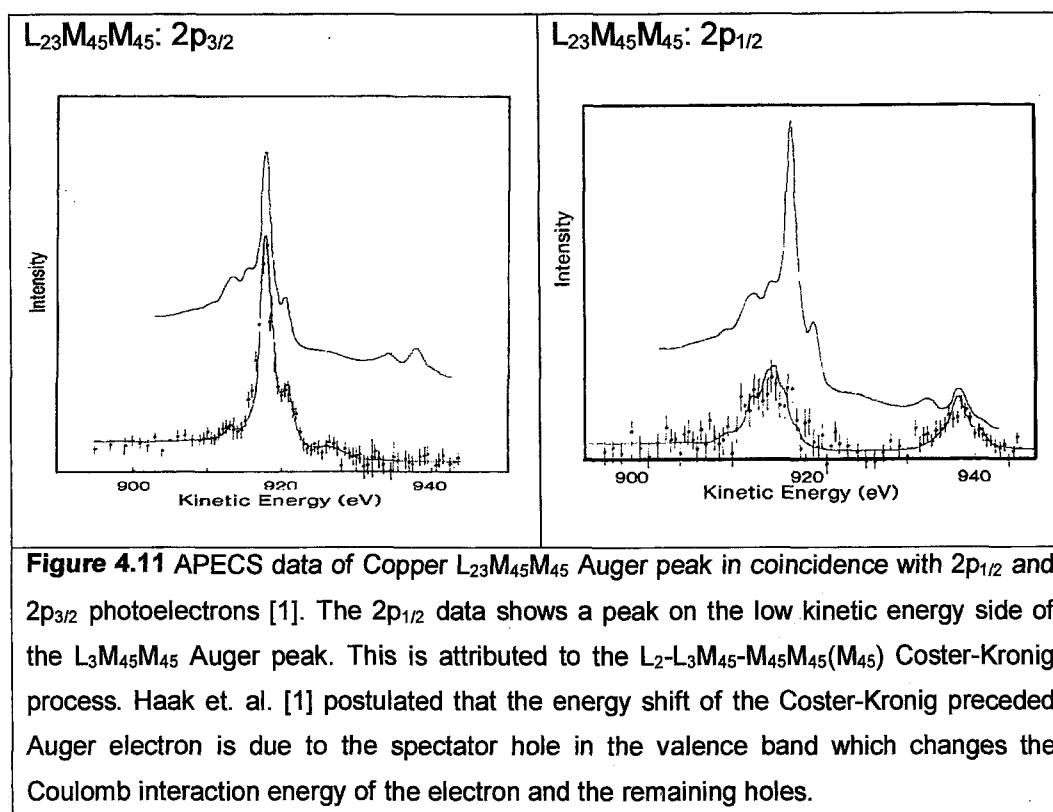
Another difference between the singles and coincidence spectra may arise because on average the escape depth of the coincidence electrons is less than the average escape depth of the singles electrons. In other words the events that are counted in coincidence spectroscopy come from closer to the surface than events that are recorded in singles Auger spectroscopy. The electrons counted in coincidence suffer less energy loss than electrons counted in the singles spectrum and this results in narrower Auger peaks in coincidence [11] (discussed further in section 4.4.3).

4.3. Historical Perspective of APECS

In 1978 the power of APECS was demonstrated by Haak [1, 12] who used it to differentiate between the intensity arising from the Coster-Kronig process $L_2-L_3M_{45}-M_{45}M_{45}(M_{45})$ and a final-state shake processes which placed intensity in the same part of the Copper Auger spectrum.

As can be seen in Figure 4.11 the Copper Auger spectrum has been physically separated into its component peaks. The Auger lineshape contains intensity arising from the simple 2-hole Auger processes $L_2-M_{45}M_{45}$ and $L_3-M_{45}M_{45}$ and also the more complex Coster-Kronig process $L_2-L_3M_{45}-M_{45}M_{45}(M_{45})$. There have been several other APECS experiments since 1978, many carried out by the Murdoch group, with the same intention of investigating the processes that contribute to the Auger lineshape.

Investigation of Tin and Palladium in this thesis adds to the knowledge and aids in the understanding of the Auger lineshape of elements.



Other interesting aspects of Haak's work

- Haak [1] found two peaks in the $L_{3}M_{45}M_{45}$ energy range of the Copper Auger spectrum. The first was the basic 2-hole Auger process and the second the Coster-Kronig $L_{2}-L_{3}M_{45}-M_{45}M_{45}(M_{45})$ process. The second peak was shifted to a lower kinetic energy with respect to the first because of the spectator hole in the valence band which increases the value of U . This made the peak more atomic-like and shifted the centroid to lower kinetic energies. This was a practical demonstration of the Cini-Sawatzky

theory. He provided another demonstration by comparing the widths of Nickel and Copper Auger spectra. The Nickel data had increased linewidth because the lower U/W value for Nickel resulted in more intensity in the band-like part of the spectrum [12].

- He demonstrated the existence of the $L_1-L_2M_{45}-M_{45}M_{45}(M_{45})$ Coster-Kronig processes in Copper [12].
- He also studied a CuNi alloy and was able to remove the overlapping Copper Auger spectrum from the Nickel spectrum by examining it in coincidence with the Nickel 2p lines [12].
- He found that the low kinetic energy tail associated with a characteristic feature was greatly reduced in coincidence when compared to the conventional Auger or photoelectron spectra [1]. This was due to the surface sensitivity of the experiment.

Sawatzky, Haak's thesis supervisor, demonstrates a great understanding about the inter-relationship between photoemission and Auger spectroscopy and the experimental apparatus needed to do APECS in his chapter on APECS in the book *Treatise on Materials Science and Technology* [13]. He discusses Haak's data in depth with respect to the Cini-Sawatzky theory. While this chapter did not add any new experimental information the amount

of thought and the depth of explanation makes this an essential document for the toolbox of the APECS research student.

Haak et. al. [1] proposed APECS could be used for

- surface studies because of the surface sensitivity of the procedure
- intrinsic versus extrinsic contributions to lineshape and satellites because the extrinsic contributions are strongly reduced.
- studying satellite structure – resolving the Auger peak into curves relating to the main photoelectron excitation and those originating from the satellites
- studying the contributions to the XPS and AES lineshapes.

The work by Haak and Sawatzky formed the basis for following APECS experimentation.

4.4. The Advantages of APECS Spectra

4.4.1. Selection of specific decay processes

When using APECS different decay processes can be selected by the placement of the stationary analyser. For example placing it on a low kinetic energy shoulder of an XPS line would select the 3-hole initial-state shake-up/off process, which would place intensity in the 3-hole position of the Auger peak. Placing it on the peak of the XPS line will select the 2-hole process

(including intrinsic plasmon loss/gain), Coster-Kronig process and any 3-hole final state shake-up/off process, all of which place intensity in different parts of the Auger spectrum.

A reverse experiment could also be done where the Auger analyser is fixed and the XPS line is scanned. This would give information about the photoelectrons and thus the decay processes that placed intensity in the selected part of the Auger spectrum. This technique is useful for distinguishing between 3-hole processes that place intensity on a low kinetic energy shoulder of the Auger peak, for example initial state shake-up/off, and Coster-Kronig processes. A more detailed description of how APECS can be used to differentiate between selected decay processes can be found in Appendix iv.

The main disadvantage of APECS is the low count rate. Where an XPS or AES spectrum can be done in a matter of minutes each APECS spectrum of Palladium and Tin for $M_{45}N_{45}N_{45}:3d_{3/2}$ and $M_{45}N_{45}N_{45}:3d_{5/2}$ took months. Fortunately recent improvements in the electron detection equipment have reduced the time for the most intense Auger peak and photoelectron line coincidence experiments to a matter of weeks. Even with these improvements less intense coincidence spectra such as Tin $M_{45}N_{45}N_{45}:3p_{3/2}$ still have collection times above the one-month mark.

4.4.2. Reduction of non-related background

In the electron energy spectrum the background intensity increases when going from high to low kinetic energy. This intensity is from electrons that have lost energy as they leave the material or from electrons released by cascade processes. Background electrons under an Auger peak may not even be linked to the Auger peak being investigated but may be from XPS and AES peaks at higher kinetic energies. APECS removes all this background from the Auger peak because it is not related to the selected initiating photoelectron. The most spectacular demonstration of this effect was by Bartynski et. al. [14] in the N_3VV Auger spectrum of Silver. In the singles spectrum there is no detectable feature associated with the Auger peak whilst in the coincidence spectrum there is well-defined structure.

4.4.3. Reduction of low kinetic energy broadening of the Auger peak

Scanning the Auger peak in coincidence with defined photoelectron energy removes low kinetic energy broadening of the peak due to inelastic scattering of the Auger electron. The effective IMFP for coincidence depends on the IMFP for both the photoelectron and Auger electron as in Equation 4.1 The coincidence IMFP should therefore be used with Tougaard's formula to subtract the inelastic background from the coincidence data.

$$1/\lambda_{\text{coincidence}} = 1/\lambda_{\text{Auger}} + 1/\lambda_{\text{photoelectron}}$$

Equation 4.1 [13]

$\lambda_{\text{coincidence}}$ is the effective IMFP for coincidence

$\lambda_{\text{photoelectron}}$ is the IMFP for the photoelectron

λ_{Auger} is the IMFP for the Auger electron

Sometimes this modification is described as a reduction of IMFP in coincidence, which is not strictly true. The IMFP of the photoelectrons and Auger electrons remain unchanged. What the coincidence experiment does is select peak photoelectrons with minimal energy loss. These on average would be closer to the surface than other photoelectrons that contribute to the photoelectron line [1]. As the Auger electrons arise from these self-same atoms they must also on average be closer to the surface. So APECS is more surface sensitive than XPS or AES. More surface sensitive means less inelastic scattering and a reduction of intensity on the low kinetic energy side of the coincidence Auger peak compared to the singles peak for the same energy region. This reduction in intensity was first demonstrated by Haak et. al. in 1978 [1] and has since been proven many times by the Thurgate group.

Equation 4.1, originally given by Sawatzky [13] defined λ as the escape depth for a single event. The MED as previously discussed is dependent not only on the energy of the electron and the material under investigation but also on the geometry involved in the experiment. When this equation was first used the assumption would have been that elastic scattering had no

effect on the energy of the emitted electrons and so the MED would be proportional to the IMFP and either value could be used. Jablonski and Powell [15] recommended the use of the IMFP for quantitative AES rather than other measurements because it is more reliable and accessible.

In performing lineshape analysis at Murdoch the photoelectron or Auger electron IMFP used with the singles spectrum would be one of the values calculated by Tanuma et. al. [16-20]. The IMFP values for Palladium are given in Table 4.1 with the error in IMFP being about 13% for electron energies in this range.

Table 4.1 Palladium IMFP - Electron Energies in the Range 200 to 1000eV

eV	50	100	150	200	300	400	500	600	700	800	900	1000
Pd IMFP (A)	4.8	4.8	5.4	6.2	7.8	9.4	11	12.5	14	15.4	16.8	18.2

[16, 17]

4.4.4. Identification of shake processes

Once the inelastic background has been removed from the singles and coincidence spectrum these two spectra can then be compared. The coincidence spectra will now contain only primary and diffuse primary electrons that are initiated with the photoionisation of the energy level under investigation i.e. the simple Auger 2-hole process, the 3-hole final-state

shake, Coster-Kronig and plasmon loss process. Initial-state shake processes will not place intensity in the coincidence spectrum. They rob the initiating photoelectron of energy placing it at a lower kinetic energy than the selected photoelectron at maximum intensity. Initial-state shake processes will however be included in the singles Auger spectrum. A difference between the singles and coincidence spectrum on the low kinetic energy side of any Auger peak, after the effect of their respective IMFP values have been taken into account, could be due to initial-state shake processes. Using this logic Lund and Thurgate [21, 22] were able to show that there were no initial-state shake processes in either Silver $M_{45}NN$ or Gallium $L_{23}M_{45}M_{45}$ Auger peaks as intensity was comparable for both singles and coincidence spectra on the low kinetic energy side of the Auger peak. These shake processes can extend 2 – 3 inelastic scattering events (~ 50 eV) below the peak. By using the Tougaard background subtraction process, which does not depend on the person doing the analysis to determine how far down this intensity extends, it is safe to say the Auger peak contains all the intensity arising from intrinsic processes. Figure 4.12 demonstrates the contribution to the background on the low kinetic energy side of the Auger peak of the above-mentioned effects.

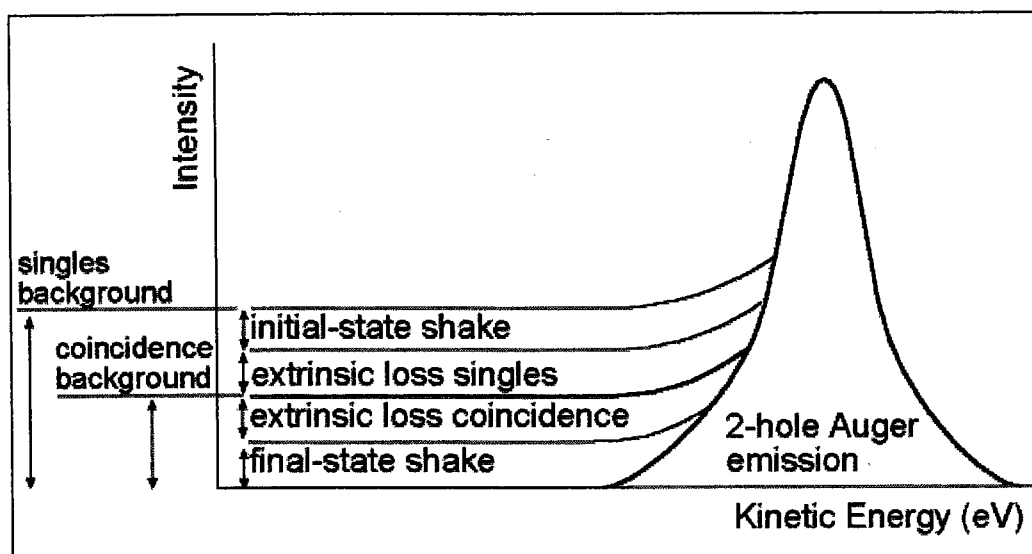


Figure 4.12 Diagram showing the components of the low energy tail of the Auger peak [23]

When looking at $M_{45}NN:3d_{3/2}$ or $L_{23}MM:2p_{1/2}$ coincidence data any intensity above that due to extrinsic loss processes in the low kinetic energy tail is most likely from final-state shake processes. Plasmon loss processes are possible but intensity from Coster-Kronig processes are usually sufficiently removed to have no impact on intensity in this area. Final-state shake processes are detected in coincidence data because they originate with photoelectrons from the peak of the photoelectron line in the coincidence experiment.

In their coincidence investigation of the $M_{45}NN$ Auger spectrum of Silver Arena et. al. [24] found removing the extrinsic background from Auger peaks of atoms with closely spaced core levels to be rather difficult. This was because intensity from the diffuse primary electrons of the higher kinetic

energy photoelectron line added intensity to its lower kinetic energy counterpart. When this lower kinetic energy line was used as the energy for the fixed analyser in the coincidence experiment the coincidence Auger spectrum produced had intensity related to both the photoelectron line under investigation and to the higher kinetic energy photoelectron line. They were using Ultra Violet radiation that produced Ag $3d_{3/2}$ and $3d_{5/2}$ photoelectrons in the energy range of 100eV-125eV. The lower the energy of the electrons under investigation the greater the inelastic background. So the inelastic background would be much larger for Arena et. al. than similar experiments performed by the Thurgate group who use Mg $K\alpha$ X-rays as their ionising radiation. This places the same photoelectron lines in the 870eV-890eV energy range.

4.5. The Work of the Murdoch Group

In 1988 Thurgate and Todd [6] built the APECS system at Murdoch University. Originally it was designed to do electron excited coincidence Auger spectroscopy but was easily modified to use X-rays. The Murdoch studies include elements, alloys and oxidised surfaces (Table 4.2). The origins of the three-hole final state in the $L_3M_{45}M_{45}$ Auger spectrum of Copper [25, 26] was the area of investigation for the honours thesis of this author.

For the 3d transition metals the $L_{23}M_{45}M_{45}$ Auger spectra was studied in coincidence with $2p_{1/2}$ and $2p_{3/2}$ photoelectron lines and for 4d elements the

$M_{45}NN$ Auger spectra was investigated in coincidence with $3d_{3/2}$ and $3d_{5/2}$ and $3p_{3/2}$ photoelectron lines. The Auger spectra of the 4d metals are more complex than the 3d because of the greater number of possible decay processes following ionisation of a core energy level. The energy difference between the core levels initiating the Auger processes are also closer together in the 4d metals so the 4d Auger spectra overlap more.

Table 4.2 3d and 4d Transition Metals

3d	$L_{23}M_{45}M_{45}$ with $2p_{3/2}$ and $2p_{1/2}$	Mn	Fe	Co	Ni	Cu	Zn	Ga in Ge		
4d	$M_{45}N_{45}N_{45}$ with $3d_{5/2}$, $3d_{3/2}$ and $3p_{3/2}$	Tc	Ru	Rh	<u>Pd</u>	Ag	Cd	In in Sn	InP	Sb

Elements in bold have been studied by the Murdoch group. Those underlined are the focus of this thesis.

In the 3d transition metals several trends can be seen in the processes contributing to the Auger lineshape as atomic number increases. These have been demonstrated at Murdoch using the APECS technique. For example the Auger spectrum changes from band-like in Iron and Cobalt, to mixed in Nickel and atomic-like in Copper and Gallium [5, 11, 27, 28]. Changes in intensity due to Coster-Kronig processes are also seen being most probable in Iron and Cobalt less probable in Copper and not occurring at all in Gallium [5, 27, 28]. A summary of the information gleaned from the investigations at Murdoch is given in Table 4.3 and 4.4 and Table 4.5 shows a sample collection of Murdoch coincidence spectra for the 3d and 4d elements.

Table 4.3 Information on the 3d and 4d Transition Metals

	Fe	Co	Ni	Cu	Zn	Ga in GaAs	Ge
Electronic configuration	(Ar)3d ⁶ 4s ²	(Ar)3d ⁷ 4s ²	(Ar)3d ⁸ 4s ²	(Ar)3d ¹⁰ 4s ¹	(Ar)3d ¹⁰ 4s ²	(Ar)3d ¹⁰ 4s ² 4p ¹	(Ar)3d ¹⁰ 4s ² 4p ²
Valence band width (W) [29]	3.5eV	3.2eV	2.9eV	2.75eV	1.6eV	1.6eV	1.4eV
Hole-hole interaction energy (U _{eff}) [29]	1.3eV	1.3eV	2.4eV	8.1eV 6.7eV [7]	9.6eV	11.2eV	12.9eV
U/W	0.37	0.41	0.83	2.44 - 2.95	6	7	9.21
Type of peak	Band-like	Band-like	Mixed	Mostly Atomic-like	Atomic-like	Atomic-like	
Work function [30]	4.5eV	5.0eV	5.15eV	4.65eV	4.33eV	4.2eV	5.0eV
Binding energy M ₅ [30]					10.1eV	18.7eV	29.2eV
Binding energy M ₄ [30]					10.2eV	18.7eV	29.8eV
Binding energy M ₃ [30]	52.7eV	58.9eV	66.2eV	75.1eV	88.6eV	100.0eV	120.8eV
Energy differ 2p energy levels (ΔE_{2p}) [4]	13.10eV	14.97eV	17.27eV	19.80eV	22.97eV	26.84eV	
FWHM of L _{2,3} :cK _{MM} [27]	6.3eV + /-2%	3.7eV + /-2%	2.5eV + /-2%			No C-K	
Initial-state shake	yes	yes	yes	yes		no	
Final-state shake	yes	yes	yes	yes		no	
Plasmons	no	no	no	no		yes	

	Ru	Rh	Pd	Ag	Cd	In in InP	Sn
Electronic configuration	(Kr)4d ⁷ 5s ¹	(Kr)4d ⁸ 5s ¹	(Kr)4d ⁸ 5s ²	(Kr)4d ¹⁰ 5s ¹	(Kr)4d ¹⁰ 5s ²	(Kr)4d ¹⁰ 5s ² 5p ¹	(Kr)4d ¹⁰ 5s ² 5p ²
Valence band width (W) [29]	6.1eV	5.5eV	5.1eV	4.0eV	2eV	2eV	2eV
Hole-hole interaction energy (U) [29]			7.1eV [31]	3.6+/-0.2eV [32]	1.9+/-0.1eV [32]	1.9+/-0.1eV [32]	2.0+/-0.1eV [32]
U/W			3.1eV	5.1eV	6.1eV	6.5eV	6.7eV
			2.8 - 3.1eV [33]	5.1+/-0.7eV [32]	6.0+/-0.6eV [32]	6.8+/-0.7eV [32]	6.9+/-0.6eV [32]
			0.39 - 0.61	1.28 - 1.42	3.05 - 3.12	3.25 - 3.58	3.35 - 3.45
			0.4 this thesis				
Type of peak			Band-like	Mixed		Atomic-like	Atomic-like
Work function [30]	4.71eV	4.98eV	5.12eV	4.26eV	4.22eV	4.12eV	4.42eV
Binding energy N ₅ [30]					10.7eV	16.9eV	23.9eV
Binding energy N ₄ [30]					11.7eV	17.7eV	24.9eV
Binding energy N ₃ [30]	15.3eV	47.3eV	50.9eV	58.3eV	63.9eV	73.5eV	83.6eV
Energy difference 3p energy levels [4]	4.17eV	4.74eV	5.26eV	6.00eV	6.74eV	7.54eV	8.41eV
Ratio 3d _{3/2} :3d _{5/2} linewidth [34]	3.04	3.04	1.22	1.00	1.00	1.00	1.00
M ₄ :M ₅ :cK _{NNN}			yes	no		no	yes
Energy differ 3p _{3/2} 3d _{3/2} energy levels [30]	177.0eV	184.5eV	191.5eV	198.6eV	206.0eV	213.5eV	221.1eV
Ratio 3p _{3/2} :3p _{1/2} linewidth [34]	0.98	1.00	1.06	1.06	1.11	1.10	1.05
M ₃ :M ₄ :cK _{NNN} and M ₃ :M ₅ :cK _{NNN}				both		both	both
Initial-state shake				no			
Final-state shake			yes	no			
Plasmons			no	no		yes	yes

Information from the investigations at Murdoch (red text – this thesis, blue text – other experiments)

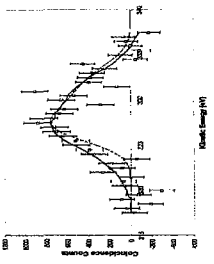
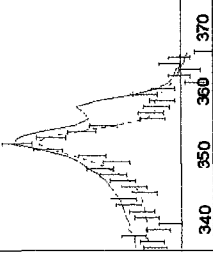
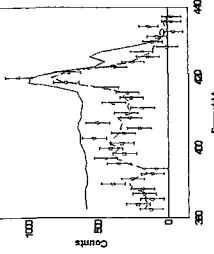
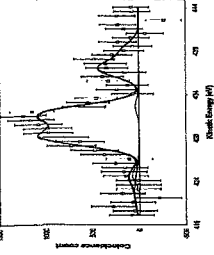
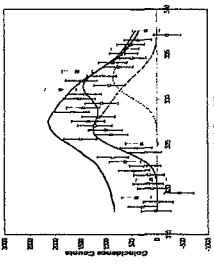
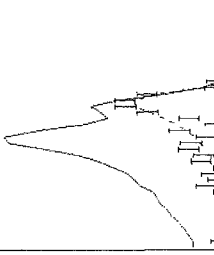
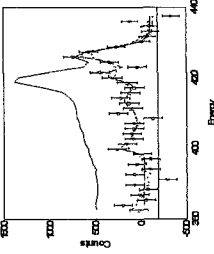
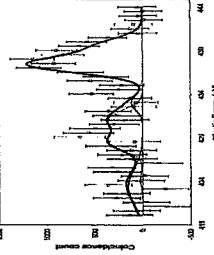
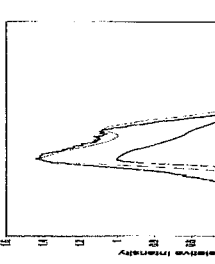


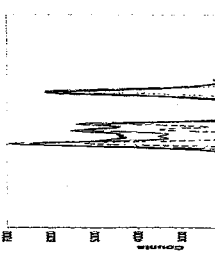
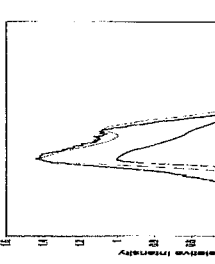


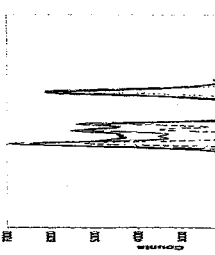
Table 4.4 Murdoch University APECS Experiments

3d Element	Type of spectra	Other Comments	Reference
Fe	band	$L_2:L_3:CKM_{45}M_{45}M_{45}$ satellite $0.8+/-0.2$ eV below $L_3M_{45}M_{45}$ 2-hole position. Large Coster-Kronig transition rate. No change in U from 2 to 3-hole processes (Auger energy level not pulled out of band after photoionisation).	[5, 27, 28, 35, 36]
Co	band	$L_2:L_3:CKM_{45}M_{45}M_{45}$ satellite $0.5eV$ ($1.1+/-0.2eV$ depending on which paper) below $L_3M_{45}M_{45}$ 2-hole peak position. It is only $0.5eV$ and not $2.5eV$ as in Cu because the valence band is better screened from the Auger process than in Cu. The 3-hole Coster-Kronig peak is narrower than the peak for the 2-hole process indicating an increase in the value of U for the 3-hole situation. This element has the highest Coster-Kronig transition rate of these 3d materials. 2-hole U $1.8eV+/-0.2eV$, Coster-Kronig U $1.0eV+/-0.2eV$	[5, 11, 23, 27, 28, 35, 36, 36, Thurgate, 1999 #107, 37]
Ni	mixed	$L_2:L_3:CKM_{45}M_{45}M_{45}$ satellite but no energy shift. The Coster-Kronig transition rate is less than Co but more than Cu. A band-like curve seen in coincidence with $2p_{3/2}$ but not $2p_{1/2}$ this is due to the Coster-Kronig process producing a spectator hole in the valence band which increases U and makes the Auger peak for the $2p_{1/2}$ decay processes more atomic-like.	[5, 11, 27, 28, 35, 36, 38]
Ni in Ni ₇₀ Fe ₃₀		Reverse experiment from 3-hole position on Auger spectrum indicates initial state shake processes $2eV$ below $2p_{3/2}$ photoelectron line. MgK α_3 ghost satellite seen.	[38]
Ni in Ni ₅₀ Fe ₅₀	atomic	$L_2:L_3:M_{45}M_{45}M_{45}$ satellite whose rate decreases in the Ni ₅₀ Fe ₃₀ alloy process compared to pure Ni. Reduced probability of final-state shake up/off processes on alloying but increased probability of initial-state shake up/off. This results in a singles spectrum that remains the same. Evidence of narrowing of valence band (W) on alloying i.e. Auger spectra becomes totally atomic-like.	[23, 37, 39]
Cu	Atomic with small band-like part	$L_2:L_3:M_{45}M_{45}M_4$ satellite $2.5eV$ below $L_3M_{45}M_{45}$ 2-hole peak. Coster-Kronig rate is less than Ni. Evidence of $L_1-L_2M_{45}-M_{45}M_{45}(M_{45})$ Coster-Kronig process. Reverse experiment from $4.5eV$ below the $L_3M_{45}M_{45}$ 2-hole peak gave a $0.9eV$ shift in the photoelectron line to lower kinetic energies. Conservation of energy dictates that the energy lost by the Auger and photoelectron is gained by the Coster-Kronig electron. Reverse experiment from the $1G$ term of $L_3M_{45}M_{45}$ 2-hole produces a $2p_{3/2}$ photoelectron line $0.25eV$ to higher kinetic energy than centroid of singles peak. Reverse experiment from the $3F$ term on the high kinetic energy side of the Auger peak produces a photoelectron line shifted $0.15eV$ to lower kinetic energies. This indicates an interaction between the initial state following photoionisation and the final state following Auger electron release. i.e. the Auger process is not a two-step process. The lineshape of the photoelectron line can be made from the sum of these two coincidence curves.	[2, 3, 5, 7, 11, 23, 26-28, 35-37, 40-44]
Cu oxidised	more band	As the APECS technique is very surface sensitive the signal comes more from the surface ie CuO and not bulk Cu. Oxidation shifts the $L_3M_{45}M_{45}$ Cu Auger peak by $0.6eV$ to lower kinetic energy. The peak is band-like with a U/W of around 0.2	[7]
Ga in GaAs	atomic	Ga is outside the 3d series. Evidence for bulk plasmon loss $16.3eV$ and surface plasmon loss $11.5eV$ below parent Auger peaks. Data includes a reverse experiment.	[5, 22, 27, 28, 35, 36]

4d Element	Type of spectra	Other Comments	Reference
Pd	band	$M_{4L}M_{5C}CKNNN$ Coster-Kronig satellite. Ratio of peak heights $M_{4L}M_{5C}CKNNN$ to M_{4NN} is 1.45:1.00	[45]
Ag	mixed	Band-like peak 6eV higher kinetic energy than main peak and about 19+/-3% of the atomic peak intensity	[21, 46]
In in InP		Surface plasmons at 10.6eV below the parent peak. A 1S_0 term 4eV below parent peak which is more intense in the $M_{4L}N_{45}N_{45}$ than the $M_{5L}N_{45}N_{45}$ peak.	[46]
Sn	atomic	Evidence of $M_{4L}M_{5C}CKNNN$ Coster-Kronig process. Relative height of $M_{4L}M_{5C}CKNNN$ to M_{4NN} was 0.30:1.00. Also evidence of $M_{3L}M_{4C}CKNNN$ and $M_{3L}M_{5C}CKNNN$ Coster-Kronig processes with the relative height of the two 0.90:1.00 Plasmons at 14.6eV below the parent peak. Evidence of $MgK\alpha_3$ x-ray satellite. A 0.7eV shift of the singles data but not the coincidence data due to oxidation of the surface in the time between cleaning.	[47]

Table 4.5 Coincidence Plots for the Elements Studied by the Murdoch Group

	Fe	Co	Ni	Cu	Ga
$L_{23}M_{45}M_{45}2P_{3/2}$					
$L_{23}M_{45}M_{45}2P_{1/2}$					

$M_{45}N_{45}N_{45}3d_{5/2}$				
$M_{45}N_{45}N_{45}3d_{3/2}$				
$M_{45}N_{45}N_{45}3p_{3/2}$				
<p>Model derived from coincidence spectra compared to high resolution AES</p>				

It has been the intention of the group at Murdoch to do a similar study of the 4d transition metals and this thesis looks at two of them, Palladium and Tin.

The lineshape of the Auger spectrum is complex but not beyond understanding. It is the sum total of several processes which place intensity not only in the peak energy position but also some distance away in a low energy tail. This tail can contain intensity from initial-state shake, final-state shake, Coster-Kronig and plasmon loss processes. If the first three of these processes are allowable then the rate with which they proceed depends upon the structure of the electron orbitals within the atom, the binding energy of the valence electrons and the separation of the core energy levels [11, 27, 46, 48]. The shape of each component peak in the Auger lineshape is determined by the width of the valence band and the Coulomb interaction of the holes created as the Auger electron leaves the atom (see chapter on Cini-Sawatzky theory). As the structure of the atomic energy levels are characteristic of the element no two elements can expect to have exactly the same processes with the same relative intensity combining to create the Auger lineshape. The changes that take place in the structure of the energy levels of the atom as one moves across the periodic table are not random and as a pattern can be seen in these changes so too a pattern emerges in the changes in the Auger lineshape.

As atomic number increases across the 3d and 4d rows of the periodic table the valence bandwidth (W) decreases and the hole-hole interaction energy or Coulomb force (U) increases [29]. This coincides with a progression in the type of Auger spectra from band-like for values of $U/W \ll 1$ e.g. Fe, Co, Pd to mixed for values of $U/W \sim 1$ Ni, Ag to atomic-like for values of $U/W \gg 1$ Ga, In, Sn as the atomic number increases (see Tables 4.3 to 4.5 and the chapter on Cini-Sawatzky Theory).

The Murdoch group found in the 3d transition metals the Coster-Kronig rate decreases as the atomic number of the element increases [27]. The Coster-Kronig rate depends on a balance between the energy released by the electron transition in the core levels and the amount of energy a valence electron needs to escape. The energy difference between the core holes increases with atomic number [4] so if all other things remain constant the Coster-Kronig rate should increase across the row. It does not therefore other factors must therefore be contributing to the declining Coster-Kronig rate. The minimum amount of energy needed for the valence electron to escape from the material depends upon the work function of the material and the binding energy of the electron with respect to the Fermi level in the solid. The values given in Appendix iv show the work function of the 3d metals increases from Fe to Ni then decreases from Ni to Ga and so it is unlikely that decrease in Coster-Kronig rate can be a result of the changes in the work function. Increasing binding energy with atomic number for all given energy levels could however be the reason for the declining Coster-Kronig rate in the 3d metals.

The 4d elements are more complex. The energy released by the electron transition between core levels ($M_4 - M_5$) increases (less than the rate of the 3d materials) [4] and the binding energy of the outer electrons also increases [30] but the Coster-Kronig rate does not have a steady trend as with the 3d elements. There seems to be no simple answer to the problem of what determines the Coster-Kronig process in the 4d transition metals and this would be a further profitable area for APECS studies.

Shake processes complicate the Auger lineshape further. They contribute to the low intensity tail of the Auger peak and are more likely in elements with a high density of filled and unfilled states close to the Fermi level i.e. the Fermi level is within the incomplete d-band. It is therefore no surprise that the APECS experiment found there are no initial or final-state shake processes in Gallium [27] as the Fermi level is outside the 3d band. They would also not be expected in pure Indium or Tin for the same reasons. No shake processes means that plasmon loss processes are more obvious and this effect was observed in the APECS spectrum of Gallium [30].

4.6. Other APECS Research

Another group of scientists have been doing APECS experiments since 1988 at the National Synchrotron Light Source at Brookhaven National Laboratory, Upton, NY, USA [10]. They are using bright, tuneable synchrotron radiation from the vacuum ultra-violet (VUV) storage ring to

produce a monochromatic photon source. A list of the people who have worked in this group can be found in the Appendix v.

They have studied Silver [14, 49], Aluminium [10], Copper [10, 50], Ruthenium [51], Tantalum [10, 52, 53], Titanium [54] and Gallium Arsenide [55]. An advantage of using synchrotron radiation is that the energy of the photons can be selected which in turn determines the atomic orbitals to be ionised. Any electron with a binding energy greater than the photon energy will not be ionised. This removes complexities in the Auger singles spectrum from Coster-Kronig processes originating in higher binding energy orbitals and allows comparisons between the coincidence and singles spectrum to give information about shake processes.

Arena et. al. [56] have performed APECS on Palladium surface alloys and found d-band movement away from the Fermi Energy on alloying but not as great as expected. They attribute this discrepancy to the neglect of lattice relaxation in the calculations. Their findings have only been released as a conference paper to date and further papers are expected.

In their work Jensen et. al. [10, 50] have experienced narrowing of the linewidths in coincidence and reduction of background intensity when going from singles to coincidence due to the nature of the coincidence experiment as we have. Ohno [57] has recently considered the mechanisms involved in the Auger process and why intensity in

coincidence spectroscopy differs from that in AES. He postulates that APECS researchers even though they are investigating individual processes are still considering the average outcome of that process. The APECS spectrum however may differ from the expected average because particular outcomes even within the same process are selected by the experimental configuration. Another interesting point he raises that has not previously been considered is that the photoelectron spectrum in coincidence is dependant on the final density of states. In recent communications with the Murdoch group Ohno has raised doubts about the intensity ratios obtained for the Palladium model curves. These doubts are based on a multiplet splitting approach to the structure of the Palladium $M_{45}NN$ Auger lineshape made by Martensson and Nyholm [34]. As will be seen in the next chapter this was also the approach used by Weightman [33]. Martensson et. al. [58] did indicate the difficulties in creating a model Auger lineshape using this approach

“the multiplet levels of the $N_{45}N_{45}$ final-state configuration will be considerably broadened.....and therefore the quasiautomic aspects of the Auger spectrum are not immediately discernible”

The APECS data for the $M_{45}NN:3d_{5/2}$ spectrum indicated that it was not possible to use this approach.

In studies on Tantalum [52] Jensen et. al. found that the Auger signal from surface atoms was different to that from the atoms in the bulk of the material due to the different bonding environment of the surface atoms compared to the bulk. They also found the threshold energy of the

photons needed to produce photoelectrons was higher for surface atoms than for bulk atoms because of the increased binding energy of the surface atoms. In a reverse experiment on Aluminium (2p photoelectron lines in coincidence with the LVV Auger peak) [10] the surface sensitivity of the APECS process was demonstrated by looking at the surface and bulk plasmon loss section of the 2p Aluminium photoelectron spectra. In coincidence the relative height of the peak due to the bulk plasmon was reduced by about 40% from the singles while the surface plasmon peak shows little change in intensity. This correlates with our experiments on Gallium, which could also differentiate between surface and bulk plasmons

In 1992 Jensen et. al. [10] studied the Auger spectrum of Aluminium metal exposed to Oxygen. They used the parts of the Aluminium 2p photoelectron spectrum arising from clean metal, chemisorbed oxygen on aluminium and ionically bonded aluminium oxide in coincidence with the Auger spectrum. Each position on the photoelectron peak produced a different coincidence spectrum and from this they were able to determine which parts of the Al $L_{23}VV$ Auger peak were related to which oxidation states. We have studied Copper extensively and noted Auger spectrum changes from atomic-like to band-like [7] as the surface becomes oxidised.

As stated before the Brookhaven group have the ability to tune the energy of the ionising photons and with a count rate of 0.5 counts/s [10]

compared to the Murdoch count rate of 9 counts/hr APECS using synchrotron radiation is very effective. The ionising radiation on the synchrotron VUV beamlines U14A and U16B, where it is possible to perform APECS experiments, is in the range 15-300eV and 50-1000eV respectively [59]. Thus the Brookhaven group are limited to electrons from core levels with binding energy less than 1000eV. The system at Murdoch has an Mg $K_{\alpha_{1,2}}$ X-ray source that produces photons with 1253.6eV and can therefore probe deeper into the atom than the Brookhaven group can.

Another group capable of performing APECS are using the ALOISA beamline at the ELETTRA Synchrotron Light Source in Trieste, Italy [60]. A list of the people working on this project can also be found in the Appendix viii. Beamline 7.2 R - Surface Diffraction ALOISA became operational at the end of 1996. The energy range of the ionising photons in the beam is 200 - 2000 eV. So far there have been test experiments that include momentum resolved coincidence spectroscopy. An interesting result from a Cu(111) sample showed an angular dependence between photoelectrons and $L_3M_{45}M_{45}$ Auger electrons [61].

Recently APECS experiments on Silicon have been performed at the European Synchrotron Radiation Facility in Grenoble Cedex, France [62]. The group working there is attempting to combine APECS with the X-ray Standing Wave technique (XSW). At the moment it appears they are still working out the capabilities of the equipment but access to 5keV monochromatic X-rays should produce some very interesting results. A

low secondary background because of high energy X-rays, high count rates and K-shell ionisations promise to add a new dimension to APES studies.

It has been 24 years since Haak [1] performed the first APECS experiments. Since then there have been technical and conceptual improvements in APECS which have made it possible for the experiment to become a useful tool in lineshape analysis of the electron emission spectrum. Murdoch University APECS experiments have been an integral part of this investigative process and the result of this thesis are a small but important part of the whole picture.

-
1. Haak, H.W., G.A. Sawatzky, and T.D. Thomas, *Auger-Photoelectron Coincidence Measurements in Copper*. Physical Review Letters, 1978. **41**(26): p. 1825 - 1827.
 2. Thurgate, S.M., *Auger Photoelectron Coincidence Spectroscopy*. Australian Journal of Physics, 1990. **43**: p. 443 - 451.
 3. Thurgate, S.M., et al., *More Auger Photoelectron Coincidence Spectra From Copper*. Journal of Electron Spectroscopy and Related Phenomena, 1998. **93**: p. 209 - 214.
 4. Moulder, J.F., et al., *Handbook of X-ray Photoelectron Spectroscopy*, ed. J. Chastain. 1992: Perkin Elmer Corporation.
 5. Thurgate, S.M., *Auger Photoelectron Coincidence Experiments from Solids*. Journal of Electron Spectroscopy and Related Phenomena, 1996. **81**: p. 1 - 31.
 6. Todd, W., *Electron Excited Coincidence Auger Electron Spectroscopy off Solid Surfaces*, in *School of MPS*. 1989, Murdoch University: Perth, WA.
 7. Jiang, Z.-T., S.M. Thurgate, and P. Wilkie, *Line Structure in Photoelectron and Auger Electron of CuO_x/Cu and Cu by Auger Photoelectron Coincidence Spectroscopy (APECS)*. Surface and Interface Analysis, 2001. **31**: p. 287 - 290.

8. Thurgate, S.M., et al., *An Auger Photoelectron Coincidence Spectrometer*. Review of Scientific Instruments, 1990. **61**(12): p. 3733 - 3737.
9. Volkel and Saunder, *Journal of Physics E: Scientific Instruments*, 1983. **16**: p. 456.
10. Jensen, E., et al., *Auger Photoelectron Coincidence Spectroscopy Using Synchrotron Radiation*. Review of Scientific Instrumentation, 1992. **63**(5): p. 3013 - 3026.
11. Thurgate, S.M., C.P. Lund, and A.B. Wedding, *Applications of Auger Photoelectron Coincidence Spectroscopy (APECS) to Understanding Inner-Shell Transitions*. Nuclear Instruments and Methods in Physics Research B, 1994. **87**: p. 259 - 266.
12. Haak, H.W., *Auger Photoelectron Coincidence Spectroscopy - A Study of Correlation Effects in Solids*. 1983, University of Groningen: Groningen.
13. Sawatzky, G.A., *Auger Photoelectron Coincidence Spectroscopy*, in *Treatise on Materials Science and Technology*. 1988, Academic Press Inc. p. 167 - 243.
14. Bartynski, R.A., Q. Qian, and S.L. Hulbert. *Line Shape of the Ag N₂₃VV Auger Spectrum Measured by Auger-Photoelectron Coincidence Spectroscopy*. in *International Conference on Coincidence Spectroscopy*. 1999. Brest, France: Journal de Physique IV.
15. Jablonski, A. and C.J. Powell, *Formalism and Parameters for Quantitative Surface Analysis by Auger Electron Spectroscopy and X-Ray Photoelectron Spectroscopy*. Surface and Interface Analysis, 1993. **20**(9): p. 771 - 786.
16. Tanuma, S., C.J. Powell, and D.R. Penn, *Calculations of Electron Inelastic Mean Free Paths for 31 Materials*. Surface and Interface Analysis, 1988. **11**: p. 577 - 589.
17. Tanuma, S., C.J. Powell, and D.R. Penn, *Calculations of Electron Inelastic Mean Free Paths II. Data for 27 Elements Over the 50-2000 eV Range*. Surface and Interface Analysis, 1991. **17**: p. 911 - 926.
18. Tanuma, S., C.J. Powell, and D.R. Penn, *Electron mean-Free-Path Calculations Using a Model Dielectric Function*. Surface and Interface Analysis, 1991. **17**(13): p. 927 - 939.

19. Tanuma, S., C.J. Powell, and D.R. Penn, *Calculations of Electron Inelastic Mean Free Paths (IMFPs). IV. Evaluation of Calculated IMFPs and of the Predictive IMFP Formula TPP-2 for Electron Energies Between 50 and 2000eV*. Surface and Interface Analysis, 1993. **20**(1): p. 77 - 89.
20. Tanuma, S., C.J. Powell, and D.R. Penn, *Calculations of Electron Inelastic Mean Free Paths. V. Data for 14 Organic Compounds Over the 50 - 2000eV Range*. Surface and Interface Analysis, 1994. **21**(3): p. 165 - 176.
21. Lund, C.P. and S.M. Thurgate, *Analysis of the $M_{4,5}N_{4,5}N_{4,5}$ Spectrum of Ag by Auger Photoelectron Coincidence Spectroscopy*. Surface Science, 1997. **376**: p. L403 - L408.
22. Lund, C.P. and S.M. Thurgate, *Auger Photoelectron Coincidence Studies of the Intrinsic and Extrinsic Processes in the Ga $L_{23}M_{45}M_{45}$ Auger Line of GaAs*. Physical Review B, 1994. **50**: p. 17166 - 17171.
23. Lund, C.P., S.M. Thurgate, and A.B. Wedding, *Intrinsic Satellites in the $L_{23}VV$ Auger Spectra of 3d Transition Metals*. Physical Review B, 1994. **49**(16): p. 11352-11357.
24. Arena, D.A., R.A. Bartynski, and S.L. Hulbert, *A Method for Determining Intrinsic Shapes of Overlapping Spectral Lines in Auger-Photoelectron Coincidence Spectroscopy*. Review of Scientific Instruments, 2000. **71**(4): p. 1781 - 1787.
25. Creagh, C.A., *The Use of Auger Photoelectron Coincidence Spectroscopy to Study the Origins of the Three-Hole Final State in the $L_3M_{45}M_{45}$ Auger Spectrum of Copper*, in *Physics*. 1996, Murdoch University: Perth. p. 60.
26. Creagh, C.A., et al., *Auger Photoelectron Coincidence Spectroscopy of the $2p_{1/2}$ Line in Coincidence with the $L_3-M_{45}M_{45}$ Peak of Copper*. Surface Science, 1999. **432**: p. 297 - 304.
27. Lund, C.P., S.M. Thurgate, and A.B. Wedding, *Auger Photoelectron Coincidence Spectroscopy Studies : Trends in the $L_{2,3}M_{4,5}M_{4,5}$ Line Shapes Across the 3d Transition Metal Series*. Physical Review B, 1997. **55**(8): p. 5455 - 5465.
28. Thurgate, S.M. and C.P. Lund, *Auger-Photoelectron Coincidence Spectroscopy (APECS) A Tool for Understanding Auger Emission From Solids*. Journal of Electron Spectroscopy and Related Phenomena, 1995. **72**: p. 289 - 297.

29. Ramaker, D.E., *The Past, Present, and Future of Auger Line Shape Analysis*. Critical Reviews in Solid State and Materials Sciences, 1991. **17**(3): p. 211 - 276.
30. Lide, D.R., *CRC Handbook of Chemistry and Physics*. 76 ed, ed. D.R. Lide. 1995 - 1996, Boca Raton, New York, London, Tokyo: CRC Press.
31. Papaconstantopoulos, D.A., *Handbook of the Band Structure of Elemental Solids*. 1 ed. 1986, Washington, D.C., New York, London: Plenum Press. 410.
32. Parry-Jones, A.C., P. Weightman, and P.T. Andrews, *The $M_{4,5}N_{4,5}N_{4,5}$ Auger Spectra of Ag, Cd, In and Sn*. Journal of Physics C: Solid State Physics, 1979. **12**: p. 1587 - 1600.
33. Weightman, P., et al., *Local Lattice Expansion Around Pd Impurities in Cu and Its Influence on the Pd Density of States: An Extended X-ray-Absorption Fine-Structure and Auger Study*. Physical Review B, 1987. **36**(17): p. 9098 - 9105.
34. Martensson, N. and R. Nyholm, *Electron Spectroscopic Determination of M and N Core-Hole Lifetimes for the Elements Nb - Te (Z = 41 - 52)*. Physical Review B, 1981. **24**(12): p. 7121 - 7134.
35. Lund, C.P. and S.M. Thurgate. *What Can We Learn From a Systematic Auger Photoelectron Coincidence Spectroscopy (APECS) Study of the 3d Transition Metal $L_{23}VV$ Auger Lines - Fe to Ga? in 3rd Vacuum Society of Australia Congress*. 1995. University of Newcastle, NSW.
36. Thurgate, S.M., *Auger Spectroscopy and Surface Analysis*. Australian Journal of Physics, 1997. **50**: p. 745 - 757.
37. Thurgate, S.M., *Coincidence Measurements in the Electron Spectroscopies: Surface Studies*. Surface and Interface Analysis, 1993. **20**: p. 627 - 636.
38. Lund, C.P. and S.M. Thurgate, *Auger Photoelectron Coincidence Studies of the Origin of the Three-Hole Final State Contribution to the Ni L_3VV Auger Line*. Journal of Electron Spectroscopy and Related Phenomena, 1995. **77**: p. 283 - 290.
39. Thurgate, S.M., C.P. Lund, and A.B. Wedding, *Auger-Photoelectron-Coincidence Spectra of Ni in Pure and Alloy Systems*. Physical Review B, 1994. **50**(7): p. 4810 - 4815.

40. Thurgate, S.M., *Auger Photoelectron Coincidence Spectroscopy*. Journal of Electron Spectroscopy and Related Phenomena, 1999. **100**: p. 161 - 165.
41. Neale, J., *Auger Coincidence Spectroscopy - Valence Level Decay in Copper*, in *Physics*. 1990, Murdoch: Perth. p. 85.
42. Thurgate, S.M. and J. Neal, *Origins of the Satellites in the $L_2M_{45}M_{45}$ Auger Spectrum of Cu: Coincidence Measurements*. Surface Science Letters, 1991. **256**: p. L605 - L 608.
43. Coward, D.M. and S.M. Thurgate, *Post Collision Interaction in the $L_3-M_{45}M_{45}$ Auger Spectra in Solid State Copper*. Journal of Electron Spectroscopy and Related Phenomena, 2000. **107**: p. 193 - 199.
44. Thurgate, S.M. and Z.-T. Jiang, *Asymmetric Broadening of the Cu $2p_{3/2}$ Photoelectron Line*. Surface Science, 2000. **466**: p. L807 - L810.
45. Creagh, C.A. and S.M. Thurgate, *The Use of Auger Photoelectron Coincidence Spectroscopy to Deconvolute the $M_{45}N_{45}N_{45}$ AES of Palladium*. Journal of Electron Spectroscopy and Related Phenomena, 2001. **114 - 116**: p. 69 - 74.
46. Thurgate, S.M. and C.P. Lund, *Comparison of the Auger Photoelectron Coincidence Spectroscopy (APECS) Spectra of Ag and InP with Cu and GaAs*. Surface and Interface Analysis, 1997. **25**: p. 10 - 16.
47. Creagh, C.A., S.M. Thurgate, and Z.-T. Jiang, *Investigating the Structure of the Tin $M_{45}N_{45}N_{45}$ Auger Spectrum Using Auger Photoelectron Coincidence Spectroscopy*. Journal of Electron Spectroscopy and Related Phenomena, 2002. **ELSPEC 4311**.
48. Antonides, E. and G.A. Sawatzky., *The $L_2L_3M_{45}$ Coster-Kronig Process in Zn and ZnO in the Solid State*. Journal of Physics C: Solid State Physics, 1976. **9**: p. L547 - L552.
49. Arena, D.A., et al., *Line Shape of the Ag $M_{45}VV$ Auger Spectra Measured by Auger-Photoelectron Coincidence Spectroscopy*. Physical Review B, 2001. **63**: p. article number 155102.
50. Jensen, E., et al., *Line narrowing in photoemission by coincidence spectroscopy*. Phys. Rev. Lett., 1989. **62(1)**: p. 71 - 73.
51. Bartynski, R.A., et al., *Auger Photoelectron Coincidence Spectroscopy using Synchrotron Radiation*. Progress in Surface Science, 1996. **53(2-4)**: p. 155 - 162.

52. Jensen, E., et al., *Observation of surface to bulk interatomic Auger decay from tantalum (100)*. Phys. Rev. B: Condens. Matter, 1990. **41(18)**: p. 12468 - 12472.
53. Hulbert, S.L., et al., *A comparison of the surface electronic structure of tantalum(100) and tantalum carbide (TaC)(111) using Auger-photoelectron coincidence spectroscopy*. J. Vac. Sci. Technol., A, 1991. **9(3, Pt.2)**: p. 1919 - 1923.
54. Siu, W.K., R.A. Bartynski, and S.L. Hulbert, *The Role of Defects at Low Concentrations in the NH₃/TiO₂(110) Adsorption System: An Auger-Photoelectron Coincidence Spectroscopy Study*. Journal of Chemical Physics, 2000. **113(23)**: p. 10697 - 10702.
55. Bartynski, R.A., et al., *Surface electronic structure of gallium arsenide(110) studied by Auger photoelectron coincidence spectroscopy*. J. Vac. Sci. Technol., A, 1991. **9(3, Pt. 2)**.
56. Arena, D.A., R.A. Bartynski, and S.L. Hulbert. *The Electronic Structure of Ag/Cu(100) and Pd/Cu(100) Surface Alloys Studied by Auger-Photoelectron Coincidence Spectroscopy*. in *Many Particle Spectroscopy. Atomic, Molecular, Clusters and Surfaces*. 2000: Kluwer Academic / Plenum New York.
57. Ohno, M., *On the L₃ Level Photoelectron Spectrum of Cu Metal Measured in Coincidence With the L₃-VV Auger-Electron Line*. In print, 2002.
58. Martensson, N., R. Nyholm, and B. Johansson, *Chemical-Shift Effects and Origin of the Pd 3d Core-level satellite in CuPd alloys*. Physical Review Letters, 1980. **45(9)**: p. 754 - 757.
59. NSLS, U.A.O., *Beamline Research Programs and Techniques*. 1999.
60. Attili, A., et al., *The ALOISA beamline: first results*. ELETTRA News, 1998. **21**.
61. Gotter, R., et al. *Angular Correlation in Auger Photoelectron Coincidence Spectroscopy from the Cu(111) Surface*. in *International Conference on Coincidence Spectroscopy*. 1999. Brest, France: Journal de Physique IV.
62. Calicchia, P., et al., *A Study on Background Subtraction in Auger and Photoelectron Time Coincidence Spectroscopy using Third Generation Synchrotron Radiation Source*. 1999. **Review of Scientific Instruments(70)**: p. 3529 - 3536.

Part 3

Palladium and Tin

APECS Spectra

Chapter 5

Experimental Results

5.1. Introduction

Previous research by the Murdoch group examined the 3d metals Iron, Cobalt, Nickel, Copper, and Gallium [1, 2] and some of the 4d metals Silver and Indium [3]. The shape of the coincidence Auger spectra was observed to change from band-like for Iron and Cobalt, to mixed for Nickel, to mostly atomic-like for Copper and atomic-like in Gallium. In the 4d metals Silver had a mixed coincidence Auger spectra while Indium was atomic-like. This raised the question of a complementary trend in the 4d metals and it was therefore decided to use APECS to investigate the possibilities. It was expected that the Palladium coincidence Auger spectrum would be mixed or even band-like while the Tin coincidence spectrum would be atomic-like. The $M_{45}NN$ Palladium Auger spectrum was examined in coincidence firstly with $3d_{5/2}$ photoelectrons and then with $3d_{3/2}$ photoelectrons. The same coincidence spectra were collected for Tin with the addition of one extra spectrum in coincidence with the $3p_{3/2}$ photoelectron line.

5.2. Sample Preparation and Cleaning

The Palladium and Tin samples were examined sequentially however both were subjected to similar cleaning regimes. The first sample examined was 99.95% pure Palladium and the second sample was 99.99% pure Tin. Both were obtained from Goodfellows Cambridge Ltd. Before a sample

was introduced to the UHV chamber it was mounted onto a sample holder using a small patch of Tantalum. Both sample and holder were then rinsed sequentially in Propane, Water and Acetone to remove as much contamination as possible before installation in the UHV chamber. As the chamber did not have a fast entry lock it was necessary to bring the whole system up to air pressure to install the sample. To return the system to UHV it had to be baking for 12 hours to remove absorbed gas from the chamber walls. Then each of the working components within the system had to be out-gassed i.e. X-ray tube anode and filaments, ion gun and for Palladium the sample heating filament. Thus changing the sample and any maintenance or repair that involved bringing the chamber up to air took at least two working days.

Once installed the sample was then cleaned, in situ, by Argon ion bombardment and in the case of Palladium also annealed, until there was no trace of contamination as determined by XPS. Annealing was achieved by bombarding the sample with electrons from behind the sample using a Tungsten filament. The filament current was 2.5A and the voltage difference between filament and sample was 1000V producing an emission current of 21.6mA. The sample was annealed for 5 min. The Palladium sample glowed slightly red. The melting point of Palladium is 1825K and the recommended annealing temperatures ranged from 913K to 1500K [4]. Tin was not annealed because its melting point was too low (505K).

The sample position had then to be optimised to give the maximum coincidence count rate for the energy of the electrons under investigation. This could take anywhere between one day and a month particularly if the magnetic field from the Helmholtz coils around the apparatus was part of the optimisation process. Notes from the laboratory logbook about optimising the magnetic fields can be found in Appendix vi.

When the sample was changed from Palladium to Tin, Palladium peaks were found on the Tin singles spectrum. It was therefore necessary to bring the system up to air pressure again and thoroughly clean or replace any parts with Palladium contamination even though they were no where near the sample.

During the experiment the sample was cleaned daily within the UHV system. The X-ray source and channel plates were turned off and Argon was allowed to enter the chamber until the pressure reached 4.0×10^{-5} Torr. It was necessary to change the sample position so it could be bombarded. Palladium was bombarded for 30 min and the Tin sample was bombarded for 15 min. The Palladium sample was also annealed for 2min using the settings mentioned above. This process removed any Oxygen and Carbon contamination that had built up on the surface over the previous 24hrs. The cleanliness was checked using XPS. Examples of cleaning and experimental settings can be seen in Appendix vii. The experiment was not restarted until the system pressure was below 2×10^{-9} Torr and often it operated in the 10^{-10} Torr range.

5.3. Palladium Experimental Results

5.3.1. Weightman's model of the $M_{45}NN$ Auger peak

The Palladium $M_{45}NN$ Auger spectrum is composed of at least two overlapping peaks, the $M_{5}NN$ (327.6 eV) peak and the higher kinetic energy $M_{4}NN$ (332.9 eV) peak. Weightman et. al. [5] calculated the lineshape of each of these peaks from first principles using a set of curves each of which represented a different multiplet state. The multiplet structure of the $M_{45}NN$ Auger spectrum as determined by Weightman [5] is given in Table 5.1

Table 5.1 The Multiplet Structure of Palladium $M_{45}NN$

		Relative intensities	
(L,S,J) term	Splittings (eV)	$M_{4}NN$	$M_{5}NN$
1S_0	-2.41	2.28	2.55
1G_4	0.0	27.69	24.48
1D_2	0.22	21.38	5.92
3P_0	0.30	5.43	3.20
3P_1	0.32	8.89	5.91
3P_2	0.73	7.57	14.47
3F_2	1.33	9.45	9.13
3F_3	1.49	14.89	10.06
3F_4	1.89	2.42	24.28

The lineshape of each multiplet curve was derived by applying the Cini-Sawatzky theory to the self-convolution of the local single electron DOS. Each component was then broadened by a Gaussian instrumental contribution of 0.5 eV FWHM and by a Lorentzian lifetime broadening of

around 1.0 eV. A value of $U(^1G_3) = 3.0$ eV was used when applying the Cini-Sawatzky theory as previous studies had indicated a value of U between 2.8eV to 3.1eV [5].

The validity of this methodology was not under dispute. What Weightman et. al. were investigating at the time was the effect of local lattice expansion around Palladium impurities in Copper and which impurity calculations for the DOS gave the best fit to the experimental Palladium $M_{45}NN$ Auger impurity profile.

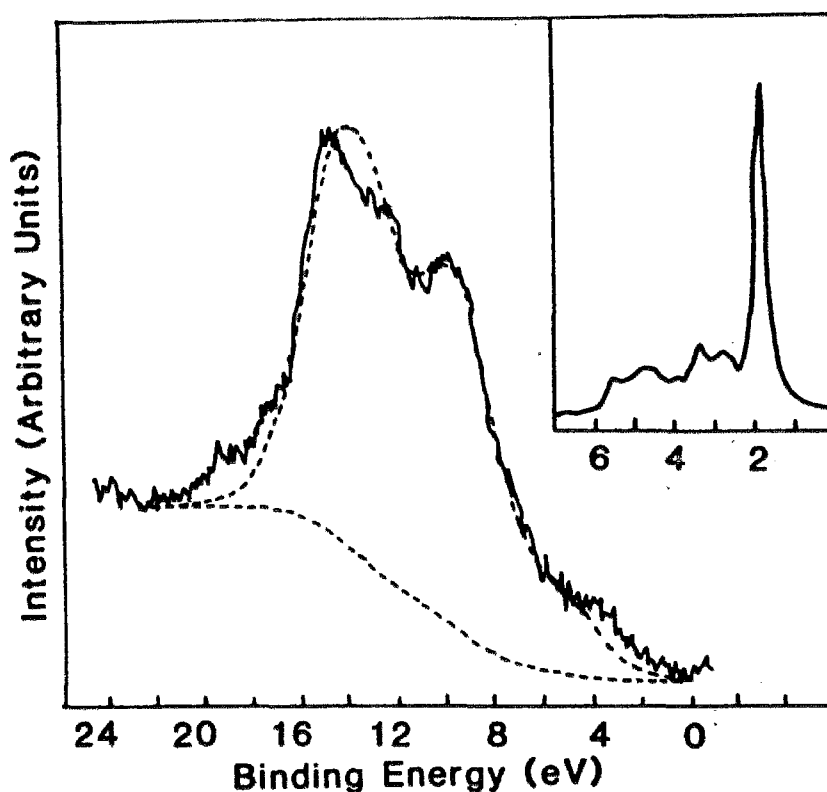


Figure 5.1 From the paper by Weightman et. al. [5] The inset shows the calculated DOS for Pd impurities in Cu. This DOS gave the best agreement between theory and experiment when the Auger profile was calculated with a $U(^1G_4)$ of 3.0eV

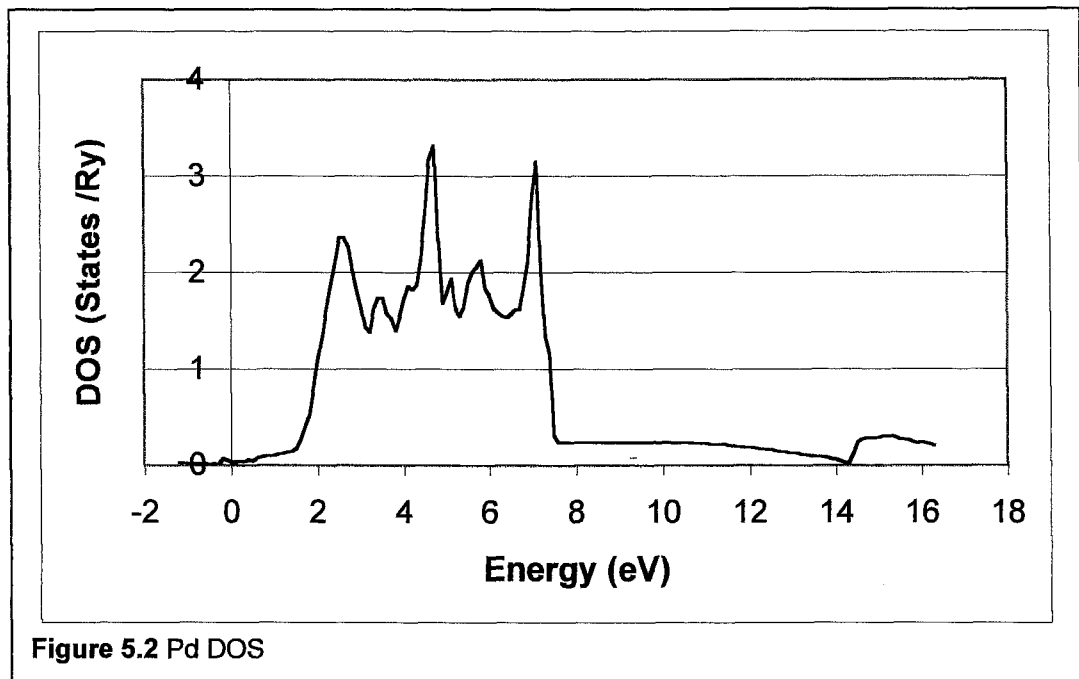
They obtained a good fit to the Palladium impurity profile by using a modification of the Clogston-Wolff model of the local impurity DOS (Figure 5.1). This positive result indicated that the multiplet structure as given in Table 5.1 and the methodology of constructing the Auger lineshape, was a reliable starting point in understanding the coincidence data for this thesis.

In creating their model Weightman et. al. [5] gave an M_5NN to M_4NN intensity ratio ranging from the experimental 1.0:0.3 to a calculated 1:0.69. The first ratio was suggested by their work on an $Ag_{80}Pd_{20}$ alloy and the second ratio was derived from calculations of the initial-state photoelectron cross sections. Kucherenko et. al. [6] infers that the difference in these two ratios is due to a Coster-Kronig transition between the $3d_{3/2}$ and $3d_{5/2}$ orbital, which removes intensity from the M_4NN peak and places it in the low kinetic energy side of the M_5NN peak.

5.3.2. Creating the Model Curves

Weightman's methodology was used on the DOS of pure Palladium [7] (Figure 5.2) to construct a model of the $M_{45}NN:3d_{5/2}$ coincidence Auger peak using a set of multiplet curves. The bulk of the intensity of the model curve was centered around the main 2-hole position of the M_5NN Auger peak with minimal intensity in the M_4NN section as expected. This model was then compared to the coincidence data of the $M_{45}NN$ Auger lineshape originating with an initial $3d_{5/2}$ photoelectron. The coincidence spectrum contained intensity arising from the initial $3d_{5/2}$ ionisation only and it was expected from Weightman's model that no, or at most very little intensity

would be found in the energy range expected to be occupied by the M_{4NN} part of the Auger peak. The coincidence data however had substantial intensity in this area indicating the Weightman model was not a complete explanation and an alternate model was therefore needed to explain the origins of the intensity in the M_{4NN} area of the Auger peak.



The new model consisted of only one curve for each Auger process and ignored multiplet-splitting effects. To construct the curve the density of filled states for pure Palladium [7] was used (Figure 5.2). It was convoluted with itself to give a first approximation to the line-shape of the Auger peak as postulated by Lander in 1953 [8]. A modifying factor (Equation 5.1) [9, 10] was then applied to the resultant curve.

This modification allows for the Coulomb interaction of the two holes created during the Auger process as discussed by Cini [10-13] and Sawatzky et. al. [9, 14]. The amount of modification is based on the ratio

of U/W where U is the effective hole-hole interaction energy related to the departing Auger electron and W is the width of the valence band (see p 37 to 42). For a $U \ll 0.66W$ the line-shape appears broad and band-like [9]. In creating the model $U = 2.8\text{eV}$ and 3.1eV [5] and $W = 7.1\text{eV}$ [7] were used giving U/W ratios of 0.4 and 0.44. The resultant curve was then broadened with a Gaussian curve (FWHM 2.7eV) to allow for instrument broadening.

$$d\sigma/d\varepsilon_k = \frac{D(\omega)}{[1-(U/W)F(\omega)]^2 + [\pi(U/W)D(\omega)]^2} \quad \text{Equation 5.1}$$

$d\sigma/d\varepsilon_k$ – transformed DOS at energy ω
 $D(\omega)$ – initial DOS energy ω
 U – hole-hole interaction energy
 W – band width

$$F(\omega) = P \int_{-\infty}^{+\infty} \frac{D(\omega') d\omega'}{(\omega - \omega')}$$

ω' – another energy in the initial DOS

Using the Cini-Sawatzky theory in this way assumes that Palladium has a full d-band however it does not. There are two holes in the d-band of a neutral Palladium atom. The effect of these holes would be to broaden the peak [15]. According to Treglia et. al. [15] in situations where the band is partially filled the unfilled section should also be included in the self-convolution of the DOS. We ignored this work in the light of the results of Bennett et. al. [16] who found that Nickel alloys with varying hole densities all had similar values for U . They attributed this to screening of the d-band by the s-p orbitals. Palladium is in the same column of the periodic table

as Nickel and so each curve was first constructed using the Cini-Sawatzky theory for full d-bands. As this gave a curve that resulted in a good fit between the final model and high-resolution AES data no further complications were necessary.

The following sections describe how the complete model for the $M_{45}NN$ Auger peak was built from curves created using the methodology described above. Each curve represented an independent process, which added intensity to the $M_{45}NN$ Auger lineshape. Relative intensities of the curves representing the $M_4-N_{45}N_{45}$ and $M_4-M_5N_{45}-N_{45}N_{45}(N_{45})$ processes were determined by fitting the model curve to the related APECS data. The intensity ratio of the M_4NN to M_5NN transitions given by Weightman et. al. [5] was used when the curves representing each process were summed together to create the complete model of the total Auger lineshape. The model compared favourably to a high resolution AES scan of the Palladium $M_{45}NN$ Auger peak.

5.3.3. Results

5.3.3.1. *Background subtraction*

The Palladium singles spectrum (Figure 5.3) contains all emitted Auger electrons and so the count rate is very high compared to the coincidence spectrum (Figure 5.4). For there to be a comparison between the two, the singles spectrum was scaled to the coincidence data (Figure 5.5).

In order to analyse the lineshape of the Palladium data it was necessary to remove as much unrelated background intensity as possible. This was done in two stages. Firstly a fixed amount of intensity across the whole coincidence peak was removed bringing the high-energy side of the peak to zero. A similar process was applied to the singles data. The removed intensity represented inelastic scattering of electrons with higher kinetic

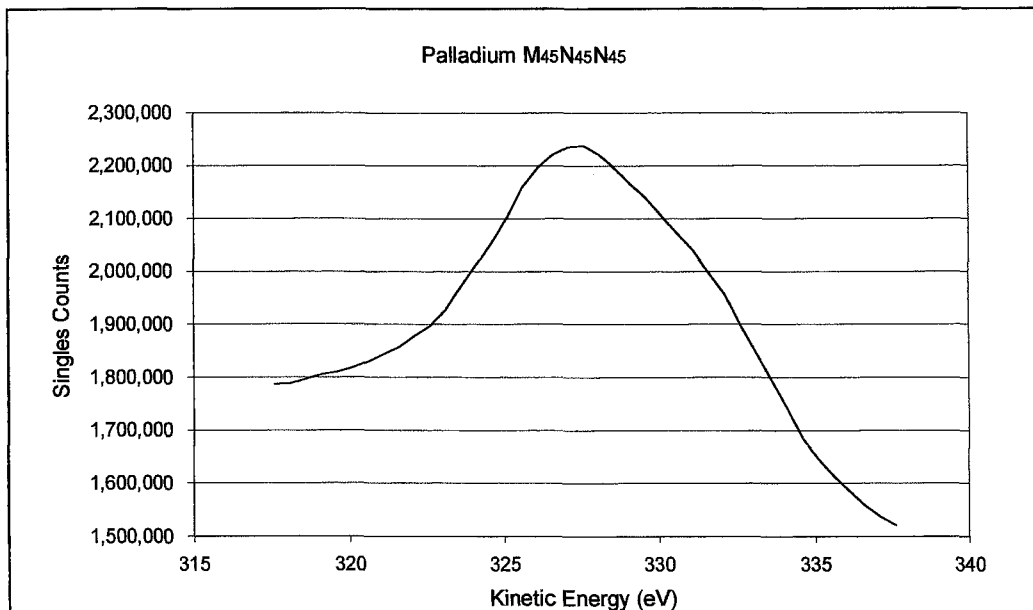


Figure 5.3 Raw singles data

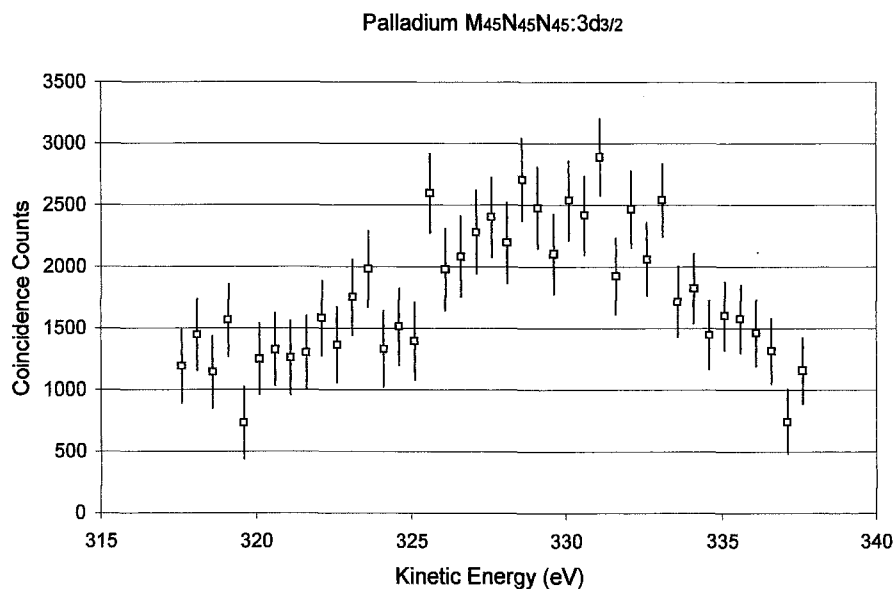
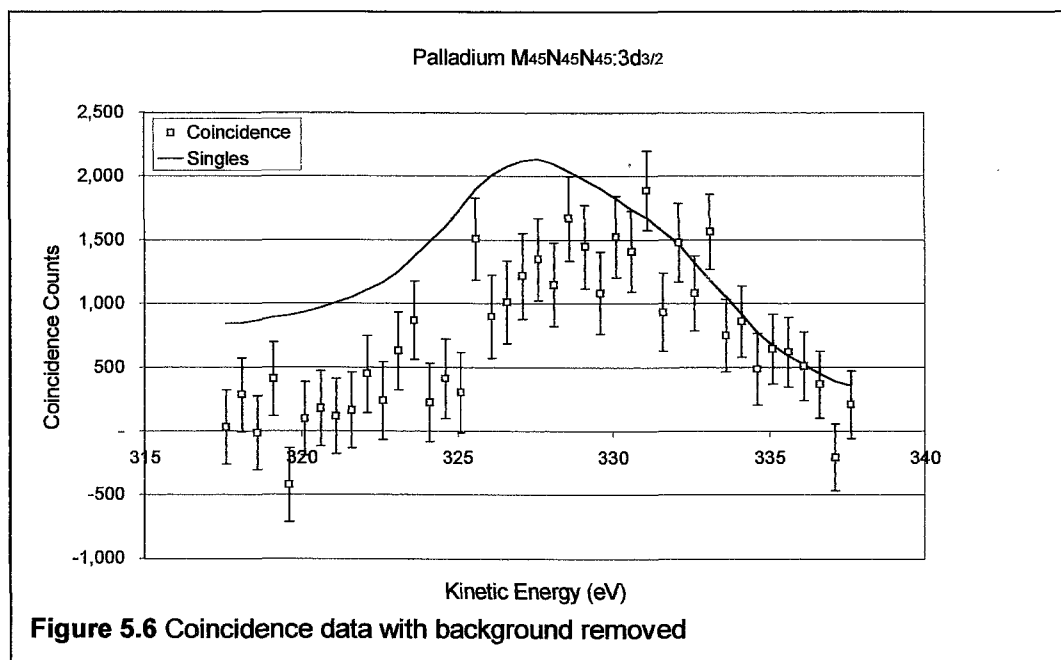
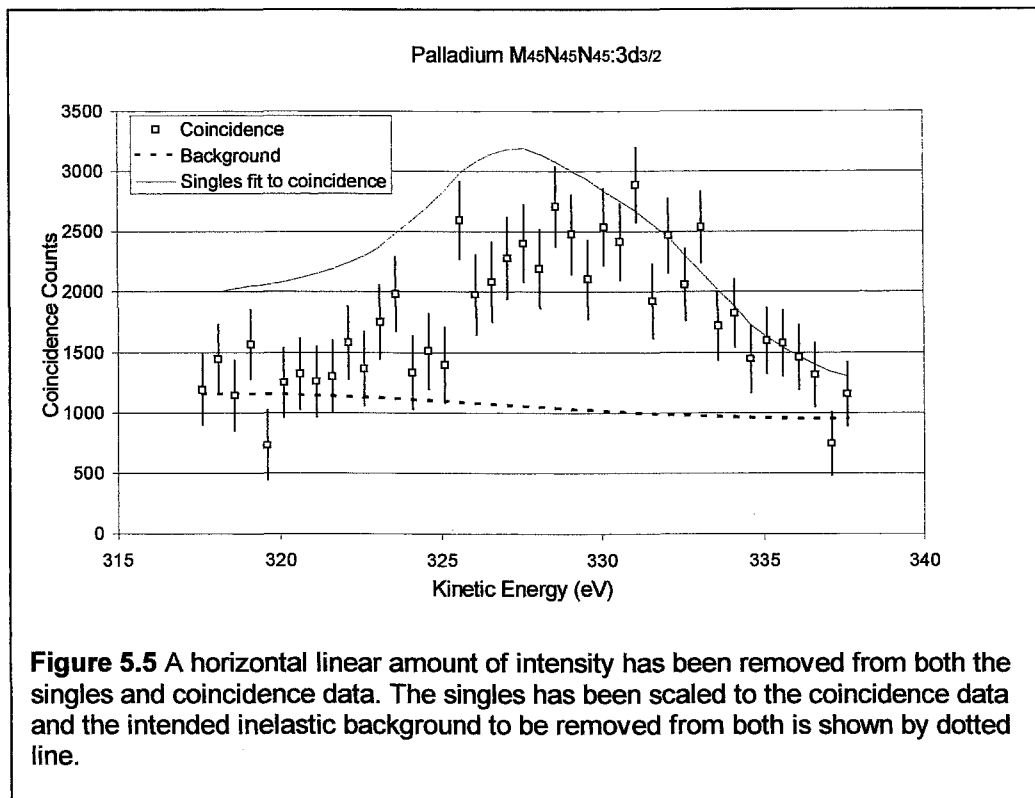


Figure 5.4 Raw coincidence data

Secondly it was necessary to remove the inelastic background relating to the Auger processes under investigation. Factors that could effect the inelastic background intensity were minimised by cleaning the surface of the 99.95% pure sample so there were no oxidised or carbonaceous over-layers. The samples used could be considered to have a homogeneous depth distribution profile because of their purity. There would however still be some background intensity from inelastic scattering remaining.

The Tougaard Background subtraction method would have been the preferable method to use in removing this background intensity. It has been developed into a software program (QUASES) that can perform background subtraction on a spectrum recorded from a material under a variety of emission situations [17]. The minimum energy range required by the software to give a reliable result is around 65eV. As the coincidence data for this thesis and most of the data produced by the Murdoch group has an energy range 20 – 25eV it was not possible to use this software on the APECS data and so another method had to be found.

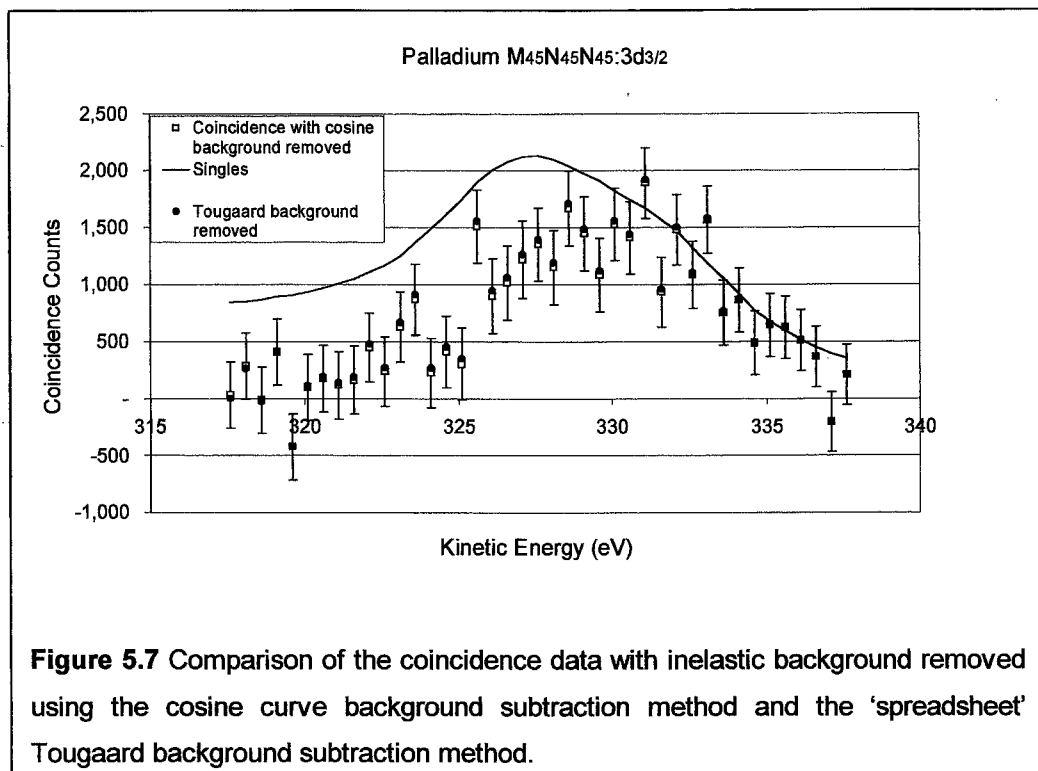
A cosine curve was used to approximate the shape of the Tougaard background. Starting at zero at the high kinetic energy end of the spectrum the curve gently sloped upwards to reach a maximum equalling the intensity of the coincidence spectrum at the low kinetic energy end of the energy range (Figure 5.5).



This intensity was then removed from both the coincidence and singles spectrum leaving the data as shown in Figure 5.6. It is probable that more inelastic background should have been removed from the singles

spectrum because of the differences in effective IMFP (see section 4.4.3 Reduction of low kinetic energy broadening of the Auger peak). The singles spectrum however is not used quantitatively in the curve fitting process. Its main purpose is to give a visual indication of the position of the centroid of the coincidence peak with respect to the singles Auger lineshape.

An attempt was made, over the limited energy range, to compare the cosine curve background subtraction method with a spreadsheet representation of the Tougaard background subtraction method using the algorithm given by Tougaard and Jansson in their 1993 paper [18]. The results (Figure 5.7) showed that the difference between the two was well within the tolerance limits of the data.



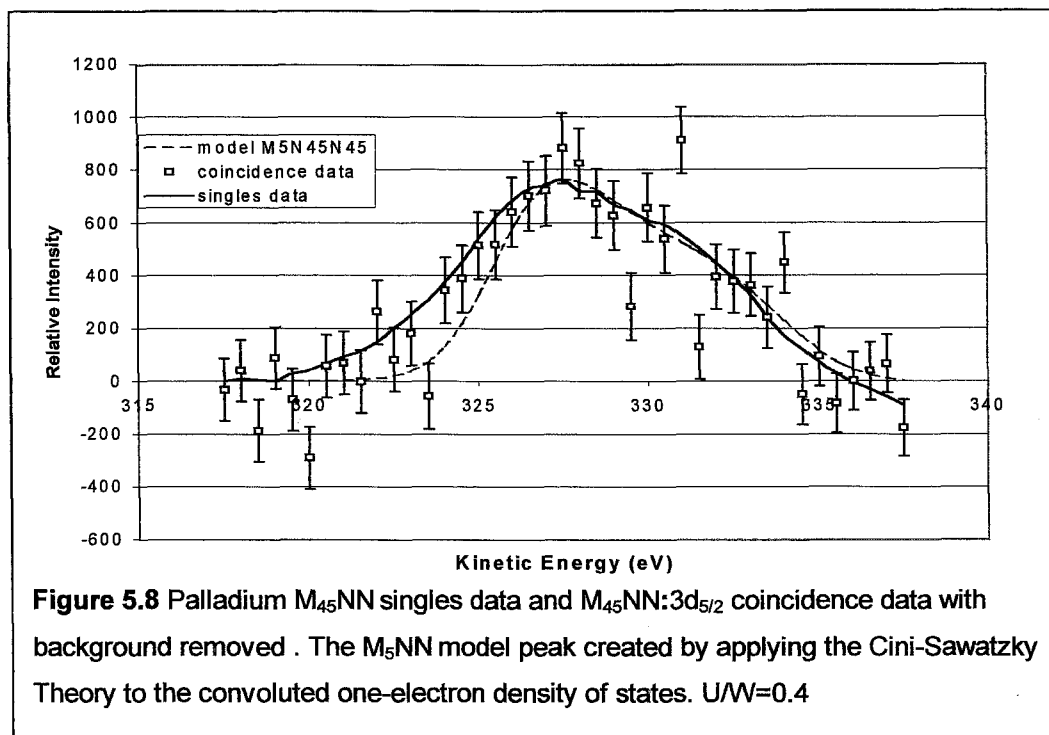
Unfortunately using spreadsheets to subtract the Tougaard background in this way was too difficult to use on a regular basis. It was expected that Tougaard's method would leave more intensity on the low kinetic energy side of the peak but because of the limited energy range it was impossible to calculate the background to 20 or 30 eV below the peak as required. Under the circumstances the background subtraction technique used was reasonable. It may have however removed some intensity from any $M_4:M_5:CK$ NNN Coster-Kronig process present.

As with the Straight Line method it is expected that the cosine curve background subtraction method would have the following advantages and limitations.

- It compensates for the method used to remove intensity arising from higher kinetic energy events, which is why it was possible to remove a baseline amount of intensity from the whole energy range.
- It was necessary to specify the maximum and minimum energy range. The total intensity in the peak area was sensitive to the selection of the minimum energy position and in this respect it was necessary to depend on a personal interpretation of the data. The minimum energy was chosen so that the average intensity on the low kinetic energy side of the peak was zero.

5.3.3.2. $M_{45}NN:3d_{5/2}$

For this part of the APECS experiment one analyser was fixed on the $3d_{5/2}$ photoelectron line, while the other analyser was scanned across the $M_{45}NN$ Auger peak. The coincidence data $M_{45}NN:3d_{5/2}$ with background removed is shown in Figure 5.8.



The coincidence data points with the error bars were obtained by counting only those electrons in the Auger peak associated with initiating photoelectrons from the $3d_{5/2}$ level. The continuous line (scaled to fit the coincidence data) is the AES spectrum produced by counting all detected electrons within that kinetic energy, i.e. the singles spectrum. The singles spectrum includes electrons within that energy range which may not have been produced by initial ionisation of the $3d_{5/2}$ energy level.

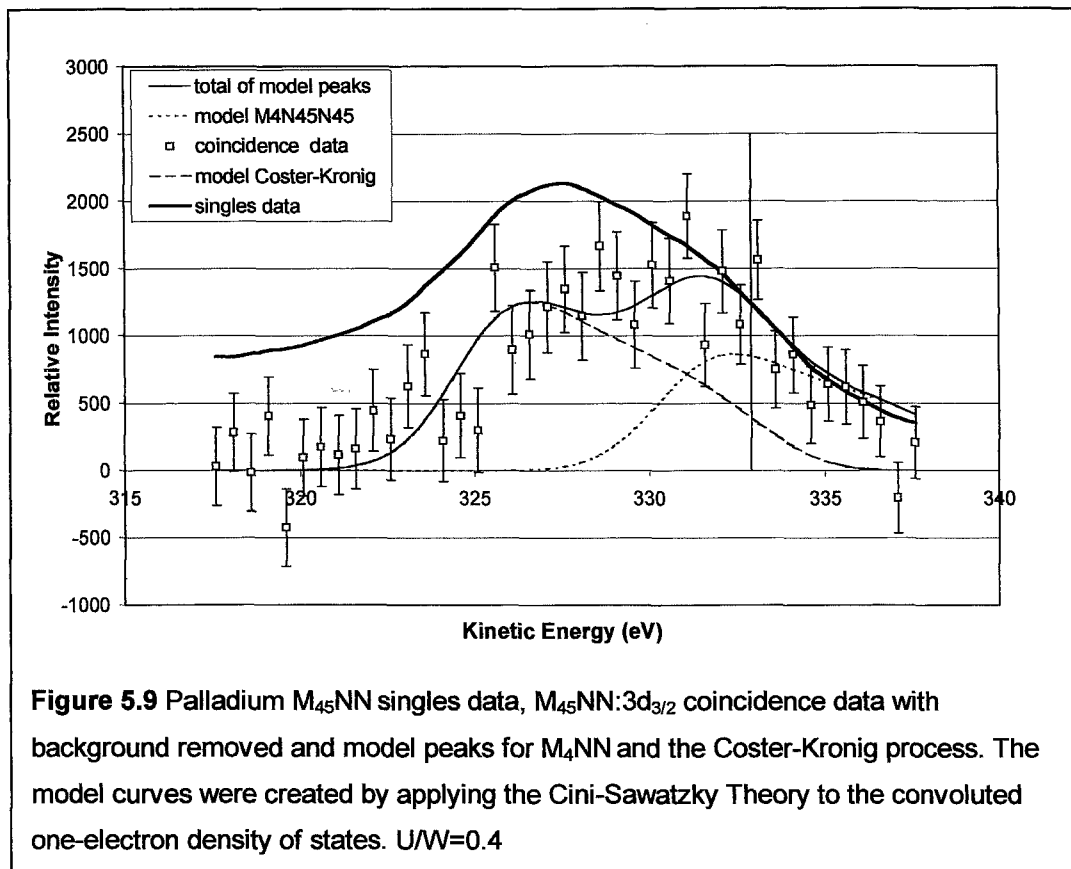
The range of the coincidence data was unexpected. The most intense part of the M_5NN Auger peak (singles and coincidence) at a kinetic energy of 327.6eV can be attributed to the simple 2-hole Auger process $M_5-N_{45}N_{45}$. This process is initiated by a $3d_{5/2}$ photoionisation. The unexpected intensity was in the 332.9eV range. Using Weightman's model the $M_4-N_{45}N_{45}$ process initiated by $3d_{3/2}$ photoionisation was expected to give rise to intensity in this higher kinetic energy range (332.9 eV) and the two overlapping peaks would sum to give the familiar Auger peak. No high kinetic energy intensity in the $M_{45}NN:3d_{5/2}$ coincidence data was expected even though there is intensity in the singles because only Auger electrons resulting from initial $3d_{5/2}$ photoelectrons were recorded. The intensity found in this region was explained however using the model created from the convolution of the DOS with application of the Cini-Sawatzky theory. The peak produced in this manner has a large band-like component, which fits the coincidence data well, as shown in Figure 5.8.

This model curve for the $M_{45}NN:3d_{5/2}$ data was created using a $U/W = 0.4$ (which gave a better fit than $U/W = 0.44$) convoluted with a 2.7eV Gaussian curve. This was scaled to the $M_{45}NN:3d_{5/2}$ coincidence data (Fig. 5.8). using a χ^2 test for goodness of fit.

5.3.3.3. $M_{45}NN:3d_{3/2}$

The $M_{45}NN:3d_{3/2}$ data collected with background removed is shown in Figure 5.9. The data points with the error bars are the coincidence spectrum and the bold continuous line is the scaled singles spectrum. The

coincidence data has intensity in the 2-hole (332.9eV [19]) position of the M_4NN spectrum as expected and is represented by the finely dotted curve.



Removing the background from the coincidence data may not have eliminated all the contribution of the final state shake up/off process to the total intensity at lower kinetic energies. The residual amount however is expected to be small so the large amount of intensity in the coincidence data in the 320 eV to 328 eV range under the M_5NN part of the Auger spectrum can only be attributed to a Coster-Kronig process.

In constructing the model peak for this part of the spectrum it was reasoned that the simple 2-hole process $M_4-N_{45}N_{45}$ would produce a peak with a line-shape the same as the $M_5-N_{45}N_{45}$ process because the final

state for the atom is the same for both processes. It was therefore reasoned that the hole-hole interaction energy (U) would be the same for both processes. The M_4NN peak would be at 5.3eV higher kinetic energy than the M_5NN peak because the energy supplied by the difference in binding energy between core level and valence band is greater for the $3d_{3/2}$ level than for the $3d_{5/2}$ level by this amount.

5.3.3.4. $M_4M_5^{CK}NNN$ Coster-Kronig Process

The 3-hole Coster-Kronig process starts with a $3d_{3/2}$ photoelectron and places intensity in the M_5NN Auger peak. The initial ionisation is followed by an intermediate state where an electron from an outer shell with the same primary quantum number drops down to fill the inner core hole. This releases enough energy to liberate an outer valence electron.

This Coster-Kronig electron has very little kinetic energy and so is not often detected. If the Coster-Kronig process is fast the extra hole in the valence band does not have time to delocalise before the Auger electron is released in the final state. Thus the Auger electron has the same possible energy range as one initiated with a $3d_{5/2}$ photoelectron but feels the effect of this 'spectator hole' as an increase in the strength of the spherical potential of the atom as it leaves. The extra work done by the Auger electron in overcoming this increase in potential reduces its kinetic energy and places it in the low kinetic energy section of the M_5NN Auger peak.

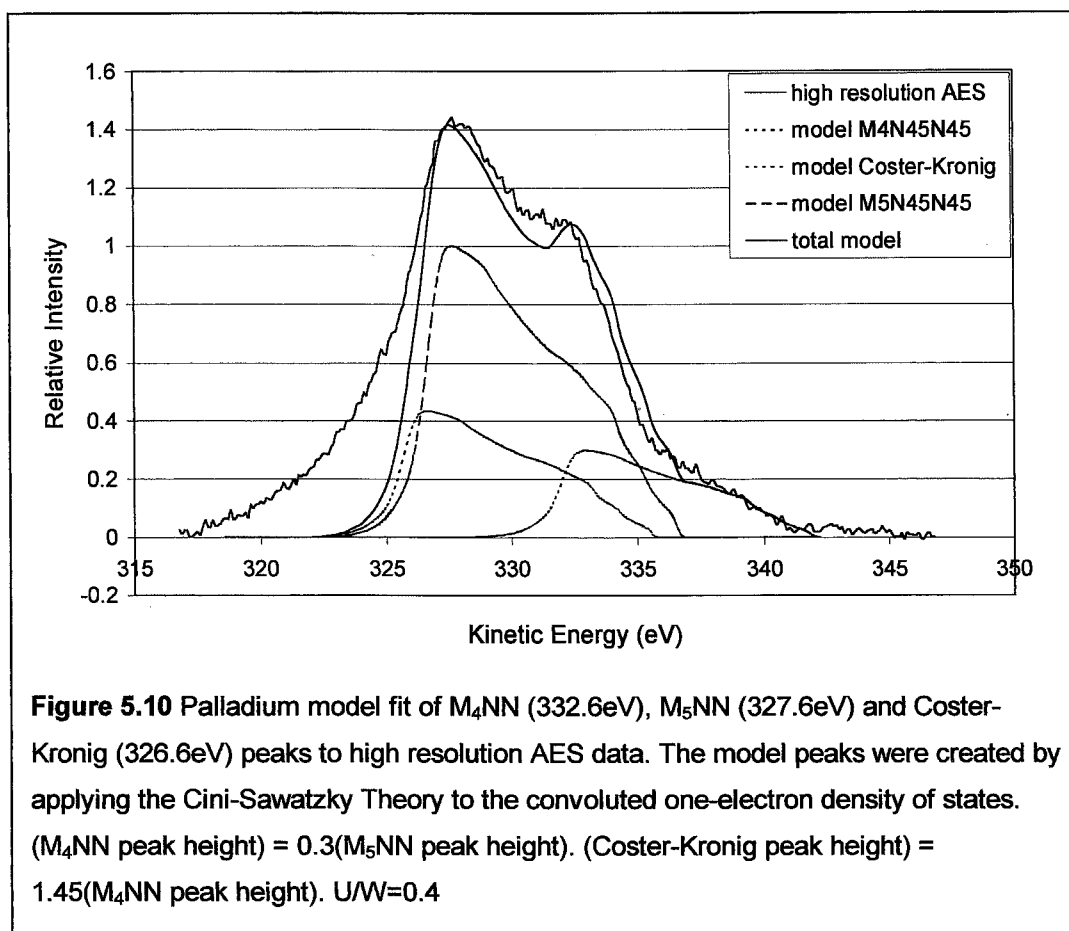
If the spectator hole from this process is localised in the valence band then this will increase U and the Coster-Kronig component of the Auger peak will become more atomic-like. At this stage it is not possible to detect a change in U for the Coster-Kronig process, and so the model peak has the same lineshape as the other component peaks.

The model fit of Coster-Kronig and M_4NN peaks to the coincidence data for the $M_{45}NN:3d_{3/2}$ photoelectron is shown in Figure 5.9. The ratio of the height of the Coster-Kronig peak to the M_4NN peak was found to be 1.45:1.00. The apex position of the Coster-Kronig peak is 326.6eV and the apex position of the M_4NN peak is 332.6eV. The actual height of the Coster-Kronig peak may be a little less than the value given here because there is a possibility of some contribution from a $3d_{5/2}$ initial state shake process. Martensson et.al. [20] found there was an initial-state shake peak 6eV below the $3d_{5/2}$ photoelectron line. From their plot the shake intensity under the peak of the $3d_{3/2}$ line is 0.156 the intensity of the $3d_{3/2}$ line. This could therefore place intensity in the M_5NN 2-hole position of the Auger spectrum reducing the Coster-Kronig intensity by this amount from 1.45:1.00 to 1.29:1.00. The model could be adjusted to include the peak from the initial state shake process and reduce the intensity of the Coster-Kronig peak. This was seen to be an unnecessary complication, as the two curves would still sum to give the model curve, which fits the APECS data. The combination of possible initial-state shake processes resulting in a smaller Coster-Kronig curve than indicated and the background subtraction method resulting in a larger Coster-Kronig curve than indicated

means that the ratio of the height of the Coster-Kronig peak to the M_{4NN} peak is open to consideration.

5.3.4. Total Model of the $M_{45}NN$ Auger Spectrum

Weightman [5] gave the relative intensity of the M_{5NN} and M_{4NN} Auger peaks from a minimum of 1.0:0.3 to a maximum of 1.00:0.69. Using this information it is possible to put both sets of model peaks together and compare the result with a high resolution AES scan taken with the Kratos Axis Ultra Imaging XPS system at Murdoch University (Figure 5.10).



It was necessary to change the instrument function that the model peaks were convoluted with from 2.7eV to 0.35eV, this second value is the

instrument broadening of the Kratos XPS equipment, used for the high-resolution scan.

A good fit of the model to the data (background removed) was achieved with the ratio of the relative intensity of the $M_5NN:M_4NN$:Coster-Kronig peaks set at 1.00:0.30:0.435 (i.e. the Coster-Kronig: M_4NN height is 1.45:1.00). The M_5NN peak was found to be at 327.6eV, the Coster-Kronig peak at 326.6eV and the M_4NN peak was at 332.6eV. A U/W of 0.4 was used for all curves.

5.3.5. Discussion

The coincidence data $M_{45}NN:3d_{5/2}$ (Figure 5.8) shows the expected intensity at 327.6eV. This is the peak position for the simple, 2-hole, $M_5-N_{45}N_{45}$ Auger process. Coincidence intensity in the low kinetic energy 3-hole position of the M_5NN data (320 eV to 327 eV range) could be due to final state shake up/off processes, which would be observed in the coincidence data but has not been included in the model. Also any intensity in this area due to inelastic collisions of the electrons as they leave the metal would also show up in the singles and coincidence spectrum but not been included in the model. The intensity in the higher kinetic energy 332.9 eV part of the coincidence spectrum, (Figure 5.8) while unexpected using Weightman's [5] model, proved to be an integral part of the M_5NN peak when using the self-convoluted density of states modified in accordance with the Cini-Sawatzky Theory [9-14].

In Figure 5.9 the singles data has been scaled to fit the M_4NN part of the coincidence data only and the extra intensity in the singles with respect to the coincidence data is due to the above-mentioned M_5NN process. The coincidence data $M_{45}NN:3d_{3/2}$ shows intensity in the 2-hole $M_4-N_{45}N_{45}$ position (320 eV to 337.5 eV range) as expected. The magnitude of the intensity in the 320 eV to the 328 eV range was much larger than expected and necessitated the inclusion of a Coster-Kronig component to the model of the $M_{45}NN:3d_{3/2}$ data.

The position of the Coster-Kronig peak (326.6eV) is 1eV lower in kinetic energy than the M_5NN peak (Figure 5.10). This places the Coster-Kronig peak within the envelope of the M_5NN peak and while it adds intensity it does not produce a characteristic shoulder on the low kinetic energy side of the Auger peak.

There is intensity in the low kinetic region of the high resolution AES data (Figure 5.10) that is not accounted for by the complete coincidence model. This intensity could be ascribed to intrinsic final state shake up/off effects not fully removed from the high resolution AES data when the background was subtracted. It could also be due to extrinsic effects, for example, inelastic scattering of the Auger electrons after they leave atom, which has not been included in the model.

5.3.6. Palladium in summary

A good fit was achieved between a model of the Auger lineshape and a high resolution AES spectrum for Palladium. The model was built by fitting individual curves to APECS data each representing a different decay process. The intensity in the APECS Auger peak is directly related to specific initiating photoelectron. By examining the Auger region in coincidence with each photoelectron line it was possible to physically deconstruct the Auger spectrum and determine the relative intensity of the Coster-Kronig process $\bar{M}_4:M_5^{CK}NNN$ to the intensity of the simple Auger process $M_4-N_{45}N_{45}$. The line-shape of each component curves was based on the self-convolution of the density of states for Palladium, which was then modified in accordance with the Cini-Sawatzky model and finally broadened with an instrument Gaussian function.

5.4. Tin Experimental Results

5.4.1. Introduction

In this section the model making skills developed while deciphering the Palladium Auger lineshape [21] have been applied to Tin. Unlike Palladium the model created to fit the Tin APECS data was compiled from sets of Gaussian curves as the Tin spectra proved to be more atomic-like than band-like. In a previous attempt to understand the complexity of the $M_{45}NN$ Tin Auger spectra Parry-Jones et. al. [22] developed a model using multiplet-splitting calculations (see Figure 5.11). They produced curves for the $M_4-N_{45}N_{45}$ and $M_5-N_{45}N_{45}$ processes each composed of a set of curves representing the individual multiplet states.

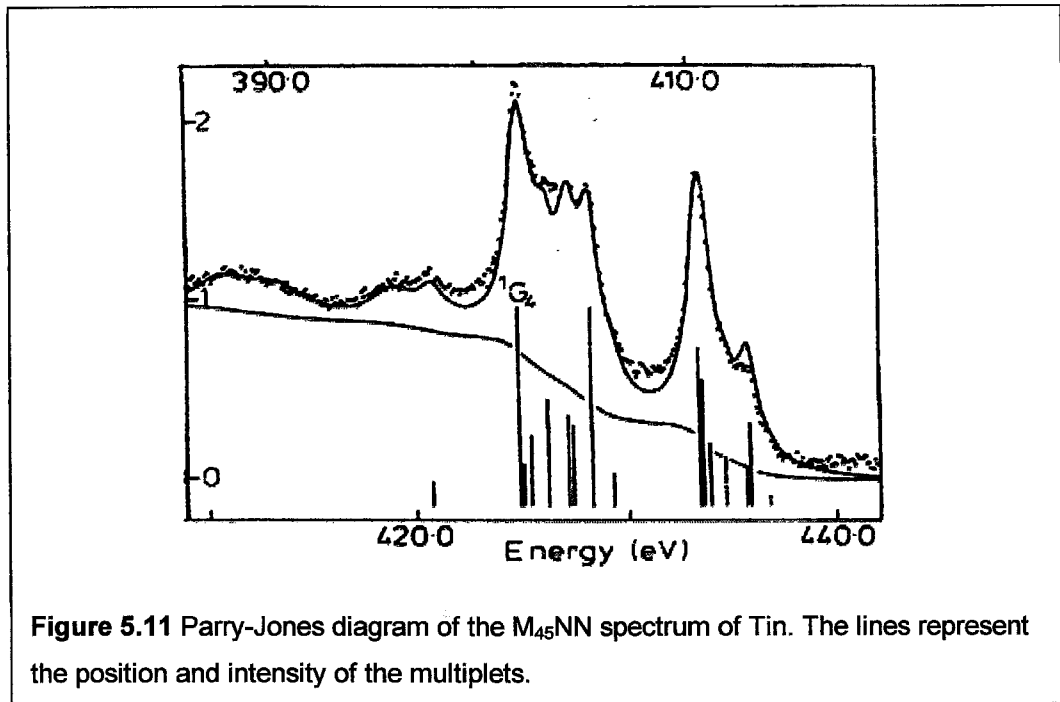


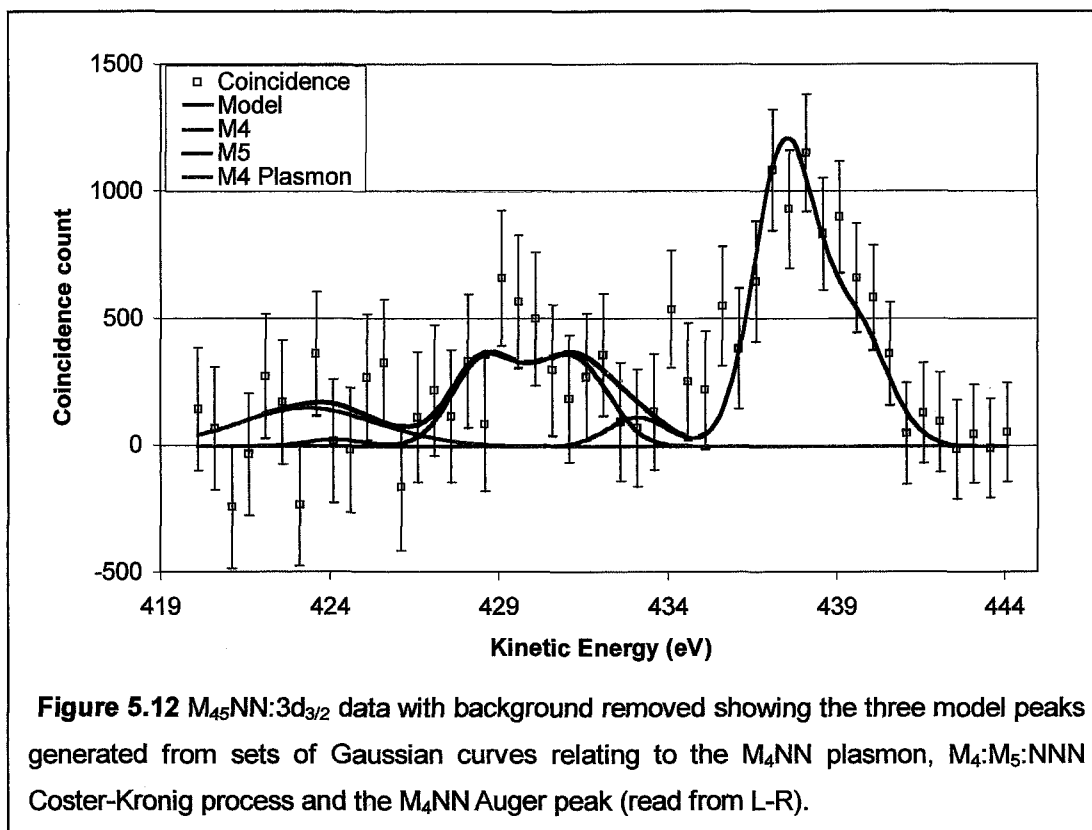
Figure 5.11 Parry-Jones diagram of the $M_{45}NN$ spectrum of Tin. The lines represent the position and intensity of the multiplets.

Using APECS it was possible to extend this model by investigating the intensity in the $M_{45}NN$ Auger spectrum arising from photoionisation of the $3p_{3/2}$, the $3d_{3/2}$ and the $3d_{5/2}$ electron energy levels independently. A model spectrum was built up by using the APECS data for each of the main processes associated with photoionisation of these energy levels. This increased the number of processes included in the final Auger model from 2 to 5 and provided a unique way of experimentally deconstructing the Tin $M_{45}NN$ Auger spectrum.

5.4.2. Constructing a model of the Tin Auger spectra using APECS data

5.4.2.1. $M_{45}NN:3d_{3/2}$

APECS data was collected for the $M_{45}NN$ Auger peak of Tin in coincidence with the $3d_{3/2}$ photoelectron line. Figure 5.12 shows the data after the background has been removed. The technique used to remove the background was the same as that used on the Palladium data. Expected intensity was found at the $M_{4}NN$ peak position of 437.3eV^1 and 14.6eV lower. This lower kinetic energy peak is related to a $M_{4}NN$ plasmon [22].



¹ Value obtained from a high resolution AES scan of the sample using the Kratos Axis Ultra Imaging XPS system at Murdoch University

Additional intensity was also found under the M_5NN part of the Auger peak, which can only come from the $M_4-M_5(N_{45})-N_{45}N_{45}(N_{45})$ Coster-Kronig process (427 eV to 434 eV).

The model of the coincidence spectra was developed using multiplet structure calculations provided by Parry-Jones et. al. [22]. The model was compiled from three sets of curves, each set representing a different process and a unique area of intensity. The highest kinetic energy set of curves are shown collectively in Figure 5.12 by the blue line, belong to the two-hole $M_4-N_{45}N_{45}$ processes. The mid-range set taken together form the red curve in Figure 5.12 represent the Coster-Kronig process. The final lower kinetic energy set, in sum, form the green curve belong to the two-hole processes which had been energy shifted due to plasmon loss effects. Both the plasmon and the 2-hole process curve therefore have the M_4NN multiplet structure. The curve representing the Coster-Kronig process however has the M_5NN multiplet structure because the final transition, which releases the Auger electron, is between the valence band and the $3d_{5/2}$ energy level.

Each set of curves was constructed from nine Gaussian curves of the intensity and energy separation stipulated by Parry-Jones et. al. [22] as given in Table 5.2. The FWHM of 4.1eV used for the Gaussian curves was the experimentally determined line broadening of the APECS equipment with the 127° cylindrical electron energy analysers.

Table 5.2 Multiplet Splitting Information given by Parry-Jones et. al.

	Energy Position	Intensity M ₄ NN	Intensity M ₅ NN
¹ S ₀	-4.14	0.25	0.13
¹ G ₄	0.0	1.16	1.00
¹ D ₂	0.19	0.93	0.20
³ P ₀	0.55	0.08	0.12
³ P ₁	0.51	0.37	0.25
³ P ₂	1.28	0.40	0.50
³ F ₂	2.25	0.25	0.51
³ F ₃	2.48	0.61	0.41
³ F ₄	3.36	0.08	1.10

[22]

The relative intensity between the M₄:M₅:^{CK}NNN Coster-Kronig peak, the M₄NN peak, and the position of the ¹G₄ of both peaks was determined by a χ^2 best fit to the coincidence data and is given in Table 5.3. The plasmon peak was a copy of the M₄NN peak with the intensity reduced to 10% of the parent peak, double the FWHM and at 14.6eV lower kinetic energy. The ratios for the plasmon peak with respect to the parent peak are given by Parry- Jones et. al. [22]

Table 5.3 Peak Energy Positions and Relative Heights

Coincidence Data	Position of ¹ G ₄		Relative Peak Height		Relative Height of ¹ G ₄	
	M ₅ NN	M ₄ NN	M ₅ NN	M ₄ NN	M ₅ NN	M ₄ NN
M ₄₅ NN:3d _{3/2}	428.3eV C - K	437.25eV two-hole	0.30 C - K	1.00 two-hole	0.38 C - K	1.00 two-hole
M ₄₅ NN:3d _{5/2}	428.8eV two-hole	436.8eV Mg K α_3 satellite	1.00 two-hole	0.41 Mg K α_3 satellite	1.00 two-hole	0.32 Mg K α_3 satellite
M ₄₅ NN:3p _{3/2}	427.9eV C - K	436.3eV C - K	1.00 C - K	0.9 C - K	1.00 C - K	0.86 C - K

Peak positions and relative heights of the curves used to fit the data in the three sections of the APECS experiment. (determined by χ^2 best fit to the coincidence data)

5.4.2.2. $M_{45}NN:3d_{5/2}$

The $M_{45}NN$ Auger peak was scanned in coincidence with the $3d_{5/2}$ photoelectron line and the coincidence data with background removed is shown in Figure 5.13. Intensity was observed in the M_5NN part of the spectrum between 428.8eV and 432eV as expected.

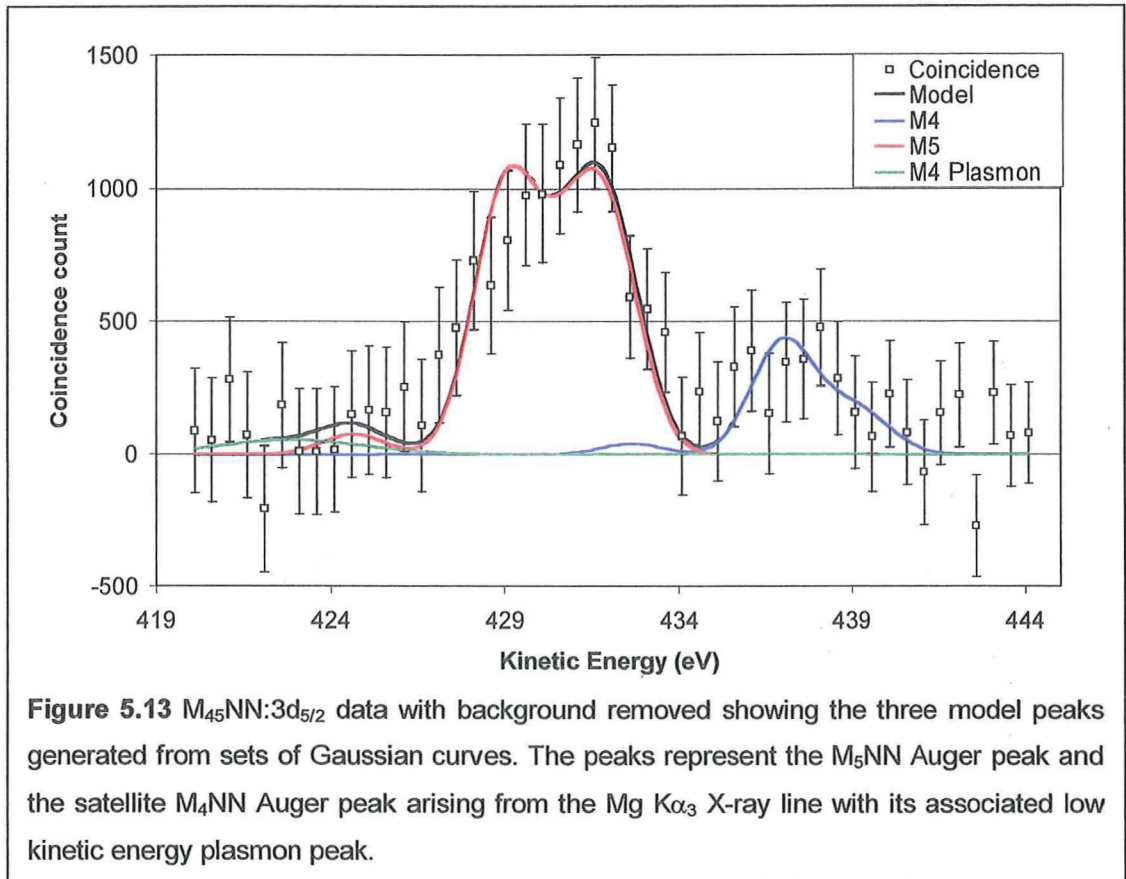


Figure 5.13 $M_{45}NN:3d_{5/2}$ data with background removed showing the three model peaks generated from sets of Gaussian curves. The peaks represent the M_5NN Auger peak and the satellite M_4NN Auger peak arising from the $Mg K\alpha_3$ X-ray line with its associated low kinetic energy plasmon peak.

The extra intensity at 437.4eV is due to the $Mg K\alpha_3$ X-ray line, which creates a copy of the $3d_{3/2}$ photoelectron line 8% as intense as the parent line and at 8.4eV higher kinetic energy [19]. The satellite of the $3d_{3/2}$ photoelectron line produced by the $Mg K\alpha_3$ X-ray line sits directly under the $3d_{5/2}$ photoelectron line. When the stationary analyser is positioned at the energy of the $3d_{5/2}$ line it detects electrons that arise from not only the $3d_{5/2}$ energy level but also those from the $3d_{3/2}$ level that have been

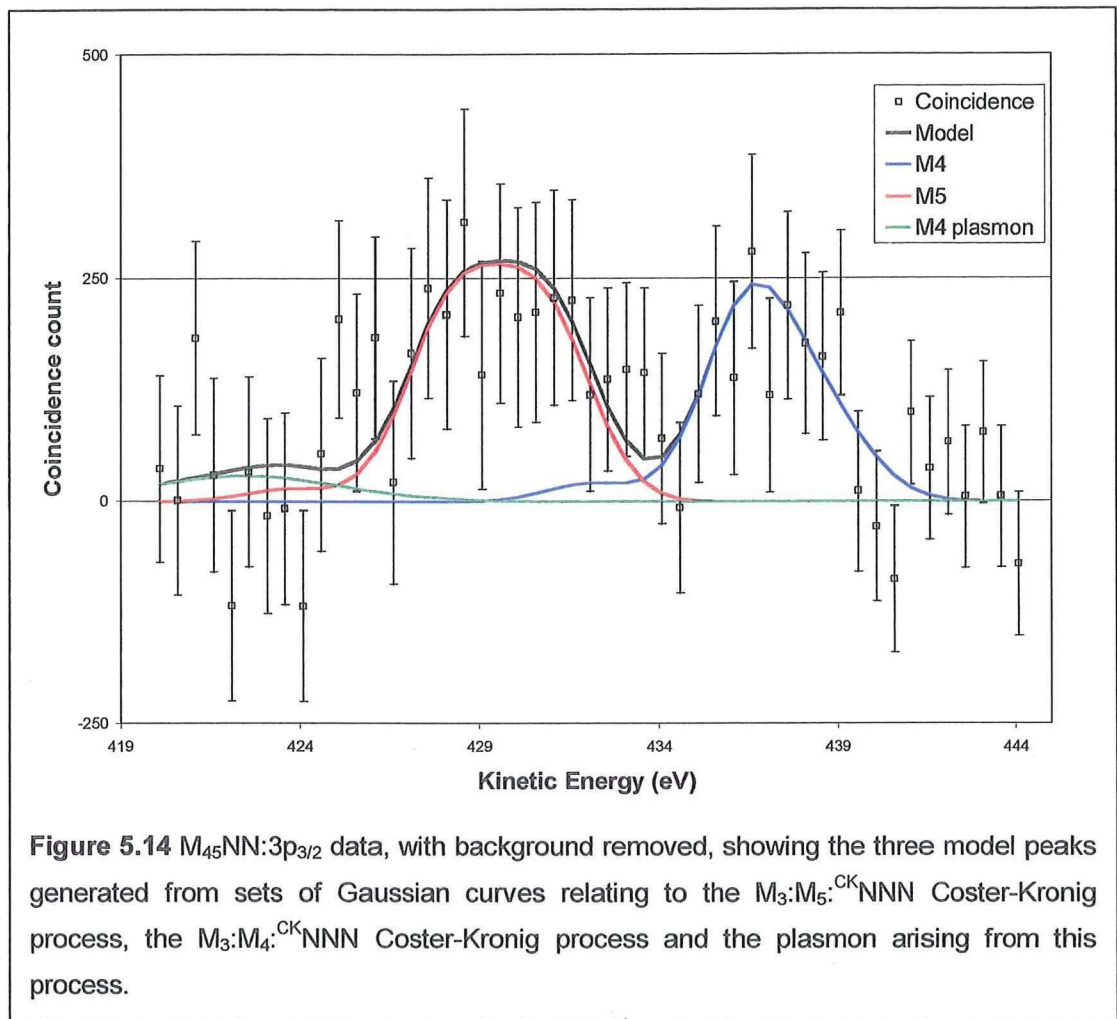
excited by photons from the $K\alpha_3$ part of the Mg spectrum. The resulting two-hole Auger processes put intensity in both the M_5NN and the M_4NN area of the Auger spectrum as observed.

The model of the M_4NN peak produced by the Mg $K\alpha_3$ X-ray line has the M_4NN multiplet structure as does its plasmon. The M_5NN model curve however has the M_5NN multiplet structure. The specifications of the model curves can be found in Table 5.3. The relative intensities and positions of the model curves was determined by a χ^2 best fit to the coincidence data.

5.4.2.3. $M_{45}NN:3p_{3/2}$

In the final section of this experiment the $M_{45}NN$ Auger peak was scanned in coincidence with the $3p_{3/2}$ photoelectron line (Figure 5.14). This part of the experiment could not have been performed without the installation of new hemispherical electron energy analysers, which gave better energy resolution and signal-to-noise ratio [23]. The $3p_{3/2}$ photoelectron line is approximately 10% as intense as the $3d_{3/2}$ line and thus the coincidence rate with the 127° cylindrical analysers would have been too low to contemplate performing this part of the experiment earlier.

Intensity in the $M_{45}NN:3p_{3/2}$ coincidence spectrum with background removed indicates Coster-Kronig transitions involving both the $3d_{3/2}$ and $3d_{5/2}$ levels. The processes would be as follows $M_3-M_4N_{45}-N_{45}N_{45}$ (N_{45}) and $M_3-M_5N_{45}-N_{45}N_{45}$ (N_{45}). It is difficult to know what the shape of the model curves should be for this data.



An attempt was made to fit the data first with three broad base Gaussian curves, one for each process. This did not produce a very good fit between the final total model and the high resolution AES lineshape. Next three sets of Gaussian curves each set representing multiplet splitting within an individual process was tried. The $M_3:M_4^{CK}NNN$ curve was given the same multiplet structure as the M_4NN model Auger curve and the $M_3:M_5^{CK}NNN$ curve had the same multiplet structure as the M_5NN model Auger curve. The FWHM of the Gaussian curves in each set was determined by the best fit to the data and was found to be 5.8eV (the instrument broadening was experimentally determined as 2.6eV for the

APECS equipment with the new hemispherical analysers). When the final model of the Auger spectrum was created from the sum of the APECS model spectra and fitted to the high-resolution AES spectra, it was found that the curves formed from the sets of Gaussian curves gave the best comparison (Figure 5.16). This indicated that there is a need for some form of structure in these Coster-Kronig peaks but the exact nature of that structure has yet to be determined.

The Coster-Kronig process places intensity on the low kinetic energy side of the two-hole Auger peak produced by initial photoionisation of the intermediate energy level. This is because the spectator hole in the valence band effectively increases the electrostatic potential of the atom as seen by the emitted Auger electron in the final decay of the atom. Table 5.3 shows the 1G_4 of both peaks are at 0.9eV and 0.95eV lower kinetic energies than the corresponding two-hole positions of the M_4NN and M_5NN peaks.

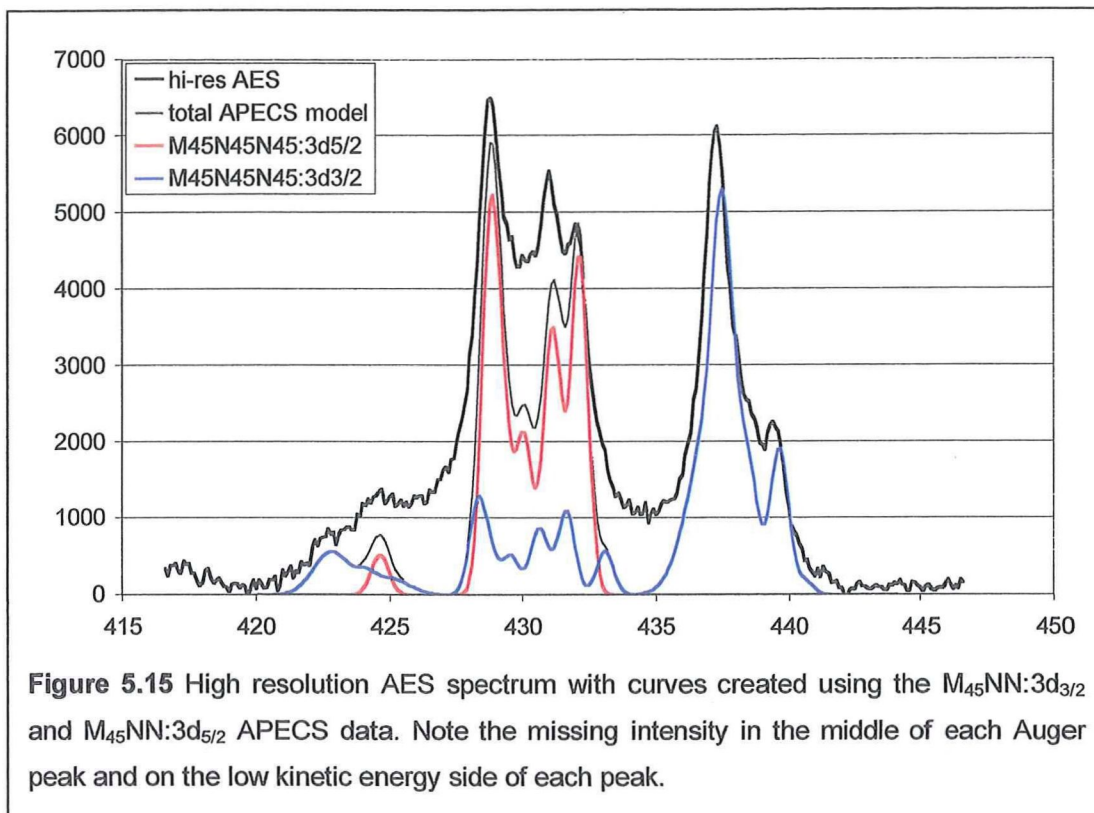
5.4.3. Comparing the model and high resolution Auger spectra

For each of the models developed to fit the APECS data time was spent investigating a band-like component. The band-like components were found to be very broad based and of low intensity because $(U/W) > 2$ [9-12, 14]. When the individual APECS model spectra were compiled the band-like parts of the spectra produced a small linear background. This intensity complicated the curve fitting process greatly without providing any extra

information and was therefore removed before fitting the model to the Tin data.

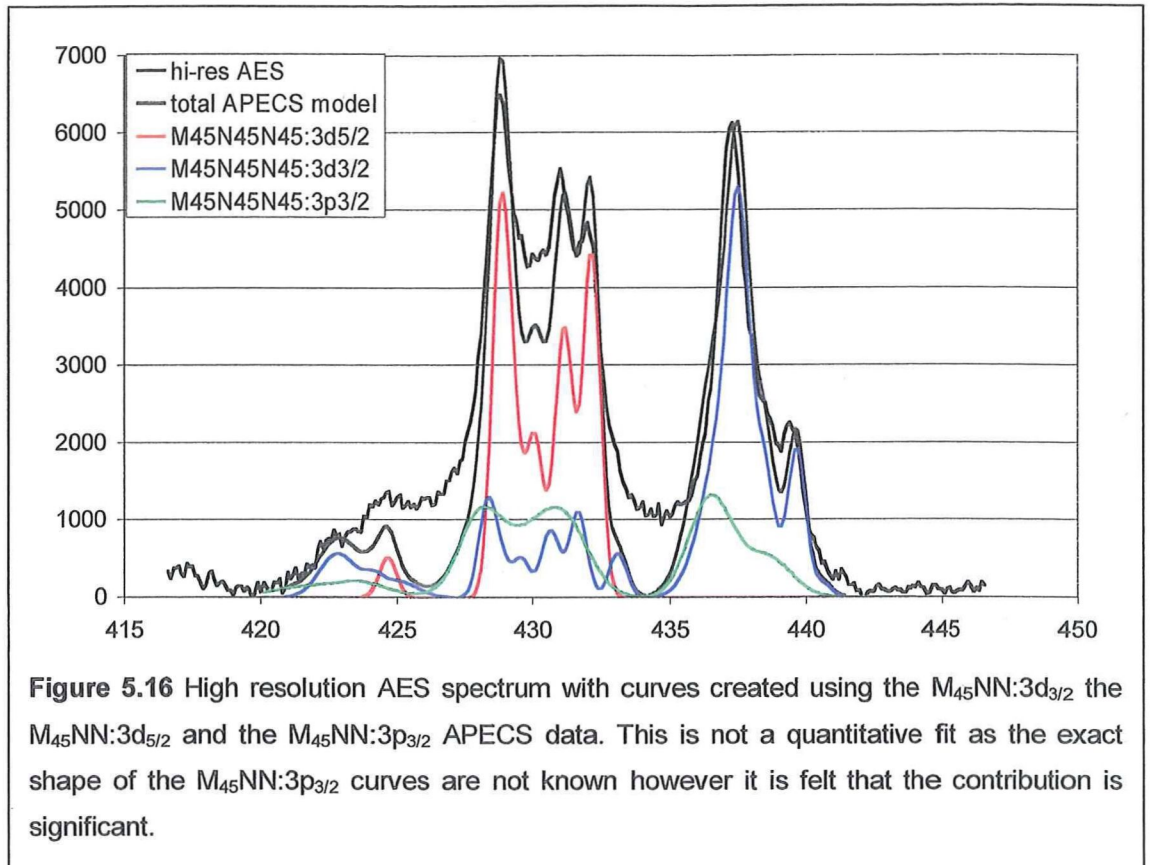
When the $M_{45}NN:3d_{5/2}$ model was added to the other APECS model peaks for comparison with the high resolution AES spectrum the intensity due to Mg $K\alpha_3$ satellite was removed. The aluminium anode on the Kratos Axis Ultra Imaging XPS system was used to produce monochromatic X-rays for the high-resolution AES spectrum. This X-ray spectrum would therefore not contain the extra satellite peak intensity found in the spectrum produced by the non-monochromate Mg anode of the APECS system.

All the APECS model spectra had to be modified to fit the high resolution AES spectrum because the instrument broadening of the APECS equipment was greater than the instrument broadening of the Kratos Axis Ultra Imaging XPS system used to produce the high-resolution AES spectra. Initially the model Auger spectrum was created from the sum of the two APECS models for $M_{45}NN:3d_{3/2}$ and $M_{45}NN:3d_{5/2}$ and a visual fit was made to the high-resolution AES spectra (Figure 5.15) in such a way that no part of the model was more intense than the high-resolution AES spectra.



When combining the APECS models of the $M_{45}N_{45}N_{45}:3d_{3/2}$ and $M_{45}N_{45}N_{45}:3d_{5/2}$ peaks the ratio of the 1G_4 lines in the two-hole peaks were provided by the calculations of Parry-Jones et. al. [22] multiplied by the ratio of the $M_4NN:M_5NN$ photoelectron cross sections determined by Scofield [24]. The ratio of the 1G_4 lines were thus found to be 0.80 to 1.00.

The component Gaussian curves in each set were made as broad as possible without losing too much structure resulting in a FWHM of 1.5eV. This compared favourably with the 1.1eV used by Parry-Jones et. al. [22] in their model of the same spectra. A better fit was achieved however when the $M_{45}N_{45}N_{45}:3p_{3/2}$ APECS model of the Coster-Kronig processes was added and scaled to give the best visual fit (Figure 5.16).



The FWHM for the component curves in the sets representing the Coster-Kronig processes in the $M_{45}NN:3p_{3/2}$ APECS model were 3.55eV (3.2eV line-width from APECS model + 0.35eV instrument broadening of Kratos). The composite Gaussian peaks in the plasmon for each model are two times the FWHM of their parent peaks in the $M_{45}NN$ curve and 10% of their height.

The main differences between Figures 5.15 and 5.16 is the added intensity in the mid peak region of both Auger peaks and the broadening of both peaks on the low kinetic energy side due to the intensity from the $M_3:M_{45}:^{CK}NNN$ Coster-Kronig processes.

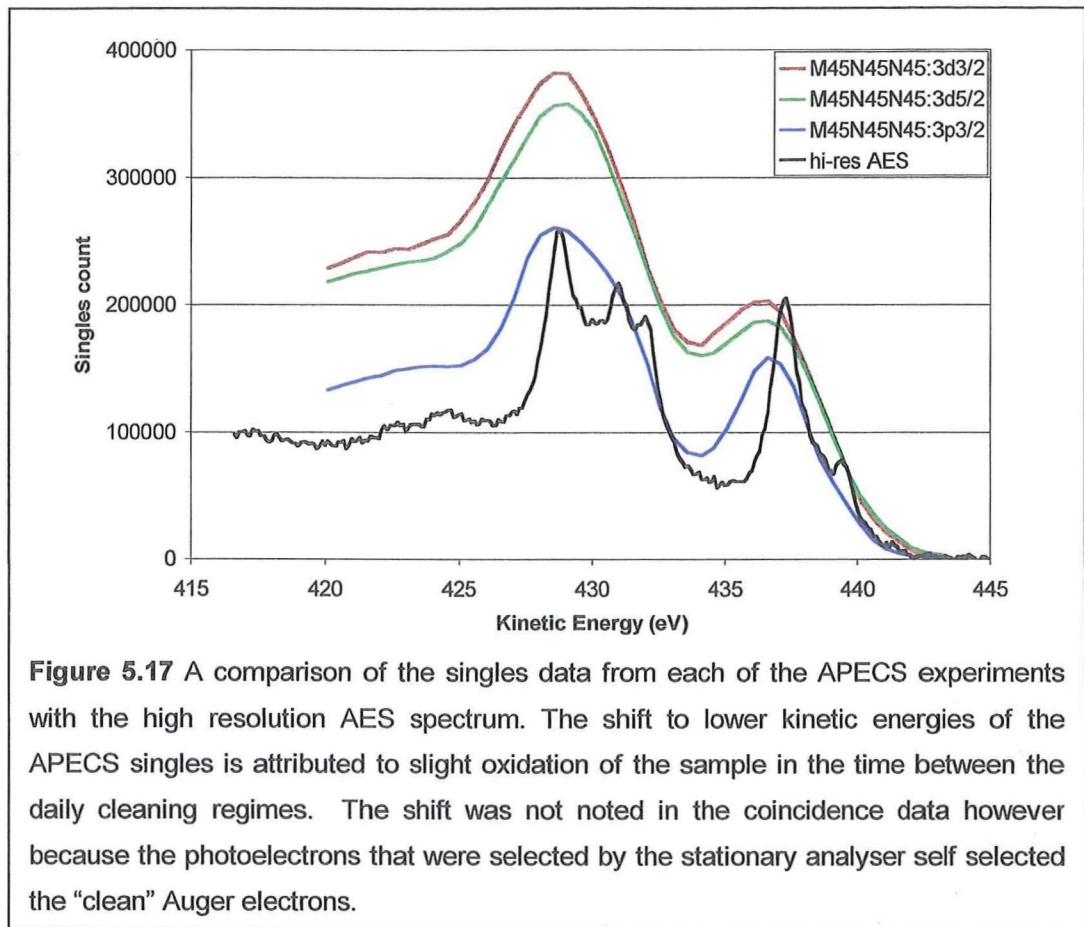
While it is not possible to put a quantitative value on the intensity due to the Coster-Kronig processes originating with the $3p_{3/2}$ photo-ionisation, this experiment shows that these processes make a significant contribution to the intensity in both the M_5NN and M_4NN Auger region. A theoretical calculation of the shape of these Coster-Kronig peaks would be the next step in obtaining this quantitative information. The intensity difference between the coincidence model and the AES spectrum on the low kinetic energy side of the peaks is due to extrinsic energy loss processes and possible intrinsic shake processes not included in this model.

5.4.4. Oxidation and coincidence data

There appeared to be a 0.7eV energy shift between the singles and the coincidence peaks in the APECS data (Figure 5.17), which is why the Coster-Kronig processes originating in the $3p_{3/2}$ electron energy level were originally investigated. As can be seen from Figures 5.15 and 5.16 the intensity derived from these processes was not the solution to the problem. A possible explanation of the energy shift could lie in the nature of the APECS experiment itself.

During the collection of the APECS data the sample was cleaned daily to remove all traces of carbon and oxygen contamination and this was checked using XPS. When the singles data from all three APECS experiments was compared to the high resolution AES data from the Kratos Axis Ultra Imaging XPS equipment (Figure 5.17) the energy shift of

the curves can clearly be seen, even though the coincidence data aligned with the high-resolution data perfectly.



An energy shift of up to 5eV to lower kinetic energies can be attributed to oxidation (Sn M₅NN 437.4 eV and SnO₂ 432.7ev [19]) with the amount of shift dependant on the amount of oxidation of the surface. So the explanation for the energy shift is as follows. The sample was cleaned (as verified by XPS) and the fixed energy analyser of the APECS experiment was positioned on the clean photoelectron line experimentally. If the photoelectron line shifts during the course of the experiment due to gradual oxidation it will move away from the position of the fixed energy analyser. The fixed analyser will continue to collect photoelectrons unaffected by the chemical shift. If the selected photoelectrons are

unaffected by the chemical shift then the coincidence Auger electrons will also be unaffected. So the singles Auger spectrum will show the chemical shift but the coincidence spectrum will not. The representation is therefore of the clean Auger spectrum, despite the effect of minor oxidation of the surface. It would be expected however that the oxidation of the surface of the sample would affect the coincidence count rate causing it to decrease with the time between sample cleaning. At present it is not possible to monitor the coincidence count of each scan through the Auger spectrum, only the total coincidence count for the day. There is however a definite decrease in the total AES count for each scan. The coincidence count for each scan may be monitored in the future to enable optimisation of the cleaning routine and maximisation of the signal to noise ratio.

5.4.5. Tin in summary

A good visual fit was obtained between the model spectra developed using APECS data and a high resolution AES spectrum of Tin. Previously unresolved Coster-Kronig transitions were noted between the $3d_{3/2}$ and $3d_{5/2}$ energy levels placing intensity on the low kinetic energy side of the M_5NN Auger peak. Further investigation uncovered intensity in the M_4NN and M_5NN regions arising from Coster-Kronig processes originating in the $3p_{3/2}$ energy level. The quantitative contribution to the $M_{4,5}NN$ Auger spectrum from photoionisation in the $3p_{3/2}$ energy level could not be determined from this experiment however it is considered to be significant.

-
1. Lund, C.P., S.M. Thurgate, and A.B. Wedding, *Auger Photoelectron Coincidence Spectroscopy Studies : Trends in the $L_{2,3}-M_{4,5}M_{4,5}$ Line*

Shapes Across the 3d Transition Metal Series. Physical Review B, 1997. **55**(8): p. 5455 - 5465.

2. Thurgate, S.M., *Auger Photoelectron Coincidence Experiments from Solids*. Journal of Electron Spectroscopy and Related Phenomena, 1996. **81**: p. 1 - 31.
3. Thurgate, S.M. and C.P. Lund, *Comparison of the Auger Photoelectron Coincidence Spectroscopy (APECS) Spectra of Ag and InP with Cu and GaAs*. Surface and Interface Analysis, 1997. **25**: p. 10 - 16.
4. Musket, R.G., *Preparation of Atomically Clean Surfaces of Selected Elements: A Review*. Applications of Surface Science, 1981. **10**: p. 143 - 207.
5. Weightman, P., et al., *Local Lattice Expansion Around Pd Impurities in Cu and Its Influence on the Pd Density of States: An Extended X-ray-Absorption Fine-Structure and Auger Study*. Physical Review B, 1987. **36**(17): p. 9098 - 9105.
6. Kucherenko, Y., et al., *Local Electronic Structure and $M_{45}VV$ Auger Spectra of Pd in Cu-rich Cu-Pd Alloys*. Physical Review B, 1998. **57**(7): p. 3844 - 3849.
7. Papaconstantopoulos, D.A., *Handbook of the Band Structure of Elemental Solids*. 1 ed. 1986, Washington, D.C., New York, London: Plenum Press. 410.
8. Lander, J.J., *Auger Peaks in the Energy Spectra of Secondary Electrons from Various Materials*. Physical Review, 1953. **91**(6): p. 1382 - 1387.
9. Sawatzky, G.A. and A. Lenzelink, *Auger Line Shape in Narrow-Band Metals*. Physical Review B, 1980. **21**(5): p. 1790 - 1796.
10. Cini, M., *Two Hole Resonances in the XVV Auger Spectra of Solids*. Solid State Communications, 1977. **24**: p. 681 - 684.
11. Cini, M., *Density of States of Two Interacting Holes in a Solid*. Solid State Communications, 1976. **20**: p. 605 - 607.
12. Cini, M., *Comment on Quasiatomic Auger Spectra in Narrow-Band Metals*. Physical Review B, 1978. **17**(6): p. 2788 - 2789.
13. Cini, M., *Theory of Auger XVV Spectra of Solids: Many Body Effects in Incompletely Filled Bands*. Surface Science, 1979. **87**: p. 483 - 500.

14. Sawatzky, G.A., *Quasiatomic Auger Spectra in Narrow-Band Metals*. Physical Review Letters, 1977. **39**(8): p. 504 - 507.
15. Treglia, G., et al., *Correlation Effects on Auger Spectra in Unfilled d Band Metals*. Journal of Physics C: Solid State Physics, 1981. **14**: p. 4347 - 4355.
16. Bennett, P.A., et al., *Electronic Structure of Ni and Pd Alloys. III. Correlation Effects in the Auger Spectra of Ni Alloys*. Physical Review B, 1983. **27**(4): p. 2194 - 2209.
17. Jablonski, A. and S. Tougaard, *Database of Relativistic Elastic Scattering Cross-sections for Calculations of Photoelectron and Auger Electron Transport*. Surface and Interface Analysis, 1994. **22**: p. 129 - 133.
18. Tougaard, S. and C. Jansson, *Comparison of Validity and Consistency of Methods for Quantitative XPS Peak Analysis*. Surface and Interface Analysis, 1993. **20**: p. 1013 - 1046.
19. Moulder, J.F., et al., *Handbook of X-ray Photoelectron Spectroscopy*, ed. J. Chastain. 1992: Perkin Elmer Corporation.
20. Martensson, N., R. Nyholm, and B. Johansson, *Chemical-Shift Effects and Origin of the Pd 3d Core-level satellite in CuPd alloys*. Physical Review Letters, 1980. **45**(9): p. 754 - 757.
21. Creagh, C.A. and S.M. Thurgate, *The Use of Auger Photoelectron Coincidence Spectroscopy to Deconvolute the $M_{45}N_{45}N_{45}$ AES of Palladium*. Journal of Electron Spectroscopy and Related Phenomena, 2001. **114 - 116**: p. 69 - 74.
22. Parry-Jones, A.C., P. Weightman, and P.T. Andrews, *The $M_{4,5}N_{4,5}N_{4,5}$ Auger Spectra of Ag, Cd, In and Sn*. Journal of Physics C: Solid State Physics, 1979. **12**: p. 1587 - 1600.
23. Jiang, Z.-T., S.M. Thurgate, and P. Wilkie, *Line Structure in Photoelectron and Auger Electron of CuO_x/Cu and Cu by Auger Photoelectron Coincidence Spectroscopy (APECS)*. Surface and Interface Analysis, 2001. **31**: p. 287 - 290.
24. Scofield, J.H., *Hartree-Slater Subshell Photoionization Cross-Sections at 1254 and 1487eV*. Journal of Electron Spectroscopy and Related Phenomena, 1976. **8**: p. 129 - 137.

Chapter 6

Conclusion

The primary aim of this thesis “To demonstrate the effectiveness of the APECS technique in deconstructing a specific section of the Auger spectra of Palladium and Tin allowing quantitative analysis of the component parts”, has been achieved. The main components of both the Palladium and Tin spectra have been identified. Their contribution to the Auger lineshape was demonstrated by the creation of a model Auger peak, derived from APECS data, which was a good fit to high-resolution Auger spectra.

The component curves used to create the Palladium model represented the 2-hole M_4NN and M_5NN Auger processes and the $M_4:M_5^{CK}NNN$ Coster-Kronig process. These curves were also used for the Tin model as well as ones for the M_4NN plasmon and the two Coster-Kronig processes $M_3:M_4^{CK}NNN$ and $M_3:M_5^{CK}NNN$.

The Coster-Kronig process in Palladium was expected as it occurs in Nickel, its comparable element in the 3d metals and because of the ratio of the $3d_{3/2}$ to $3d_{5/2}$ linewidths given by Martensson [1] is 1.22. This ratio indicates more decay paths from the $3d_{3/2}$ energy level than the $3d_{5/2}$ energy level.

Martensson however gives a value of 1.00 for the same ratio in Tin indicating no extra decay processes ie no Coster-Kronig process. Contrary to this indication the coincidence data acquired for this thesis has definite intensity related to the $M_4:M_5:NNN$ Coster-Kronig process.

The ratios of the Tin $3p_{1/2}$ and $3p_{3/2}$ linewidths given by Martensson [1] are close to unity indicating an equivalent number of decay paths for each of these energy levels ie if one level has a Coster-Kronig process so does the other. This is confirmed by the Tin coincidence data for this thesis, which gives a peak height ratio of 1.11 for the $M_3:M_5:CKNNN$ to $M_3:M_4:CKNNN$ Coster-Kronig processes.

The model Auger peaks for Palladium and Tin were composed of several individual curves derived from the APECS data, each represented an individual decay process. These curves were created as follows.

Tin has a filled d-band therefore Cini-Sawatzky transformation of the convoluted density of states produced a curve with 90% of the intensity in a Gaussian atomic-like peak and 10% in a higher kinetic energy band-like component. This curve was used for each of the multiplet final state components in the 2-hole and Coster-Kronig peaks. It was assumed the value of U was constant for each curve and as there was a good fit between the model and the high definition Auger spectra this assumption was justified.

Although not technically correct to use the Cini-Sawatzky transformation of the self-convoluted density of states for partially filled bands, it was applied to Palladium. This was possible because the d-band in Palladium is screened by a full s-band and can be likened to studies on Ni alloys by Bennet [2]. He found that even though the 'fullness' of the valence band varied from alloy to alloy there was little change in the value of U for all of the twenty-seven Nickel alloys studied. Weightman [3] also found that the value of $U(^1G_4)$ was almost independent of alloy composition in studies of $Cu_{99}Pd_1$, $Al_{80}Pd_{20}$, $Mg_{75}Pd_{25}$, $AgPd$. So it was expected that the degree of "fullness" of the d-band in Palladium was not critical. The curve produced by applying the Cini-Sawatzky transformation to the self-convoluted density of states was broad and band-like and fitted the APECS data well. The APECS data from the $M_{45}NN:3d_{5/2}$ and $M_{45}NN:3d_{3/2}$ experiments was used to determine the relative intensity for each component curve in the final model. The model produced was a good fit to the high resolution Auger spectrum. Again the same value of U was used for each curve and if U did change in the Coster-Kronig process it was not detectable.

The difference between these two models is not subtle. In the atomic-like Tin spectrum each decay process is represented by a set of nine Gaussian-like peaks each with a small band-like part, which portray the final state multiplets. The Palladium model however is much simpler and has only one band-like curve for each of the decay processes. This is evidence that the self-convolution of the DOS with the application of the

Cini-Sawatzky Theory can take into account the complexity of the decay paths that contribute to the lineshape for each decay process.

A definite contribution from plasmon processes could be seen in the Tin coincidence data for this thesis however intensity in the low kinetic energy tail of the Palladium Auger peak could be ascribed to either plasmon or shake processes.

An interesting observation was made about the effects of oxidation on the $M_{45}NN$ Tin Auger spectrum over the 24hrs between the sample being cleaned. The singles data had an energy shift of 0.7eV compared to the coincidence data. Due to the nature of the coincidence experiment only electrons unaffected by oxidation became part of the coincidence spectrum however the singles spectrum contained all electrons collected even those affected by the oxidation of the surface. This therefore accounted for the chemical shift of the singles peak to lower kinetic energy.

The Auger spectra are complicated and quantitative use of the Auger spectrum is impossible without detailed understanding of the contributing processes and rigorous lineshape analysis. This indicates the importance of the work in this thesis in understanding the Auger lineshape of Palladium and Tin.

The secondary aim, "To produce a thesis that will facilitate the learning of future students enabling them to make a productive start in the APECS laboratory at Murdoch University" as stated in the introduction, will be determined by time. One of the people who have been reading this thesis as it develops is a first year APECS PhD student and he has asked for a copy of the final work. My hope is that he will use it as a reference and not as a doorstop.

In the near future the electron detection system at Murdoch will be upgraded to a multi-hit multi-channel plate with a delay-line detector. This will increase the count rate by at least 10 fold by improving the sensitivity and count rate and a more detailed lineshape of the 3-hole section of the Auger spectrum in coincidence with various energy positions on the photoelectron line could be obtained. It may be possible from this to distinguish between final-state shake-up and shake-off using the distinctive shape of the respective peaks.

An improved count rate would make it practical to scan a larger energy range below the Auger peak. A large enough energy range would allow the use of the QUASES [4] software for background subtraction. Using this background subtraction technique minimal intensity from 3-hole processes would be removed allowing examination of the shake and Coster-Kronig processes.

The Coster-Kronig and shake-off electrons, which add intensity to the low kinetic energy background in the 0 eV – 10 eV section, cannot normally be distinguished from secondary electrons. It would be interesting to scan this area in coincidence with the 3-hole position on the Auger peak as the APECS technique removes all unrelated electrons.

If the processing software at Murdoch could be modified to enable the coincidence count of each scan through the Auger spectrum to be monitored then any decrease in coincidence count rate as the surface degrades would be clear. This information would help to optimise the cleaning regime for the sample.

APECS spectra of other 4d transition metals may give a clue to relationships in the rate of the Coster-Kronig process. It may also be possible to determine the pivotal factors affecting this rate and the role played by the binding energy and work function.

There is still a great deal of work to be done in Auger photoelectron coincidence spectroscopy. With increased count rates it will be possible to delve deeper into the mysteries of the atom within a solid.

-
1. Martensson, N. and R. Nyholm, *Electron Spectroscopic Determination of M and N Core-Hole Lifetimes for the Elements Nb - Te (Z = 41 - 52)*. Physical Review B, 1981. **24**(12): p. 7121 - 7134.

2. Bennett, P.A., et al., *Electronic Structure of Ni and Pd Alloys. III. Correlation Effects in the Auger Spectra of Ni Alloys*. Physical Review B, 1983. **27**(4): p. 2194 - 2209.
3. Weightman, P., et al., *Local Lattice Expansion Around Pd Impurities in Cu and Its Influence on the Pd Density of States: An Extended X-ray-Absorption Fine-Structure and Auger Study*. Physical Review B, 1987. **36**(17): p. 9098 - 9105.
4. Kover, L., et al., *Determination of Overlayer Thickness by QUASES Analysis of Photon-Excited KLL Auger Spectra of Ni and Cu Films*. Surface and Interface Analysis, 2001. **31**: p. 271 - 279.

Appendix i : Acronyms

AEF	average emission function
AES	Auger electron spectroscopy
AL	attenuation length
APECS	Auger photoelectron coincidence spectroscopy
CFD	constant fraction discriminator
C-K	Coster-Kronig
DDF	depth distribution function
DOS	density of states
EAL	effective attenuation length
E_b	binding energy
ED	escape depth
EDDF	emission depth distribution function
EFWHM	effective full width at half maximum height
E_k	kinetic energy
FWHM	full width at half maximum height
ID	information depth
IMFP	inelastic mean free path
MCA	multi-channel analyser
MED	mean escape depth
MFP	mean free path
Mg	Magnesium
Pd	Palladium
Sn	Tin
TAC	time to amplitude converter
U	hole-hole interaction energy / the Coulomb force between two holes
UHV	ultra high vacuum
VUV	vacuum ultra-violet
VHF	very high frequency
W	valence band width
XPS	X-ray photoelectron spectroscopy

Appendix ii : Auger Process Notation

2-hole process placing intensity in the $M_{45}N_{45}N_{45}$ Auger peak

Name	Process	Label/Description
Basic Auger	$M_4-N_{45}N_{45}$	M_4NN
Basic Auger	$M_5-N_{45}N_{45}$	M_5NN

3-hole processes placing intensity in the $M_{45}N_{45}N_{45}$ Auger peak

Name	Process	Label/Description
Coster-Kronig	$M_4-M_5N_{45}-N_{45}N_{45}(N_{45})$	$M_4:M_5^{CK}NNN$
Coster-Kronig	$M_3-M_4N_{45}-N_{45}N_{45}(N_{45})$	$M_3:M_4^{CK}NNN$
Coster-Kronig	$M_3-M_5N_{45}-N_{45}N_{45}(N_{45})$	$M_3:M_5^{CK}NNN$
Initial-state shake	$M_4N_{45}-N_{45}N_{45}(N_{45})$	$M_4^{is}NNN$
Initial-state shake	$M_5N_{45}-N_{45}N_{45}(N_{45})$	$M_5^{is}NNN$
Final-state shake	$M_4-N_{45}N_{45}N_{45}$	$M_4^{fs}NNN$
Final-state shake	$M_5-N_{45}N_{45}N_{45}$	$M_5^{fs}NNN$

4-hole processes placing intensity in the $M_3N_{45}N_{45}$ Auger peak

Name	Process	Label/Description
Coster-Kronig followed by a Coster-Kronig	$M_3-M_4N_{45}-M_5N_{45}(N_{45})-N_{45}N_{45}(N_{45}N_{45})$	$M_3:M_4:M_5^{CK}N^{CK}NNN$
Initial-state shake followed by a Coster-Kronig	$M_4N_{45}-M_5N_{45}(N_{45})-N_{45}N_{45}(N_{45}N_{45})$	$M_4:M_5^{is}N^{CK}NNN$
Double initial-state shake	$M_4N_{45}N_{45}-N_{45}N_{45}(N_{45}N_{45})$	$M_4^{is}(NN)NN$
Coster-Kronig followed by a final-state shake	$M_4-M_5N_{45}-N_{45}N_{45}N_{45}(N_{45})$	$M_4:M_5^{CK}N^{fs}NNN$
Double final-state shake	$M_5-N_{45}N_{45}N_{45}$	$M_5^{fs}(NN)NN$
Initial-state shake followed by final-state shake	$M_5N_{45}-N_{45}N_{45}N_{45}(N_{45})$	$M_5^{is}N^{fs}NNN$

Appendix iii : Electron Path Length Definitions

The following information is taken these papers

- Jablonski A., C. J. Powell (1999). "Relationships between Electron Inelastic Mean Free Paths, Effective Attenuation Lengths, and Mean Escape Depths." Journal of Electron Spectroscopy and Related Phenomena **100**: 137 - 160.
- Powell C. J., A. Jablonski, et al. (1999). "Surface Sensitivity of Auger-Electron Spectroscopy and X-Ray Photoelectron Spectroscopy." Journal of Electron Spectroscopy and Related Phenomena **99**: 1 - 15.
- Jablonski A., C. J. Powell (1993). "Formalism and Parameters for Quantitative Surface Analysis by Auger Electron Spectroscopy and X-Ray Photoelectron Spectroscopy." Surface and Interface Analysis **20(9)**: 771 - 786.

Inelastic mean free path (**IMFP**)(λ): the average of distances, measured along trajectories, that particles with a given energy travel between inelastic collisions in a substance ie. the average distance an electron of a given energy travels between successive inelastic collisions.

Emission depth distribution function (for a measured signal)(**EDDF** or **DDF**): for particles or radiation emitted from a surface in a given direction, the probability that the particle or radiation leaving the surface in a specified state originated from a specific depth measured normally from the surface into the material.

Average emission function decay length (AEF): the negative reciprocal slope of the logarithm of a specified exponential approximation to the emission depth distribution function over a specified range of depths, as determined by a straight-line fit to the emission depth distribution function plotted on a logarithmic scale versus depth on a linear scale ie. the reduction of intensity of any radiation with distance traversed in matter ie. the probability that an electron leaving the solid at a certain emission angle was generated at a certain depth and reached the surface without energy loss.

Effective attenuation length (EAL or AL): the average emission function decay length when the emission depth distribution function is sufficiently close to exponential for a given application.

Mean escape depth (MED or ED): the average depth normal to the surface from which the specified radiation or particles escape as defined by

$$D = \frac{\int_0^{\infty} z\phi(z,\alpha) dz}{\int_0^{\infty} \phi(z,\alpha) dz}$$

where $\phi(z,\alpha)$ = the emission depth distribution function for depth z from the surface into the material and for direction of emission α with respect to the surface normal.

$$D = \Delta = \lambda \cos\alpha \quad \text{if elastic-electron scattering in the sample is ignored}$$

Information depth (ID): maximum depth, normal to the specimen surface, from which useful signal information is obtained.

Note 1 The ID can be identified with the specimen thickness from which a specified percentage (eg 95% or 99%) of the detected signal originates.

Note 2. The ID can be determined from measured, calculated, or estimated DDF for the signal of interest.

Each of these measurements has a place in calculations of signal intensity and this has been summarised by Jablonski as follows.

Quantitative application	AES		XPS	
	Exponential EDDF	Non-exponential EDDF	Exponential EDDF	Non-exponential EDDF
Overlayer thickness measurement	EAL	EDDF	needs more than one parameter	needs more than one parameter
Determination of surface composition	IMFP	IMFP	IMFP	IMFP
Estimation of the average depth of analysis	MED	MED	MED	MED

Summary of when to use various electron path length values

Appendix iv The Use of APECS to Investigate Various Decay Processes

Process investigated	XPS spectrum characteristics	AES spectrum characteristics	APECS (Coincidence) spectrum characteristics	Auger electron analyser
Basic Auger (2-hole) with no plasmon processes	Single featureless line	Includes intensity from all possible processes, may be missing intensity from Coster-Kronig processes	Fixed on maximum intensity of XPS line	Scanning Shows basic 2-hole process, final state shake-up/off processes and intensity shifted due to energetically allowable Coster-Kronig process if scan range includes Auger peak from other participating energy level. Does not show initial-state shake-up/off processes.
Basic Auger (2-hole) with XPS plasmon loss	Shows bulk and surface plasmon loss peaks - different periodicity	May show bulk and surface plasmon gain peaks for some materials with a different periodicity for each. May show bulk and surface plasmon loss peaks for other materials.	Fixed on maximum intensity of XPS line	Scanning May show surface plasmon gain peaks for some materials and surface plasmon loss peaks for others. Shows basic 2-hole process, final state shake-up/off processes and intensity shifted due to energetically allowable Coster-Kronig process if scan range includes Auger peak from participating other energy level. Does not show initial-state shake-up/off processes.
Final-state shake-up/off (3-hole)	Single featureless line	Shows low kinetic energy shoulder on peak	Fixed on maximum intensity of XPS line	Scanning Shows basic 2-hole process and final state shake-up/off processes. May be able to determine difference by shape and periodicity.

Process investigated	XPS spectrum characteristics	AES spectrum characteristics	APECS (Coincidence) spectrum characteristics	
			Photoelectron analyser	Auger electron analyser
Initial-state shake-up/off (3-hole)	Shows low kinetic energy shoulder on line	May show as low kinetic energy shoulder on peak because of spectator hole in Auger process changes the hole-hole interaction energy	Fixed on low kinetic energy shoulder of XPS line, which has no intensity due to plasmon loss.	Scanning Shows peak shifted within singles envelope to lower kinetic energies due to presence of spectator hole. Peak should be similar shape to basic 2-hole peak. The amount of difference determined by ΔU (see chapter on Cini-Sawatzky Theory)
Coster-Kronig	Single featureless line broader than expected by looking at energy levels with the same quantum number because of the shorter core hole lifetimes / higher transition probabilities	Diminished intensity of AES peak from inner energy level and enhanced intensity of AES peak from outer energy level with the same principle quantum number—by comparison with the intensity ratio of the corresponding XPS lines.	Scanning Peak moves to low kinetic energy side of singles envelope. Shows initial-state shake-up/off peaks – may be able to determine difference by periodicity of peaks.	Fixed on low kinetic energy shoulder of AES peak which has no possibility of plasmon loss intensity
			Fixed on maximum intensity of XPS line from inner energy level	Scanning Intensity in AES spectrum associated with energy level selected (2-hole simple Auger process) and intensity in low kinetic energy shoulder of AES spectrum of outer energy level with same principle quantum number. Fixed on low energy shoulder of AES spectrum from outer energy level
			Scanning Shows mid peak intensity under XPS line from inner energy level corresponding to origin of Coster-Kronig process and intensity on low kinetic energy side of XPS line from outer energy level which could be associated with initial-state shake-up/off	

Process investigated	XPS spectrum characteristics		AES spectrum characteristics		APECS (Coincidence) spectrum characteristics	
	XPS spectrum characteristics	AES spectrum characteristics	Photoelectron analyser	Auger electron analyser		
Inelastic scattering	Broadening on low kinetic energy side of peak and contribution to general low energy background		Fixed on maximum intensity of XPS line	Less broadening than singles and less contribution to the background because effective escape depth for coincidence is less than XPS or AES so there is less scattering.		
Background intensity from unrelated processes	Increases almost exponentially from high to low kinetic energy		Fixed anywhere on XPS line	Scanning Background greatly reduced because not associated with initiating photoelectrons. Difficult for processes elsewhere to put intensity in both the photoelectron line and the Auger spectrum.		
Transitions between atoms	Broadening of affected line (cp. isolated atom) due to increased number of possible modes of decay	Decreased intensity of peak (compared to isolated atom) if transitions are between atoms which are different	Scanning Background eliminated because not associated with selected Auger electrons Difficult for processes elsewhere to put intensity in both the photoelectron line and the Auger spectrum	Fixed anywhere on Auger peak		
			Fixed on maximum intensity of XPS line	Scanning Reduced intensity when compared to spectra of sample with isolated atoms because of intensity shifting. The energy available to the Auger electron depends on the difference in the binding energy of the two energy levels involved in the Auger decay.		

Process investigated	XPS spectrum characteristics	AES spectrum characteristics	APECS (Coincidence) spectrum characteristics	
			Photoelectron analyser	Auger electron analyser
Overlapping lines	XPS lines and AES peaks from different materials in the solid may overlap. This can sometimes be fixed by using a different source of X-rays because the photoelectron kinetic energy is dependent on the energy of the X-rays but the Auger electron energy is not.	XPS lines and AES peaks from different materials in the solid may overlap. This can sometimes be fixed by using a different source of X-rays because the photoelectron kinetic energy is dependent on the energy of the X-rays but the Auger electron energy is not.	Fixed on clear XPS line	Shows only the intensity in the selected XPS line. So any overlapping intensity from another element is removed
Chemical shift due to alloying	Peak shifts due to change in energy levels	Peak shifts more than XPS for same change in energy levels	Fixed on maximum intensity of shifted XPS line	Possible shape change around 3-hole position (low kinetic energy shoulder) of shifted Auger peak due to turning on or off of shake or Coster-Kronig processes
Chemical shift due to oxidation during the experiment	Peak shifts a little with time	Peak shifts a little more with time	Fixed on XPS line from clean sample. As the surface oxidises the energy levels change but the analyser is still selecting the atoms with the energy levels the same as the original ones i.e. clean atoms	Auger peak does not shift because the Auger electrons are coming from atoms with unchanged energy levels. As the surface becomes oxidised there are less of these atoms and so the count rate drops.

Appendix v : List of APECS Researchers

The pioneers of APECS were H. W. Haak, G. A. Sawatzky and T. D. Thomas University of Groningen

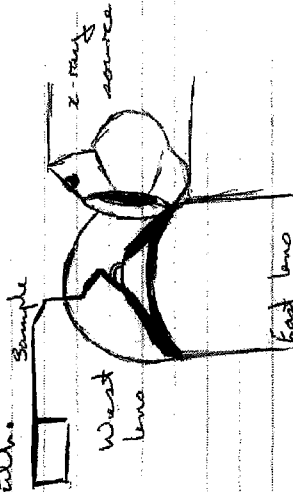
APECS Researchers	National Synchrotron Light Source, Brookhaven	ELETTRA Synchrotron Light Source, Truett	European Synchrotron Radiation Facility, Grenoble	Murdoch University, Perth
D. A. Arena	√	√		
A. Attili	√	√		
R. A. Bartynski	√	√		
S. Bernstorff		√		
F. Bruno		√		
E. Busetto		√		
P. Calicchia			√	
M. Canepa,		√		
E. Colavita		√		
D. M. Coward				√
R. P. Craig				√
C. A. Creagh				√
F. G. Curti	√			
D. Cvetko	√	√		
S. Daddato		√		
A. Di Bona		√		
B. Diviacco		√		
L. Floreano	√	√		
V. Formoso			√	
R. F. Garrett	√			
K. Garrison	√			
G.C. Gazzadi		√		
R. Gotter	√	√		
G. Granozzi		√		
S. L. Hulbert	√			
S. Iacobucci	√	√		
E. Jensen	√			
Z-T. Jiang				√
E. D. Johnson	√			
C. C. Kao	√			
S. Lagomarsino			√	
A. Lausi		√		
B. Lohmann				√
P. Luches	√	√		
C. P. Lund				√
M. Malvezzi		√		
C. Mannori		√		
L. Marassi	√	√		
C. Martinelli			√	
A. Morgante	√	√		
G. Naletto		√		
S. Nannarone		√		
R. A. Nayak	√			
J. Neal				√

APECS Researchers	National Synchrotron Light Source, Brookhaven	ELETTRA Synchrotron Light Source, Truett	European Synchrotron Radiation Facility, Grenoble	Murdoch University, Perth
H. Nozoye	√			
L. Pasquali,		√		
M. Pirlitescu		√		
Q. Qian	√			
A. Ruocco	√	√		
M. Sambi		√		
A. Santaniello		√		
F. Scarinci			√	
W. K. Siu	√			
G. Stefani	√			
A. T. Stelbovics				√
S. M. Thurgate				√
B (W). D. Todd				√
F. Tommasini	√			
A. Walker		√		
A. B. Wedding				√
M. Weinert	√			
A. H. Weiss	√			
P. Wilkie				√
X. L. Wu	√			
S. Yang	√			
D. M. Zehner	√			
M. Zitnik	√			

Appendix vi Optimising Magnetic Fields

Setting up the mag fields to maximise the collection of coincident electrons

- 1) Position the sample so that it is in the mid position between the lenses. The bottom of the sample is level with the top of the hole in the lens and just slightly removed from it.



- 3) Set retard potential & adjust sector voltages so that when an XPS is taken the strongest peaks have the correct kinetic energy.
- 4) Using the calculate analyzer software set the retard potential of the strongest peaks (W-photoelectron, G-Auger) and adjust the gain of the lenses to maximise the count rate. i.e. lenses are now focused for electrons of the required kinetic energy.
- 5) Adjust the magnetic fields. If the lenses are looking at the same spot on the target then raising & lowering the target or moving the target in a WS direction will affect the count rate on both rotometers in the same way. They will also reach peak counts at the same time. Other-wise...

167
Sketch p 168

$E \rightarrow W$ Mag field direction
balanced

$U \rightarrow D$ Mag field direction
balanced

$N \rightarrow S$ Mag field direction
balanced

Raising/lowering sample and WS movement makes no difference. So this field strength only needs adjusting if optimum of the other fields completely.

As sample is raised/lowered or moved WS one analyzer will peak before another if the field is not balanced. By changing the field strength the physical distance the sample has to be moved between where one analyzer sees peak counts & where the other analyzer sees peak counts will change & may even reverse. Minimize the distance ~~to the sample~~ needs to be moved to produce peak count in both analyzers by varying the mag field strength.

Then mag for the case if the maximum count for both analyzers is to be found within the sample is not in the midline.

Appendix vii Cleaning and Experimental Settings

Settings for Palladium $M_{45}N_{45}N_{45} : 3d_{32}$ (Data/Palladium/130499)

Retard and Focus														
Analyser	Line / Peak	Kinetic Energy (eV)	Pass Energy (eV)	Retard Energy (eV)	Sector Voltage (V)	Offset F1	Offset F2	800eV Gain F1	800eV Gain F2	Retard F1	Retard F2	Channel Plate Voltage (kV)	TAC delay	Peak Counts
West	$M_{45}VV$	327.6	150.0	177.6	50.3	000	190	641	2567	128	699.5	2.75	Start	3.6×10^4
East	$3d_{32}$	913.6	150.0	763.6	48.6	000	0.5	355	2312	337	2167.0	2.70	Stop	2.1×10^4

Sample Positions

	Run Position	Bombard Position
U/D	7.475	17.5
E/W	1.10	1.10
N/S	6.15	0.0 + 0.75
Angle	332	317.5

X-ray Settings

High Tension Voltage (kV) 13.5
 Emission Current (mA) 40
 Water Temp 17.8 - 18°C

Magnetic Field Settings

U/D 0.34
 E/W 0.21
 N/S 0.00

Electron Gun Settings

Focus 4.5
 x deflection max
 y deflection min
 Ion current 0.43 uA

Computer Program Settings

Gain 256
 Units 1
 Memory Groups 64
 Active Analyser West 317.6 - 337.6
 Increment 0.5
 Static Analyser East 913.6
 Relax Time 2100

Data Processing

Zero Channel 67

Cursor positions 46 60 67 202

Rate Meter Settings (E starts count W stops count)

TAC Full Scale Time 0.1us
 W CFDISC lower level 25
 E CFDISC lower level 20
 ChA Dual Amp Coarse 20
 ChA Dual Amp Fine 0.02
 ChB Dual Amp Coarse 20
 ChB Dual Amp Fine 0.5050

General

Pump the Ar⁺ after bombardment using the turbo to 1.5×10^{-7} torr before starting ion pump.
 C 1s 968.6eV O $K_{23}L_{23}$ 508.6eV S $2p_{1/2}$ 1088.6eV

Checklist

Ion gauge off
 TSP off
 Mag field settings
 LED noise
 Rate meters on
 Channel plate settings
 x-ray settings
 Ion gun off
 Helmholtz coil position
 Sample in position and earthed
 Rotary pump isolated
 Turbo pump off

Settings for Tin $M_{45}N_{45}N_{45} : 3d_{32}$ (Data/Tin/120799)

Retard and Focus														
Analyser	Line / Peak	Kinetic Energy (eV)	Pass Energy (eV)	Retard Energy (eV)	Sector Voltage (V)	Offset F1	Offset F2	Retard F1	Retard F2	800eV Gain F1	800eV Gain F2	Channel Plate Voltage (kV)	TAC delay	Peak Counts
West	$M_{45}VV$	428.6	150.0	278.6	50.6	000	192.5	127	1014.0	387	2600	2.76	Start	1.3×10^4
East	$3p_{3/2}$	538.6	150.0	388.6	50.0	000	0.5	300	650	796	2267	2.80	Stop	2.0×10^4

Sample Positions

	Run Position	Bombard Position
U/D	7.0	17.0
E/W	0.01	0.01
N/S	5.8	0 + 0.75
Angle	330	315

X-ray Settings

High Tension Voltage (kV) 13.5
 Emission Current (mA) 30
 Water Temp 17.8 - 18°C

Magnetic Field Settings

U/D 0.34
 E/W 0.21
 N/S 0.00

Electron Gun Settings

Focus 5.5
 x deflection min
 y deflection max
 Ion current

Computer Program Settings

Gain 256
 Units 1
 Memory Groups 64
 Active Analyser West 420.1 - 444.1
 Increment 0.5
 Static Analyser East 538.6
 Relax Time 2030
 Count time 105

Data Processing

Zero Channel 67
 Cursor positions 46 60 67 193

Rate Meter Settings (E starts count W stops count)

TAC Full Scale Time 0.1us
 W CFDISC lower level 25
 E CFDISC lower level 20
 ChA Dual Amp Coarse 20
 ChA Dual Amp Fine 0.02
 ChB Dual Amp Coarse 20
 ChB Dual Amp Fine 0.5050

General

Pump the Ar⁺ after bombardment using the turbo to 1.5×10^{-7} torr before starting ion pump. Calibrate analysers before starting new sample.
 C 1s 968.6eV O 1s 722.6

Checklist

Ion gauge off
 TSP off
 Mag field settings
 LED noise
 Rate meters on
 Channel plate settings
 x-ray settings
 Ion gun off
 Helmholtz coil position
 Sample in position and earthed
 Rotary pump isolated
 Turbo pump off

Diagram Index

Figure	Page
Figure 1.1 Electron energy spectrum of Palladium	1
Figure 1.2 XPS process and spectrum. The energy separation between the peaks in the photoelectron spectrum is the same as that of the energy levels.	3
Figure 1.3 XPS notation – photoelectron lines are named using the quantum number notation representing the original energy level of the photoelectron	4
Figure 1.4 AES notation – Auger electron peaks are named using atomic shell notation. In this situation the initial photoionisation takes place in the $4d_{3/2}$ or $4d_{5/2}$ energy level (M_{45}). The subsequent decay process leaves two holes in the valence band.	8
Figure 1.5 $M_5-N_{45}N_{45}$ basic 2-hole Auger process. Initial photoionisation of a core level is followed by an outer electron filling the core hole. The amount of energy released is transferred to another outer electron - the 'Auger' electron that escapes with a characteristic amount of kinetic energy.	9
Figure 1.6 Auger curve from a 4d metal which appears to be mainly formed from the sum of two basic 2-hole Auger processes $M_5-N_{45}N_{45}$ (shown as the Gaussian curve under the full curve) and $M_4-N_{45}N_{45}$. This diagram makes many assumptions – there is no interaction between the holes made in the valence band and there is no multiplet splitting of the energy levels.	9
Figure 1.7 Fluorescence and Auger Yield vs. Atomic Number	10
Figure 1.8 Basic Auger process involving the valence band and demonstrating the situations that produce maximum and minimum Auger electron energies.	12
Figure 1.9 Auger plasmon gain satellite peak with primary peak.	15
Figure 1.10 Auger plasmon loss satellite peak with main peak.	16
Figure 1.11 Coster-Kronig process. Photoionisation of inner core level. Core hole filled by an electron from a higher energy level with the same principle quantum number. The energy produced releases a Coster-Kronig electron from an outer orbital. Normal Auger process occurs in the presence of this spectator hole.	17
Figure 1.12 Auger spectrum showing the $M_4N_{45}N_{45}$ 2-hole Auger peak and its low kinetic energy Coster-Kronig satellite peak.	18
Figure 1.13 Initial-state shake-up process and resulting position of the satellite peak in the Auger spectrum. The shake-up electron is excited to higher levels within the valence band by the incident X-ray. This robs the photoelectron of discrete amounts of energy. The spectator hole in the valence band at the time of the Auger electron's release shifts the Auger peak to a lower kinetic energy.	23

Figure 1.14 Initial-state shake-off process and resulting intensity of the initial-state shake-off satellite peak in the Auger spectrum. The end result is the same for the Auger spectrum but the photoelectron energy is reduced by a variable amount instead of discrete amounts.	23
Figure 1.15 Final-state shake-up process and position of final-state shake-up satellite peaks in the Auger spectrum. The energy shift of the peaks is determined by the energy level to which the shake electron is raised.	24
Figure 1.16 Final-state shake-off process and position of the final-state shake-off satellite peak. The maximum energy is the maximum energy of the Auger electron less the binding energy of the shake-off electron. There is only one peak, which gradually decreases in intensity with energy because the shake-off electron may remove a variable amount of energy from the Auger electron.	24
Figure 1.17 Hypothetical electronic transition between atoms	30
Figure 2.1 Generic figure showing the density of electron states near the Fermi energy. Assuming every transition between valence band and core hole is allowed and an electron may fill the core hole from any of the positions a-i. Also assume the transition probabilities are the same for each transition then the relative distribution of the transitions is determined by the DOS. The Auger electron can leave the valence band from any position r-z. If all transition probabilities are the same then the DOS determines the relative distribution of the Auger electrons. So for each possible transition that fills the core hole (set probability) there are a full range of Auger emissions with their own probabilities. The convolution of the valence band with itself therefore presents a first approximation to the shape of the Auger peak.	35
Figure 2.2 Kinetic energy range of the Auger electron in a core-valence-valence process. ΔE is the difference in binding energy between the energy levels, E is the binding energy of the Auger electron and E_k is the kinetic energy of the Auger electron.	36
Figure 2.3a Wide band allows holes to delocalised producing a band-like spectra	38
Figure 2.3b Narrow band localises holes producing atomic-like spectra.	38
Figure 2.3c Holes are in the energy level pulled out of the bottom of the band producing an atomic-like spectra	38

Figure 2.4 Hypothetical sketches of the band-like and atomic-like sections of the Auger spectrum. In (a) the valence band (W) is wide relative to the hole-hole interaction energy (U). Most of the intensity is in the broad low-intensity band-like peak with a small amount of intensity in the narrow atomic-like peak. The atomic-like peak is shifted to a lower kinetic energy from the centroid of the band-like peak by an amount approximately equal to U . The Auger peak is the sum of these band-like and atomic-like peaks. In (b, c and d) the ratio of U/W increases, as does the intensity in the atomic-like peak and the separation between the two peaks. In this way the Auger peak changes from band-like to atomic-like across the periodic table as the values of U and W change.	40
Figure 2.5 Band-like part of the Tin Auger spectrum produced using the Cini-Sawatzky theory. The kinetic energy scale is relative to the centroid of the band-like spectrum. The legend gives values of U/W . For U/W less than or equal to 1.5 the area under the curves is the same. For $U/W = 1.5$ the lineshape has formed an atomic-like spike about U below the centroid of the band-like curve. For $U/W > 1.5$ the atomic-like curve has separated from the band-like curve (so it is not shown on the diagram) and contains 90% or more of the total intensity of the atomic-like and band-like curves for that value of U/W .	42
Figure 3.1 Tin emission-electron energy spectrum	50
Figure 4.1 APECS notation. The symbols to the left of the colon represent the peak or line being scanned while the symbol to the right of the colon represents the particular part of the electron energy spectrum that determines the decay process being investigated.	64
Figure 4.2 Schematic diagram of the Murdoch University APECS system	65
Figure 4.3 Position of x-ray source (right) and electron collection lenses (bottom). The sample holder (top left) has been raised so the sample can be cleaned by Argon ion bombardment. The sample normally sits at the focus of the of the lenses and X-ray source. A copper sample can be seen superimposed over the lower lip of the ion gun (top middle).	67
Figure 4.4 Plan view of lenses, 127° analysers and multi-channel plates	68
Figure 4.5 APCS lenses, 127° analysers and channel plates.	69
Figure 4.6 APCS lenses, 127° analysers and channel plates.	69
Figure 4.7 The electron energy is selected by the 127° cylindrical analyser	70
Figure 4.8 APECS lenses, hemispherical analysers and channel plates	73
Figure 4.9 APECS lenses, hemispherical analysers and channel plates	73

Figure 4.10 TAC spectrum. The x-axis is divided into 256 channels each representing $0.1 \times 10^{-6} / 256$ sec. Distance along the x-axis represents the delay between the start and the stop signal. The y-axis shows the number of start-stop events in each channel. The total number of events in all channels is the singles count for that particular combination of photoelectron and Auger electron energy. For the coincidence count only the events under the coincidence peak and above the background level are counted. The background level in the coincidence channels (35-47) is determined by fitting a cubic function to the other channels 5-34 and 48-242. The zero channel is 47.	75
Figure 4.11 APECS data of Copper $L_{23}M_{45}M_{45}$ Auger peak in coincidence with $2p_{1/2}$ and $2p_{3/2}$ photoelectrons. The $2p_{1/2}$ data shows a peak on the low kinetic energy side of the $L_3M_{45}M_{45}$ Auger peak. This is attributed to the $L_2-L_3M_{45}M_{45}M_{45}(M_{45})$ Coster-Kronig process. Haak et. al. postulated that the energy shift of the Coster-Kronig preceded Auger electron is due to the spectator hole in the valence band which changes the Coulomb interaction energy of the electron and the remaining holes.	83
Figure 4.12 Diagram showing the components of the low energy tail of the Auger peak	91
Figure 5.1 From the paper by Weightman et. al. The inset shows the calculated DOS for Pd impurities in Cu. This DOS gave the best agreement between theory and experiment when the Auger profile was calculated with a $U(1G_4)$ of 3.0eV	116
Figure 5.2 Pd DOS	118
Figure 5.3 Raw singles data	121
Figure 5.4 Raw coincidence data	121
Figure 5.5 A horizontal linear amount of intensity has been removed from both the singles and coincidence data. The singles has been scaled to the coincidence data and the intended inelastic background to be removed from both is shown by dotted line.	123
Figure 5.6 Coincidence data with background removed	123
Figure 5.7 Comparison of the coincidence data with inelastic background removed using the cos curve background subtraction method and the 'spreadsheet' Tougaard background subtraction method.	124
Figure 5.8 Palladium $M_{45}NN$ singles data, $M_{45}NN:3d_{5/2}$ coincidence data and M_5NN model peak created by applying the Cini-Sawatzky Theory to the convoluted one-electron density of states. $U/W=0.4$	126
Figure 5.9 Palladium $M_{45}NN$ singles data, $M_{45}NN:3d_{3/2}$ coincidence data with background removed and model peaks for M_4NN and the Coster-Kronig process. The model peaks were created by applying the Cini-Sawatzky Theory to the convoluted one-electron density of states. $U/W=0.4$	128

<p>Figure 5.10 Palladium model fit of M_4NN (332.6eV), M_5NN (327.6eV) and Coster-Kronig (326.6eV) peaks to high resolution AES data. The model peaks were created by applying the Cini-Sawatzky Theory to the convoluted one-electron density of states. (M_4NN peak height) = 0.3(M_5NN peak height). (Coster-Kronig peak height) = 1.45(M_4NN peak height). $U/W=0.4$</p>	131
<p>Figure 5.11 Parry-Jones diagram of the $M_{45}NN$ spectrum of Tin. The lines represent the position and intensity of the multiplets.</p>	135
<p>Figure 5.12.1 $M_{45}NN:3d_{3/2}$ data with background removed showing the three model peaks generated from sets of Gaussian curves relating to the M_4NN plasmon, $M_4:M_5:CKNNN$ Coster-Kronig process and the M_4NN Auger peak (read from L-R).</p>	136
<p>Figure 5.13 $M_{45}NN:3d_{5/2}$ data with background removed showing three model peaks generated from sets of Gaussian curves. The peaks represent the M_5NN Auger peak and the satellite M_4NN Auger peak arising from the Mg $K\alpha_3$ X-ray line with its associated low kinetic energy plasmon peak</p>	139
<p>Figure 5.14 $M_{45}NN:3p_{3/2}$ data with background removed showing the three model peaks generated from sets of Gaussian curves relating to the $M_3:M_5:CKNNN$ Coster-Kronig process, the $M_3:M_4:CKNNN$ Coster-Kronig process and the plasmon arising from this process.</p>	141
<p>Figure 5.15 High resolution AES spectrum with curves created using the $M_{45}NN:3d_{3/2}$ and $M_{45}NN:3d_{5/2}$ APECS data. Note the missing intensity in the middle of each Auger peak and on the low kinetic energy side of each peak.</p>	144
<p>Figure 5.16 High resolution AES spectrum with curves created using the $M_{45}NN:3d_{3/2}$ the $M_{45}NN:3d_{5/2}$ and the $M_{45}NN:3p_{3/2}$ APECS data. This is not a quantitative fit as the exact shape of the $M_{45}N_{45}N_{45}:3p_{3/2}$ curves are not known however it is felt that the contribution is significant.</p>	145
<p>Figure 5.17 A comparison of the singles data from each of the APECS experiments with the high resolution AES spectrum. The shift to lower kinetic energies of the APECS singles is attributed to slight oxidation of the sample in the time between the daily cleaning regimes. The shift was not noted in the coincidence data however because the photoelectrons that were selected by the stationary analyser self selected the "clean" Auger electrons.</p>	147

Table Index

Table	Page
Table 1.1 Comparison of XPS and AES Notation	8
Table 1.2 Notation for Possible Decay Processes.	25
Table 3.1 Comparison of the Three Types of Background Subtraction Techniques	59
Table 4.1 Palladium IMFP for Electron Energies in the Range 200 to 2000eV	89
Table 4.2 3d and 4d Transition Metals	93
Table 4.3 Information on the 3d and 4d Transition Metals	94
Table 4.4 Murdoch University APECS Experiments	95
Table 4.5 Coincidence Plots for the Elements Studied by the Murdoch Group	97
Table 5.1 The Multiplet Structure of the Palladium $M_{45}NN$	115
Table 5.2 Multiplet Splitting Information given by Parry-Jones et. al	138
Table 5.3 Peak Positions and Relative Heights	138